理學博士學位論文

Abl-Interactor (Abi) Regulation of BMP-Dependent Synaptic Growth through Macropinocytosis

Abl 상호작용 단백질인 Abi 에 의한 BMP 의존적 시냅스 성장 및 macropinocytosis 의 조절

2018 년 2 월

서울대학교 대학원

협동과정 유전공학전공

김 나 진

Abstract

Abl-Interactor (Abi) Regulation of BMP-Dependent Synaptic Growth through Macropinocytosis

Najin Kim

Interdisciplinary Graduate Program in Genetic Engineering

The Graduate School

Seoul National University

Glass bottom boat (Gbb), a bone morphogenetic protein (BMP) in *Drosophila*, is a key retrograde trans-synaptic signal required for normal synaptic development and function at the neuromuscular junction (NMJ). Although endocytosis appears to be a key mechanism to attenuate BMP signaling, the underlying mechanism remains elusive. Abi (Abl interactor) is a substrate adaptor protein for the Abl tyrosine kinase protein and a key component of the SCAR/WAVE protein complex, which relays signals from Rac to the Arp2/3 complex to regulate actin dynamics during macropinocytosis. Here, I provide

evidence that Abi acts as a node of convergence of Abl- and Rac-mediated signaling to restrain BMP-dependent synaptic growth through macropinocytosis. Abi, Abl, and the Rac-SCAR/WAVE pathway regulate the growth of NMJ synapses via inhibition of BMP signaling. Genetic interactions indicate that Abi acts downstream of Abl and Rac to regulate synaptic growth. Gbb induces macropinocytosis in neurons and at the NMJ. Gbb-induced macropinocytosis critically depends on the Rac-SCAR/WAVE pathway and Abl-mediated phosphorylation of Abi, both of which are critical for the formation of F-actin-rich macropinocytic carriers. Importantly, macropinocytosis mediates Gbb-induced internalization of the BMP receptor Thickveins (Tkv) and is indispensable for its degradation. Finally, loss of other known regulators of macropinocytosis increases BMP signaling and synaptic growth at the NMJ. Based on these findings, I propose that Abi links Abl signaling with the Rac-SCAR/WAVE pathway to promote ligand-induced BMP receptor downregulation through macropinocytosis, thereby limiting this positive growth signal.

Keywords : Abi, Abl, Rac, Gbb, BMP receptor, Macropinocytosis, Synaptic growth, NMJ synapses

***Student Number* : 2010-20212**

CONTENTS

III. Results

LIST OF FIGURES

ABBREVIATIONS

A.U.	Arbitrary unit
Abi	Abl interactor
Abl	Abelson
Arp2/3	Actin related protein 2/3
BDNF	Brain-derived neurotrophic factor
BMP	Bone morphogenetic protein
Brp	Bruchpilot
CD	Clathrin-dependent
CI	Clathrin-independent
CNS	Central nervous system
co-Smad	Common partner Smad
CSF-1	colony stimulating factor 1
CSP	Cysteine-string protein
CtBP1/BARS	C-terminal-binding protein-1/brefeldinA-ADP ribosylated substrate
Da	Daughterless
Dad	Daughters against decapentaplegic
dap160	Dynamin-associated protein 160 kDa
dfmr1	*Drosophila* fragile X mental retardation 1
dFMRP	*Drosophila* fragile X mental retardation protein
Dlg	Disc large
EGF	Epidermal growth factor

EIPA	ethyl-isopropyl amiloride
ELAV	embryonic lethal abnormal visual system
EM	Electron microscopy
EndoA	Endophilin A
F-actin	Filamentous actin
FasII	Fasciclin II
Gbb	Glass bottom boat
GEEC	Glycosylphosphotidylinositol- anchored protein enriched compartments
GFP	Green fluorescent protein
GluRIIC	Glutamate receptor IIC
Graf	GTPase regulator associated with focal adhesion kinase
HHR	Homeo-domain homologous region
HRP	Horseradish peroxidase
HSPC300	Hematopoietic stem progenitor cell 300
Mad	Mothers against decapentaplegic
Med	Medea
MT	Microtubule
Nap	Nck-associated protein
NGF	Nerve growth factor
NMJ	Neuromuscular junction
Nwk	Nervous wreck
P-Mad	Phosphorylate- Mad
PDGF	Platelet-derived growth factor

PH	Pleckstrin homology domain
PIR121	p53-inducible mRNA 121
$PLC\delta_1$	Phospholipase C-delta 1
PRR	Proline-rich region
R-Smad	Receptor-regulated Smad
Rp49	Ribosomal protein 49
Sax	Saxophone
SCAR/WAVE	Suppressor of cAMP receptor/ WASP-family verprolin homology protein
SEM	Standard error of the mean
SH3	Src Homology 3
Spict	Spichthyin
SSR	Subsynaptic reticulum
Tkv	Thickveins
TMR	Tetramethylrhodamine
Trk	Tyrosine receptor kinase
Twf	Twinfilin
UAS	Upstream activation sequence
UTR	Untranslated region
VB	Vinblastine
VNC	Ventral nerve cord
WAB	WAVE-binding
WASP	Wiskott-Aldrich syndrome protein
Wit	Wishful thinking

Figure 6 and Figures 26C & 26D were reproduced from data provided as part of collaboration by Dr. Minyeop Nham (Hanyang University).

Figure 16, Figures 23A & 23B, Figure 24, Figure 25, and Figures 26A & 26B were reproduced from data provided as part of collaboration by Seungdae Kim in our laboratory (Seoul National University).

I. Introduction

1. Transsynaptic Bone Morphogenetic Protein (BMP) Signaling at the *Drosophila* Neuromuscular Junction (NMJ)

Transsynaptic communication between neurons and their postsynaptic targets is critical for the proper development and plasticity of synaptic connections. Neurons sending signals to synapses that regulate the differentiation of the postsynaptic cells are performing anterograde signaling. On the other hand, signals from postsynaptic cells that control the growth, maturation, plasticity, and function of presynaptic neurons are carrying out retrograde signaling (Tao and Poo, 2001). Bidirectional communication between pre- and postsynaptic cells is called transsynaptic signaling. Transsynaptic communication is often mediated by growth factors released by pre- or postsynaptic terminals. Retrograde signaling in neurons often involves neurotrophins, such as the neurotrophic factors nerve growth factor (NGF) and brain-derived neurotrophic factor (BDNF), which promote the survival and differentiation of presynaptic neurons (Huang and Reichardt, 2001).In the *Drosophila* NMJ, some of the most well-characterized transsynaptic retrograde signaling players are bone morphogenetic protein (BMP) homologs, which are members of the transforming growth factor β (TGF-β) superfamily. When secreted from postsynaptic muscles, the BMP homolog Glass bottom boat (Gbb) promotes presynaptic development (McCabe et al., 2003). Interestingly, retrograde BMP signaling in the mammalian central nervous system (CNS) regulates synaptic development and function in a similar manner to that seen at the *Drosophila* NMJ, which implies that retrograde BMP signaling is well conserved across species (Xiao et al., 2013). At the *Drosophila* NMJ, Gbb binds to the type II BMP receptor

Wishful thinking (Wit) at the presynaptic neuron (Aberle et al., 2002; Marques et al., 2002). Wit then recruits and phosphorylates the type I BMP receptors Thickveins (Tkv) and Saxophone (Sax), forming a tetrameric receptor complex (Rawson et al., 2003). Activated type I BMP receptors phosphorylate the receptor-regulated Smad (R-Smad) Mother against decapentaplegic (Mad), the intracellular signaling effector of the canonical BMP signaling cascade. Phosphorylated Mad (P-Mad) associates with common-partner Smad (co-Smad) Medea (Med), and the P-Mad/Medea complex translocates into the nucleus to promote or suppress the transcription of its target genes, which are responsible for synaptic growth (Keshishian and Kim, 2004). Elevated BMP signaling causes synaptic overgrowth and formation of excessive satellite boutons (Nahm et al., 2013; O'Connor-Giles et al., 2008; Sweeney and Davis, 2002). In contrast, loss-of-function mutations in components of the canonical BMP signaling pathway, including *gbb*, *wit*, *tkv*, *mad*, *med*, result in small synapses and disrupted synaptic function (Aberle et al., 2002; Marques et al., 2002; McCabe et al., 2003; Rawson et al., 2003). Thus, retrograde BMP signaling plays an instructive role in the regulation of synaptic development at the NMJ.

Drosophila NMJ studies have demonstrated that the level of presynaptic BMP signaling is regulated by endocytosis and the subsequent intracellular trafficking of BMP receptors. Endocytosis is known to downregulate signaling through receptor degradation, thereby modulating the number of receptors expressed on the plasma membrane. At the *Drosophila* NMJ, mutations in endocytic or endosomal trafficking proteins including Endophilin and Dap160 (Intersectin), Nervous wreck (Nwk), Spichthyin (Spict), and Spartin cause elevated BMP signaling that results in increased numbers of synaptic boutons and satellite

boutons (Dickman et al., 2006; O'Connor-Giles et al., 2008; Nahm et al., 2013; Wang et al., 2007). The internalized BMP receptor is subsequently targeted by lysosomes, causing BMP receptor degradation and inhibition of BMP signaling (Nahm et al., 2013). Thus, BMP receptor endocytosis and lysosomal degradation are critical negative mechanisms attenuating BMP signaling to control synaptic growth at the NMJ. However, the definite mechanism of BMP receptor endocytosis and its physiological significance are unclear.

2. Regulation of Actin Polymerization by the Rac-WAVE Complex and Abl kinase

Actin polymerization plays essential roles in endocytosis and endosomal sorting by changing the shape of the plasma membrane (Mooren et al., 2012). The actin-related protein 2/3 (Arp2/3) complex activates filamentous actin (F-actin) nucleation, promoting actin polymerization at endocytic sites (Mooren et al., 2012). To nucleate new actin filaments, the Arp2/3 complex needs to be activated by members of the Wiskott-Aldrich syndrome protein (WASP) and Suppressor of cAMP receptor/WASP family verprolin homologous protein (SCAR/WAVE) family. Under basal conditions, WASP and neural WASP are thought to exist in an auto-inhibited conformation. This auto-inhibition can be relieved by the physical interaction of WASP proteins with Cdc42. Similarly, WAVE proteins are trans-inhibited in a multimeric complex comprising the Abelson-interactor (Abi), Kette (a Nck-associated protein (NAP1)/Hem-2 homolog), Sra-1 (CYFIP, p53-inducible mRNA 121(PIR121)), and hematopoietic stem progenitor cell 300 (HSPC300). The binding of Rac to the Sra-1 component of the WAVE complex is proposed to

make WAVE proteins to activate the Arp2/3 complex (Goley and Welch, 2006; Pollitt and Insall, 2009; Takenawa and Suetsugu, 2007).

Abi was first identified as an Abelson tyrosine kinase interactor protein that contains multi-modular protein binding domains, including an N-terminal WAVE-binding (WAB) domain, a homeodomain homologous region (HHR), a proline-rich region (PRR), a C-terminal Src homology 3 (SH3) domain, and several tyrosine motifs for further phosphorylation. Through these domains, Abi physically interacts with SCAR/WAVE, Kette, and Abl. Previous studies in mammalian and *Drosophila* cells have suggested that Abi mediates WAVE complex assembly through direct interactions with Kette and WAVE and activates WAVE-dependent actin polymerization (Bogdan et al., 2005; Innocenti et al., 2004). Interestingly, Abi also binds to WASP and stimulates WASP-dependent actin polymerization (Bogdan et al., 2005; Innocenti et al., 2005), suggesting that Abi can coordinate the activities of WAVE and WASP in certain actin-based cellular processes. Previous studies have shown that mutations in components of the WAVE complex, including SCAR/WAVE, Kette, CYFIP, and HSPC300, result in synaptic growth defects (Bogdan et al., 2004; Schenck et al., 2004; Qurashi et al., 2007; Zhao et al, 2013). However, it is not clearly understood how the Abi-SCAR/WAVE complex and Rac1 regulate synaptic growth at the NMJ. Another interactor of Abi, Abl tyrosine kinase, regulates neural growth and morphogenesis by controlling actin dynamics. Previous studies have shown that, in *Drosophila*, Abl regulates the stability and subcellular localization of Abi, and that Abi is a positive regulator of Abl kinase in cultured cells (Huang et al., 2007; Juang and Hoffmann, 1999). However, these findings remain to be verified within an *in vivo* context. Moreover, the connection between Abi, Abl, and SCAR/WAVE raises the idea that these

proteins may act together to regulate actin polymerization and synaptic development.

3. Regulation and Formation of Macropinocytosis

Macropinocytosis is one of the clathrin-independent (CI) endocytic pathways and is accompanied by actin-based cell membrane ruffling to engulf extra particles and downregulate receptors expressed in the membrane. Actin-mediated membrane ruffles fold back and fuse with the plasma membrane, producing large endocytic vesicles called macropinosomes. The size of these macropinosomes is heterogeneous (0.2-5 μm in diameter), and they are larger than clathrin-coated vesicles or other pinocytic vesicles (Hewlett at al., 1994; Lim and Gleeson, 2011; Swanson and Watts, 1995). Macropinocytosis is usually induced by growth factor stimuli, such as epidermal growth factor (EGF) (Bryant et al, 2007), platelet-derived growth factor (PDGF) (Schmees et al., 2012), and macrophage colony-stimulating factor-1 (CSF-1) (Lou et al., 2014). Macropinocytosis that is important for engulfing extracellular antigens occurs constitutively in macrophages and dendritic cells; conversely, macropinocytosis in fibroblasts or epithelial cells is induced after growth factor stimulus (Lim and Gleeson, 2011). Neurotrophins such as NGF and BDNF are involved in the macropinocytic-engulfing of tyrosine receptor kinase (Trk) receptors in peripheral and hippocampal neurons (Valdez et al., 2007). However, the physiological role of macropinocytosis in neurons is largely unknown.

Macropinocytosis is initiated by the formation of membrane ruffles (sheet-like membrane extensions enriched in actin that lie beneath the membrane),

and these ruffles undergo cup closure to form macropinosomes by membrane fusion and fission (Swanson, 2008). At these early stages, the small GTPase Rac1 and phosphoinositides play an important role in the regulation of actin polymerization and membrane ruffle remodeling (Egami et al., 2014). Activated Rac1 stimulates SCAR/WAVE, which binds to phosphatidylinositol 4,5-bisphosphate [PI(4,5)P2] and the Arp2/3 complex, initiating actin polymerization underneath the plasma membrane to form ruffles (Fujii et al., 2013; Kerr and Teasdale, 2009). Then, the expression of PI(4,5)P2 increases in the plasma membrane at the circular ruffles; when the PI(4,5)P2 levels subsequently decrease, the level of PI(3,4,5)P3 increases in the membrane, and the circular ruffles undergo cup closure to form macropinosomes. At these stages, phospholipase $C\delta_1$ ($PLC\delta_1$) and Akt bind to the PI(4,5)P2- and PI(3,4,5)P3-enriched membrane (Araki et al., 2007; Yoshida et al., 2015). During cup closure, C-terminal-binding protein-1/brefeldinA-ADP ribosylated substrate (CtBP1/BARS) is involved in the dynamin-independent membrane fission that leads to the formation of macropinosomes (Liberali et al., 2008). Then, the macropinosomes mature and fuse into early endosomes by Rabankyrin-5 and Rab5 signaling (Schnatwinkel et al., 2004; Lanzetti et al., 2004) and are finally trafficked to lysosomes accompanied by Rab7 (Racoosin and Swanson, 1993).

The Rac1/WAVE/Arp2/3 complex pathway is a well-known regulatory pathway required for actin cytoskeleton remodeling. Recent studies have revealed that mutation of Abi1, SCAR/WAVE, and Kette resulted in significant defects in dorsal ruffle formation and macropinocytosis, which implicates the involvement of SCAR/WAVE and Abi1 in macropinocytosis (Dubielecka et al., 2010; Innocenti et

al, 2005; Rottner et al, 2010). However**,** the role of Rac1-WAVE-Abi signaling-dependent macropinocytosis in neurons is largely unknown.

4. The *Drosophila* Neuromuscular Junction (NMJ)

The *Drosophila* neuromuscular junction (NMJ) is an ideal model system for studying the synapse and the underlying molecular mechanisms regulating synaptic growth. The *Drosophila* NMJ consists of 32 identified motor neurons that innervate 30 identified postsynaptic muscle cells in a stereotyped pattern. To study synaptic development and function at the NMJ, *Drosophila* genetics can be used. For example, manipulation of a target gene in a temporal and tissue-specific manner is easily achievable; moreover, identifying single neurons and their synaptic contacts is possible in this system. The *Drosophila* NMJ is also accessible to various experimental techniques that can be used to study the function and development of synapses. Identification of synaptic structures is possible with immunohistochemistry, electron microscopy (EM), and live-imaging techniques, and functional studies of the synapse are possible with electrophysiological approaches. The *Drosophila* NMJ is a glutamatergic synapse that is highly conserved and resembles the features of central excitatory synapses in the vertebrate brain. Lastly, the *Drosophila* NMJ shows structural and functional plasticity. During the first to third instar larval stages, the size of postsynaptic muscle increases 100-fold, and presynaptic nerve terminals show a 10-fold increase in the number of boutons present to maintain the efficacy of the synapses (Schuster et al., 1996a).

5. Rationale and Outline of the Thesis Experiments

Abi, a substrate of Abl kinase, also plays an essential role in SCAR/WAVE complex-mediated actin regulation; however, its role in the nervous system is still poorly defined. Here, I showed that *Drosophila* Abi is an important regulator of synaptic development. Abi is highly enriched at neuromuscular junction (NMJ) synapses. Loss of Abi causes synaptic overgrowth at the NMJ and increases bone morphogenetic protein (BMP) signaling in motor neurons. Transgenic rescue experiments suggest that the SCAR-, and Kette-binding activities of Abi, as well as its phosphorylation by Abl, are required presynaptically for normal synaptic growth. A synaptic overgrowth phenotype is also induced by presynaptic depletion of Abl or Rac1 and components of the SCAR/WAVE complex. Importantly, genetic interaction experiments suggest that Abi, Abl, and Rac1-SCAR/WAVE signals restrain synaptic growth by negatively regulating BMP signaling.

A negative regulatory mechanism controlling BMP signaling is the endocytosis of BMP receptors expressed on the plasma membrane surface and their subsequent degradation (Nahm et al., 2013; O'Connor-Giles et al., 2008; Sweeny et al., 2002). Recent findings suggest that Abi and Rac1-SCAR/WAVE are key players in macropinocytosis (Dubielecka et al., 2010; Fujii et al., 2013; Innocenti et al, 2005; Kerr and Teasdale, 2009; Rottner et al, 2010), and I show that Abi interacts with endocytic proteins to inhibit synaptic growth. I found that Glass bottom boat (Gbb) induces macropinocytosis, which internalizes surface BMP receptors to downregulate BMP signaling in neurons. I also demonstrated that Abi, Abl, Rac1 and components of the WAVE complex are required for its action.

Finally, I showed that regulators of macropinocytosis, CtBP and Rabankyrin, regulate synaptic growth by inhibiting BMP signaling at the NMJ. In this thesis, the results elucidate the indirect mechanisms underlying actin polymerization-mediated synaptic growth and the endocytic mechanism resulting in the internalization of BMP receptors and subsequent downregulation of BMP signaling at the NMJ.

II. Materials and Methods

1. Fly Stocks

The wild-type *Drosophila* strain used in this study was w^{1118}. The strains with an EP insertion in the *abi* loci, abi^{G4355} and abi^{G6718}, were obtained from GenExel (Republic of Korea). The abi^{5} mutant was generated by imprecise excision of abi^{G6718}. Transgenic lines carrying *UAS-HA-abi*, *UAS-HA-*$abi^{\Delta 30\text{-}65}$, *UAS-HA-*$abi^{Q91A}$, *UAS-HA-*$abi^{\Delta 123\text{-}175}$, *UAS-HA-*$abi^{W452K}$, *UAS-HA-*$abi^{4YE}$, *UAS-HA-*$abi^{4YE}$, *UAS-*$abi^{RNAi}$, *UAS-Myc-tkv*, *UAS-Flag-wit*, *UAS-GFP-rabankyrin*, and *UAS-CtBP-GFP* were generated in the w^{1118} background with a standard procedure (Robertson et al., 1988). *Df(3R)su(Hw)7* (a deficiency covering the *abi* locus), Abl^{1}, Abl^{4}, $rac1^{J11}$, $wasp^{1}$, wit^{A12}, wit^{B11}, $dfmr1^{\Delta 50}$, *UAS-dfmr1*, *UAS-*$rac1^{N17}$, *UAS-*$rac1^{V12}$, *UAS-*$scar^{RNAi}$, *UAS-*$kette^{RNAi}$, *UAS-*$rabankryin^{RNAi}$, and *UAS-*$ctbp^{RNAi}$ flies were obtained from the Bloomington Stock Center; *UAS-Abl*, *UAS-*Abl^{KN}, $scar^{\Delta 37}$, and $kette^{J4\text{-}48}$ flies were a gift from Peter A. Kolodziej (Vanderbilt University Medical Center, Nashville, TN, USA). UAS transgenes were expressed in the following Gal4 lines: *24B-GAL4* (Fyrberg et al., 1997), C*155-GAL4* (Lin and Goodman, 1994), *da-GAL4* (Wodarz et al., 1995), *elav-GeneSwitch-GAL4* (*elavGS-GAL4*) (Osterwalder et al., 2001), and *abi-GAL4*.

Flies were cultured on standard medium at 25ºC. For pharmacological manipulation of microtubule stability, medium containing 1 μM vinblastine sulfate (Sigma) were used as previously described (Nahm et al., 2013). First instar larvae were transferred to the medium with either 1 μM vinblastine (+VB) or 0 μM vinblastine (-VB), and then larvae were grown until the wandering third instar larval stage. For Gene Switch experiments, first instar larvae were transferred to

standard medium containing 10 µg/ml RU486 (Midepristone, Sigma) as previously described (Osterwalder et al., 2001).

2. Molecular Biology

For transgenic fly constructs, various cDNAs were subcloned into pUAST or pUAST-HA vectors; for expression in BG2-c2 cells or S2R+ cells, cDNAs of target genes were subcloned into pUAST or pAc5.1 vector (Invitrogen). For tagged *abi* transgenic fly constructs, the *abi* ORF was amplified by PCR from an LD37010 clone (Drosophila Genomics Resource Center, DGRC), cloned into the pGEM-T Easy Vector (Promega), and then subcloned into the pUAST-HA vector to generate *pUAST-HA-abi*. For site-directed and deletion mutagenesis to generate *pUAST-HA-abi*^{Q91A}, *pUAST-HA-abi*^{4YE}, *pUAST-HAabi*^{4YF}, *pUAST-HA-abi*^{W452K}, *pUAST-HA-abi*$^{\Delta 30\text{-}65}$, and *pUAST-HA-abi*$^{\Delta 123\text{-}175}$, PCR mutagenesis was perform. To generate *pUAST-Myc-tkv* and *pUAST-Flag-wit*, a Myc epitope (EQKLISEEDL) and a Flag epitope (DYKDDDDK) were inserted downstream of the signal sequence via PCR-based mutagenesis, cloned into the pGEM-T Easy Vector, and subcloned into the pUAST vector. An HA epitope (YPYDVPDYA) was inserted in the N-terminus of the *abi* ORF by PCR-based mutagenesis, and cDNA encoding *abi*, *abi*$^{\Delta 30\text{-}65}$, *abi*$^{\Delta 123\text{-}175}$, *abi*^{4YE}, and *abi*^{4YF} were amplified by PCR using *pUAST-HA-abi*, *pUAST-HA-abi*$^{\Delta 30\text{-}65}$, *pUAST-HA-abi*$^{\Delta 123\text{-}175}$, *pUAST-HA-abi*^{4YE}, and *pUAST-HA-abi*^{4YF} as templates and cloned into pAc5.1 vectors to generate *pAc-HA-abi*, *pAc-HA-abi*$^{\Delta 30\text{-}65}$, *pAc-HA-abi*$^{\Delta 123\text{-}175}$, *pAc-HA-abi*^{4YE}, and *pAc-HA-abi*^{4YF}. Myc-tkv and Flag-wit were PCR amplified with *pUAST-Myc-tkv* and *pUAST-Flag-wit* as templates, respectively, and subcloned into pAc5.1 vectors to create *pAc-Myc-tkv* and *pAc-*

Flag-wit. The *rabankyrin* ORF was amplified by PCR with a *rabankyrin* cDNA clone (RE06111) and subcloned into pEGFP-C1 vectors to tag Rabakyrin with GFP at the N-terminus. PCR amplification was performed with pEGFP-C1-rabankryin as a template to obtain GFP-Rabankyrin and subcloned into pUAST and pAc5.1 vectors to generate *pUAST-GFP-rabankyrin* and *pAc-GFP-rabankyrin*. The *CtBP* ORF was PCR amplified with a *CtBP* cDNA clone (GH20987), subcloned into a pEGFP-N3 vector to tag GFP on the C-terminus of the *CtBP* ORF and subcloned into a pUAST vector to generate *pUAST-ctbp-GFP*.

To generate *abi-GAL4* transgenic flies, the Abi promoter from ORF -17 ~ -2801 was PCR amplified with BACR10E03 (BAC PAC resource), cloned into a pGEM-T Easy Vector, and subcloned into a pCasPer4 vector (DGRC). GAL4 was obtained from a pGaTB vector (DGRC) and subcloned into the pCasPer4-abi-promoter vector to create *pCasPer4-abi-promotor-GAL4*.

For the *UAS-abi*^{RNAi} construct, an inverted repeat of the *abi* coding sequence, from +1 to +240, was subcloned into a pWIZ vector (Bogdan et al., 2005).

For the GST pull-down assay, various cDNAs encoding the N-terminus of Abi (Abi-N, amino acid residues 1-387) and Abi SH3 domain region (Abi-SH3, amino acid residues 387-473) were PCR-amplified and cloned into pGEX-6P-1 vectors (GE Healthcare) to generate *pGEX-abi-N* and *pGEX-abi-SH3*. To generate *pGEX-abi-N*$^{\Delta 30\text{-}65}$, *pGEX-abi-N*$^{\Delta 123\text{-}175}$, and *pGEX-abi-SH3*^{W452K}, cDNAs were amplified by PCR using *pUAST-HA-abi*$^{\Delta 30\text{-}65}$, *pUAST-HA-abi*$^{\Delta 123\text{-}175}$, and *pUAST-HA-abi*^{W452K} as templates and cloned into pGEX-6P-1 vectors. To generate *pAc-kette-Myc*, the *kette* ORF with a C-terminal Myc-tag was amplified by PCR from

the LD43495 clone (Drosophila Genomics Resource Center, DGRC) and subcloned into the pAc5.1 vector.

For expression in S2R+ cells or BG2-c2 cells, various cDNAs were subcloned into the pAc5.1 vector. The cDNA sequences of the PH domains of PLCδ_1 (amino acids 1-170) and Akt protein kinase (amino acids 1-167) were amplified by RT-PCR from total RNA extracted from K562 leukemia cells and then cloned into pAc-EGFP vectors, a derivative of the pAc5.1 vector, to create *pAc-PLCδ_1-PH-GFP* and *pAc-Akt-PH-GFP*.

The effect of the *abi*^{5} mutation on the expression of *abi*, *twf*, and *rp49* was analyzed by RT-PCR. Total RNA was isolated from larval extracts using TRIzol reagent (Invitrogen). Reverse transcription was performed with 1 μg RNA, an oligo-dT primer, and SuperScript II Reverse Transcriptase (Invitrogen). The resulting cDNA was analyzed by PCR using the following primers: *abi*, 5'-ATGTTGACCGAAACCCCCATG-3' and 5'-CACGCCAATCTCTCTCCTG-3'; *twf*, 5'-GTCTCACCAAACGGGTATC-3' and 5'-CGAAATCCTGCTTGTGCCG-3'; *rp49*, 5'-CACCAGTCGGATCGATATGC-3' and 5'-CACGTTGTGCACCAGGAACT-3'. RT-PCR analysis was also performed to confirm the knock-down efficiency of *Abl*, *rac1*, *scar*, *kette*, *rabankyrin*, *endophilin A (endoA)*, *dap160*, and *nervous wreck (nwk)* in BG2-c2 cells using the following primers: *Abl*, 5'-CGTCAAAGTGAAAGTTCAC-3' and 5'-GCTGTATTTGAGCCACTAC-3'; *rac1*, 5'-GATCAAGTGCGTCGTCGTGG-3' and 5'-CTTGACCGCTCCGATTTCCT-3'; *scar*, 5'-CAACGTGCACTGGTGCACGGC-3' and 5'-CGGTCCGTAGATGGGCTCCGG-3'; *kette*, 5'- GAACTGCTC ACCACGATGGA-3' and 5'-TACTTCTCCGATCCGCTTGC-3'; *rabankyrin*, 5'-

CTACTCTTATCCGAGGCGGC-3’ and 5’-GCAGCGGAGATGCCTTATCT-3’; *endoA*, 5’-GCAGATCAACAAGGCCAACCAGTA-3’ and 5’-GCAGTGGCTCCAAAAAGTTCTGCT-3’; *dap160*, 5’-CAGGAGCAACTGAATGCCGCATTC-3’ and 5’-GAAGGCGATTTGAGCTTCAGTGCC-3’; and *nwk*, 5’-CGTAAGGGAAACTATGTGAAATTC-3’ and 5’-CGCCAAGCTGAGTACGTAGTCATT-3’.

To perform quantitative RT-PCR (qRT-PCR), RNA was extracted from the brains of 10 larvae using TRIzol (Invitrogen). Reverse transcription was performed with 1 μg of total RNA, an oligo-dT primer, and SuperScript II Reverse Transcriptase (Invitrogen) to synthesize cDNA. cDNA, primers for *dfmr1* and *rp49*, and Power SYBR Green PCR Master Mix (Life Technologies) were mixed in accordance with the manufacturer’s instructions. qRT-PCR was performed using the Applied Biosystems 7500 Real-time PCR System (Thermo Fisher Scientific), and quantification of relative RNA expression was performed via the ΔΔCt method according to the manufacturer’s instructions (Applied Biosystems manual).

3. Antibodies

To produce a polyclonal anti-Abi antibody, an *abi* C-terminal fragment (amino acids 253-473) was PCR amplified and cloned into a pGEM-T Easy Vector (Promega) and then subcloned into a pGEX-6P-1 vector (GE Healthcare). The GST-tagged Abi fusion protein was expressed in *E. coli* BL21 (Stratagene) and purified with Glutathione Sepharose 4B (GE Healthcare, 17075601) following the manufacturer’s instructions. Protein samples were subjected to SDS-PAGE, the

band representing the GST-tagged Abi fusion protein was excised, and the proteins were extracted using gel electrophoresis. After dialysis, the proteins were injected into rats for immunization (AbFrontier, Republic of Korea). The anti-Abi antibody was used at a dilution of 1:100 for immunostaining and of 1:500 for western blotting.

For immunostaining of the larval NMJ and ventral nerve cord (VNC) and BG2-c2 cells, the following primary antibodies were used: FITC-conjugated and Cy5-conjugated anti-HRP at 1:200 (Jackson ImmunoResearch Laboratories), rabbit anti-P-Mad (PS1) at 1:100 (Persson et al., 1998) for motor axon terminals, rabbit anti-P-Smad3 (EP823Y) at 1:200 (Epitomics, 1880-1) for motor neuron nuclei, rabbit anti-GluRIIC at 1:2500 (gift from Aaron DiAntonio, Marrus SB et al., 2004), mouse anti-HA at 1:200 (BioLegend, 901501), rabbit anti-HA at 1:100 (Cell Signaling Technology, 3724S), rabbit anti-Myc at 1:100 (Cell Signaling Technology, 2278S), and mouse anti-Myc at 1:100 (BD Biosciences, 51-1485GR). The following antibodies purchased from the Iowa Developmental Studies Hybridoma Bank were also used: rat anti-Elav (9F8A9) at 1:10, mouse anti-Futsch (22C10) at 1:50, mouse anti-Dlg (4FC) at 1:500, mouse anti-FasII (ID4) at 1:10, and mouse anti-Bruchpilot (nc82) at 1:10. FITC-, Cy3-, and Cy5-conjugated secondary antibodies (Jackson ImmunoResearch Laboratories, 715-165-151, 711-165-152, 715-095-153, 715-175-150, and 711-175-152) were used at 1:200.

For western blotting and binding experiments, the following primary antibodies were used: rabbit anti-HA at 1:1000 (Cell Signaling Technology, 3724S), rabbit anti-Myc at 1:1000 (Cell Signaling Technology, 2278S), and rabbit anti-β-actin (1:1000, Sigma). The following antibodies purchased from the Iowa Developmental Studies Hybridoma Bank were also used: mouse anti-SCAR

(P1C1) at 1:500, mouse anti-WASP (P3B1 or P5E1) at 1:500, and anti-Gbb (3D6-24) at 1: 500.

4. Western Blotting and GST Pull-Down Assay

For western blot analysis, third instar larvae were homogenized in SDS sample buffer (62.5 mM Tris-HCl, pH 6.8, 10% glycerol, 2% SDS, 2.88 mM β-mercaptoethanol, 0.02% bromophenol blue), boiled for 10 min, and centrifuged at 13,000 x g for 5 min. Proteins were separated by 10% SDS-PAGE and transferred to nitrocellulose membranes (Whatman). Blots were blocked in 5% BSA in TBST (TBS, 0.1% Tween-20) and incubated with primary antibodies overnight at 4°C. After several washes in TBST, blots were incubated with HRP-conjugated secondary antibodies for 1 hr 30 min at room temperature. Blots were washed several times with TBST, and the immunoreactive bands were visualized with SuperSignal West Pico Chemiluminescent Substrate (Thermo Scientific).

GST fusion proteins of dAbi-N (N-terminus), dAbi-SH3, Abi-N-Δ30-65, Abi-N-Δ123-175, Abi-SH3-W452K, and GST alone were produced in *E.coli* BL21 and purified using glutathione-Sepharose 4B (GE Healthcare). S2R+ cells expressing *pAc-kette-Myc* or S2R+ cells with no exogenous vector expression were homogenized in lysis buffer (25 mM Tris-HCl, pH 7.5, 150 mM NaCl, 0.5% Triton X-100, and protease inhibitors) and then centrifuged at 12,000 rpm for 15 min at 4℃. Cell lysates were incubated with 10 μg of purified GST or GST fusion proteins immobilized on glutathione-Sepharose 4B beads for 4 hr at 4℃. Beads were washed several times with lysis buffer and boiled in SDS sample buffer. The eluates were subjected to western blot analysis using rabbit anti-Myc at 1:1000

(Cell Signaling Technology, 2278S), anti-SCAR at 1:100 (DSHB), or anti-WASP at 1:100 (DSHB).

5. Immunostaining

Wandering third instar larvae were dissected in Ca^{2+}-free HL3 saline (70 mM NaCl, 5 mM KCl, 20 mM $MgCl_2$, 10 mM $NaHCO_3$, 5 mM trehalose, 115 mM sucrose, 5 mM HEPES, pH 7.2) (Stewart et al., 1994) and fixed in 4% formaldehyde in PBS for 30 min. Fixed larvae were washed with PBST-0.1 (PBS containing 0.1% Triton X-100), blocked with blocking buffer (0.2% BSA in PBST-0.1) for 1 hr at room temperature, and incubated with primary antibodies in blocking buffer at 4°C overnight. After several washes with PBST-0.1, samples were incubated with secondary antibodies in blocking buffer for 1 hr 30 min at room temperature. Stained larvae were mounted with SlowFade reagent (Invitrogen).

Brains from wandering third instar larvae were dissected in cold PBS and fixed in 4% formaldehyde for 20 min at room temperature. Fixed brains were washed with PBST-0.3 (PBS containing 0.3% Triton X-100), blocked with blocking buffer (0.2% BSA in PBST-0.3) for 1 hr at room temperature, and incubated with primary antibodies in blocking buffer for 48 hr at 4°C. After washing several times with PBST-0.3, brains were incubated with secondary antibodies in blocking buffer for 48 hr at 4°C. Stained brains were mounted with SlowFade reagent.

Fluorescent images of NMJs labeled with anti-HRP were captured with an FV300 laser-scanning confocal microscope (Olympus) using FLOUVIEW software and a

Plan Apo 40× 0.90 NA or U Plan Apo 100× 1.3 NA objective. Other fluorescent images were acquired with an LSM 700 laser-scanning confocal microscope (Carl Zeiss) using ZEN imaging software and a C-Apo 40× 1.20 W or Plan-NeoFluar 63× 1.25 oil objective and an N-SIM super-resolution microscope system (Nickon) using NIS-elements software and a CFI Apo TIRF 100× oil / NA 1.49 objective. To compare different genotypes, samples were processed simultaneously in the same tube and imaged at identical confocal settings. All quantifications were performed at NMJ 6/7 in the A2 segment. For the analysis of NMJ morphology, Z-stack image series with 1-μm intervals were projected and then analyzed. Quantification of bouton number and satellite bouton number was performed as previously described (Nahm et al., 2010a). For quantification of intensity of pMad and Futsch expression, the area midline of NMJ 6/7 was imaged, and the mean intensity was measured by ZEN imaging software.

6. Cell Transfection and RNA Interference

BG2-c2 cells were maintained at 25ºC in Shields and Sang M3 Insect Medium (Sigma) supplemented with 10% heat-inactivated (30 minutes, 55ºC) fetal bovine serum (FBS) (Gibco), antibiotics, and 10 μg/ml insulin (Sigma). *Drosophila* S2R+ cells were maintained at 25ºC in Schneider's *Drosophila* medium (Gibco) supplemented with 10% FBS and antibiotics. BG2-c2 and S2R+ cells were transfected using Cellfectin (Invitrogen), according to the manufacturer's instructions. Typically, 10^6 cells were transfected in serum-free medium with 2 μg of plasmid DNA and 5 μg of double-stranded RNA (dsRNA). Expression of all UAS plasmids was driven by cotransfection with RK241, an *actin 5C-GAL4*

plasmid.

For RNAi experiments in BG2-c2 cells, *abi*, *Abl*, *rac1*, *scar*, *kette*, *rabankyrin*, *endoA*, *dap160*, and *nwk* dsRNAs were generated by *in vitro* transcription of their cognate DNA templates containing T7 promoters at both ends, as previously described (Lee et al., 2007). DNA templates were PCR-amplified using primers containing the T7 promoter sequence upstream of the following: *abi*, 5'-GCCTCGCATCGATATTCTA-3' and 5'-ACCATATAGAGCGTATGTG-3'; *Abl*, 5'-GGATCCGGATCGGGGCTGAGC-3' and 5'-CTCTGAGATGCGGTAGTGATA-3'; *rac1*, 5'-CAGGCGATCAAGTGCGTCG-3' and 5'-GAGCAGGGCGCACTTGCGC-3'; *scar*, 5'-GTGTATCAGCAGGATGAGC -3' and 5'-CGCCGTGCACCAGTGCACG-3'; *kette*, 5'-ACCTGGTACAGTGAGGTTC-3' and 5'-CATCAGTAGACAGGCAGTG-3'; *rabankyrin*, 5'-GCCAAATCTAGTTAAGAAG-3' and 5'-GCAGCGGAGATGCCTTATC -3'; *endoA*, 5'-CGGACTCAAAAAGCAGATC-3' and 5'-GTTCTCGAGCAAATTGAAC-3'; *dap160*, 5'-ATTGAGTCAAAGAAGGAGG-3' and 5'-ACTTGCGGCTATATAATAC-3'; and *nwk*, 5'-CAGGTGGCCAAGCTGCAGC-3' and 5'-CTCCTCCAGCAGCTCCTTG-3'. The knock-down of *graf* and *chc* was performed as previously described (Kim et al., 2017).

7. Production of Gbb-Conditioned Medium

For production of HA-Gbb- and Gbb-conditioned medium, S2R+ cells were transfected with either *pAc-HA-gbb* or *pAc-gbb* in serum-free Schneider's

medium for 6 hr. Transfected cells were incubated for 48 hr at 25ºC in Schneider's medium supplemented with 10% heat-inactivated FBS and antibiotics, and then cells were maintained in fresh serum-free Schneider's medium for 120 hr to collect HA-Gbb- or Gbb-conditioned medium. Levels of secreted HA-Gbb or Gbb in the conditioned medium were measured by western blot analysis using a multiple-epitope tag (GenScript) or conditioned medium containing 50 ng/ml HA-Gbb. For Gbb treatment of BG2-c2 cells and larvae, the conditioned medium was diluted with serum-free Schneider's medium to a concentration of 50 ng/ml Gbb.

8. Macropinocytosis Assay

BG2-c2 cells were serum-starved for 6 hr in serum-free Shields and Sang M3 Insect Medium (Sigma) and then stimulated with or without conditioned medium containing 50 ng/ml Gbb for 10 min at 25ºC. Then, pulse-chase experiments were performed with 70 kDa TMR-dextran with (+Gbb) or without (-Gbb) 50 ng/ml Gbb at 25ºC; the pulse-chase times used are described in each figure. After the macropinocytosis assay, cells were washed with ice-cold PBS and fixed with 4% formaldehyde. Then, cells were washed, permeabilized, and washed three times with PBS containing 0.1% Saponin within 10 min; blocked with blocking buffer (PBS containing 0.2% BSA) for 15 min; and incubated with primary antibodies in blocking buffer for 1 hr 30 min at 25 ºC. After several washes with PBS, the cells were stained with fluorescent-conjugated secondary antibodies in blocking buffer for 1 hr at 25ºC. Stained cells were mounted using SlowFade reagent (Invitrogen). For each cell, a Z-stack of images was taken with an LSM 800 laser-scanning confocal microscope (Carl Zeiss) using a Plan Apo 63x

1.4 NA oil objective. To quantify the amount of internalized TMR-Dex, the total fluorescence per cell was determined by integrating the intracellular fluorescence on all planes of the Z stack after correcting for background fluorescence.

To perform the macropinocytosis assay at the larval NMJ, wandering third instar larvae were dissected in Ca^{2+}-free HL3.1 solution. Then, the HL3.1 solution was removed, and the larvae were treated first with 50 ng/ml Gbb-conditioned medium for 10 min and then with 70 kDa TMR-dextran with or without Gbb for 5 min. Lastly, larvae were washed with ice-cold PBS and fixed with 4% formaldehyde for 30 min. To visualize the NMJ, larvae were stained with FITC-HRP in PBS. For quantification of the amount of TMR-dextran uptake, NMJ 6/7 at the A2 segment were Z stacked**,** and the intensity of TMR-dextran and HRP (internal control) fluorescence was measured using the Zen system.

9. Tkv Receptor Degradation Assay

To monitor degradation of the BMP receptor Tkv, BG2-C2 cells were transfected with *pAc-Myc-tkv* in the presence or absence of *abi* or *rabankyrin dsRNA* and incubated in serum-containing medium for 72 hr. After 6 hr of serum starvation, cells were treated with 50 ng/ml cycloheximide for 3 hr to inhibit new protein synthesis. Cells were then stimulated with conditioned medium containing 50 ng/ml Gbb for the indicated time and homogenized in lysis buffer (25 mM Tris-HCl, pH 7.4, 150 mM NaCl, 1% Triton X-100, and protease inhibitors). Total cell lysates were mixed with SDS sample buffer, boiled for 5 min, and subjected to 10% SDS-PAGE and western blotting with anti-Myc and anti-β-actin antibodies.

10. Time-Lapse Imaging

ML-DmBG2-c2 cells transfected with GFP-Abi were incubated for 48 hr at 25ºC in Shields and Sang M3 Insect Medium (Sigma) supplemented with 10% heat-inactivated FBS, antibiotics, and 10 μg/ml insulin (Sigma). Transfected cells were transferred to a glass-bottom Confocal Dish (SPL), incubated with serum-free Shields and Sang M3 Insect Medium for 6 hr, and then placed in conditioned medium containing 50 ng/ml Gbb and 20 μg/ml carboxylate-modified FluoSpheres polystyrene microspheres (0.02 μm, Molecular Probes) during live imaging. Time-lapse images were collected at 1.86-second intervals for 10 min with an LSM 800 laser-scanning confocal microscope (Carl Zeiss) using a Plan Apo 63x 1.4 NA oil objective.

11. Survival Rate Analysis

Male and female flies of given genotypes were mated at 25°C in standard fly food for three days, and then parental flies were emptied from the bottles. After eclosion, the numbers of eclosed flies and pupal cases containing dead flies were counted for five days.

III. RESULTS

1. Generation of the *abi* Null Mutant

In an anatomical genetic screen for mutations affecting the synaptic structure at the *Drosophila* NMJ (Nahm et al., 2010a; Nahm et al., 2010b), two EP insertions (G4355 and G6718) localized in the first and second exons of the *abi* gene were identified (Figure 1A). Mutants that were homozygous for each insertion displayed larger synapses than those of the wild-type controls (w^{1118}) at the NMJ of third instar larvae. In order to establish an unambiguous null allele of *abi*, an imprecise excision of the G6178 insertion (abi^{5}) was generated. The abi^{5} allele had a 1,075-bp deletion, which removed large portions of the second and third exons of *abi* (Figure 1A). Expression of the *abi* transcript was abolished in homozygous abi^{5} larvae and in abi^{5} heterozygous larvae with the deficiency *Df(3R)su(Hw)7* (referred to as *Df*), while the neighboring *twinfilin* (*twf*) gene was normally expressed in these mutants (Figure 1B).

abi^{5}/Df mutants showed pupal lethality, as previously demonstrated for other *abi*-null mutants (Lin et al., 2009; Stephan et al., 2011). To determine whether the pupal lethality was solely due to loss of *abi* function, I used the UAS/GAL4 system. Expression of *UAS-HA-abi* under the control of an *abi* promoter-GAL4 fusion (*abi-GAL4*) or ubiquitous *daughterless* (*da*)-*GAL4* driver completely rescued the lethality of abi^{5}/Df mutants (Figure 1C). Importantly, expression of the same *UAS-HA-abi* transgene using a combination of a pan-neuronal *C155-GAL4* driver and a muscular *24B-GAL4* driver substantially rescued the *abi* lethality, while relatively weak rescue activity was observed with the use of each GAL4 driver alone (Figure 1C). Thus, the pupal lethality associated with the *abi* mutation

Figure 1. Molecular Characterization of the *Drosophila abi* Gene and Its Null Mutants

(A) The genomic structure of the *abi* gene and deletion region of the *abi* null mutant. The structure of the exons/introns of *abi* and its neighboring genes, *twf* and *140up*, are shown. White boxes indicate untranslated regions (UTRs), black boxes are coding regions, and the transcription initiation site is marked by bent arrows. G6718 (abi^{G6718}) and G4355 (abi^{G4355}) are two P element mutants marked with inverted triangles. abi^{G6718} is inserted in the coding region of *abi* (downstream of the initiator ATG), and abi^{G6718} is inserted in the 5' UTR region. On the bottom, the deletion region of the abi^{5} mutant generated by imprecise excision of abi^{G6718} is marked by the broken line. The gray bar represents the promoter region used for the generation of the *abi-GAL4*.

(B) RT-PCR analysis of wild-type (WT), abi^{5}, $abi^{5}/Df(3R)Su(hw)$ (abi^{5}/Df) third instar larvae. *abi* mRNA expression was ablated in abi^{5} and abi^{5}/Df larvae, while expression levels of *twf* and *rp49* mRNA were not affected in either wild-type or *abi* mutant larvae.

(C) Quantification of survival rate after eclosion. The abi^{5}/Df was lethal in the pupal stage, and lethality was fully rescue by *abi* expressed by *abi-GAL4* and *da-GAL4*. The survival rate of abi^{5}/Df larvae was partially rescued by *abi* expression induced by *C155-GAL4* (28.05%), *24B-GAL4* (15.56%), and both *C155-GAL4* and *24B-GAL4* (47.40%). N(experiments)=3, n<120 (number of pupa). A one-way ANOVA was used for data analysis.

All comparisons are with controls unless indicated (*$p<0.001$). Error bars are SEM for all figures.

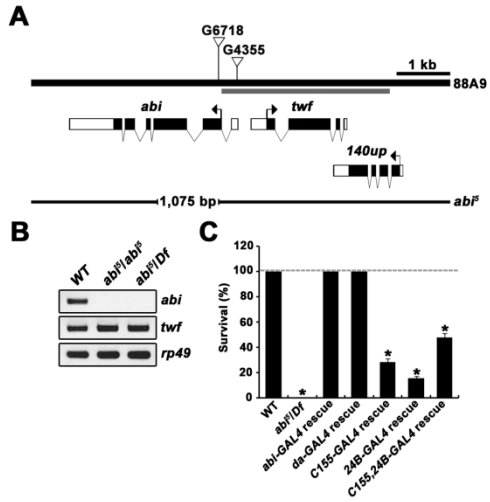
A
G6718
G4355
1 kb
88A9
abi
twf
140up
1,075 bp
abi5
B
WT
abi5/abi5
abi5/Df
abi
twf
rp49
C
Survival (%)
120
100
80
60
40
20
0
WT
abi5/Df
abi-GAL4 rescue
da-GAL4 rescue
C155-GAL4 rescue
24B-GAL4 rescue
C155,24B-GAL4 rescue

is, at least in part, attributable to essential functions of Abi in both neurons and muscles.

2. Abi Localizes to the Periactive Zone of the NMJ

Abi has been reported to localize to various axonal tracts of the embryonic and larval central nervous system (CNS) (Lin et al., 2009); however, its expression at synapses is still unknown. To investigate Abi expression at the NMJ, an antibody against amino acids 253 to 473 was generated. On immunoblots of lysates prepared from wild-type third instar larva, this antibody detected a single 50 kDa Abi band (Figure 2A). The Abi band was absent in lysates from abi^{5}/abi^{5} and abi^{5}/Df mutants, demonstrating the specificity of the antibody (Figure 2A).

Staining of wild-type third instar larval fillets with anti-Abi revealed that Abi is enriched in all types of synaptic boutons (types I, II, and III) of NMJs. Interestingly, anti-Abi signals were not uniformly distributed throughout NMJ synapses, but rather detected in a punctate pattern (Figure 2B). Anti-Abi doubly stained with the neuronal membrane marker anti-HRP showed that Abi is mostly associated with the presynaptic membrane within the bouton (Figure 2B). In contrast, abi^{5}/Df NMJs were not stained with anti-Abi, revealing the specificity of the Abi staining (Figure 2C). Postsynaptically, Abi immunoreactivity was detected in the subsynaptic reticulum (SSR), as defined by positivity for the scaffold protein Discs-large (Dlg; Figure 2D). However, it was hardly detected in the cytoplasm of postsynaptic muscles.

To further identify the precise localization of the Abi puncta, larval NMJs were double stained with antibody against Abi and Fasciclin II (FasII), a cell

Figure 2. Abi Expression at the Larval NMJ

(A) Western blot analysis of total protein extracts of wild-type, *abi*^{5}, and *abi*^{5}*/Df* third instar larvae probed with anti-Abi and anti-β−actin. The Abi protein was detected in wild-type larvae, and its expression was abolished in *abi*^{5} and *abi*^{5}*/Df* larvae.

(B-D) Single confocal slices of the NMJ 6/7 branches with type I boutons of third instar larva. (B) Wild-type and (C) *abi*^{5}*/Df* larvae stained with presynaptic membrane marker anti-HRP (green) and anti-Abi (red) antibodies. (D) Wild-type larvae doubly stained with postsynaptic SSR marker anti-Dlg (green) and anti-Abi (red) antibodies.

(E) Abi is expressed in the periactive zone of the synapse. Z series stacks confocal slices of wild-type larvae doubly stained with periactive zone marker anti-FasII (green) and anti-Abi (red) antibodies.

(F and G) Single slice SIM (structured illumination microscope) images of the NMJ 6/7 branches with type I boutons of third instar larvae. (F) *C155-GAL4*/+; *UAS-HA-abi*/+ larvae doubly stained with active zone marker anti-NC82 (green) and anti-HA (red) antibodies. (G) *UAS-HA-abi*/+; *24B-GAL4*/+ larvae doubly stained with anti-GluRIIC (green) and anti-HA (red) antibodies.

Scale bar represents 5 μm.

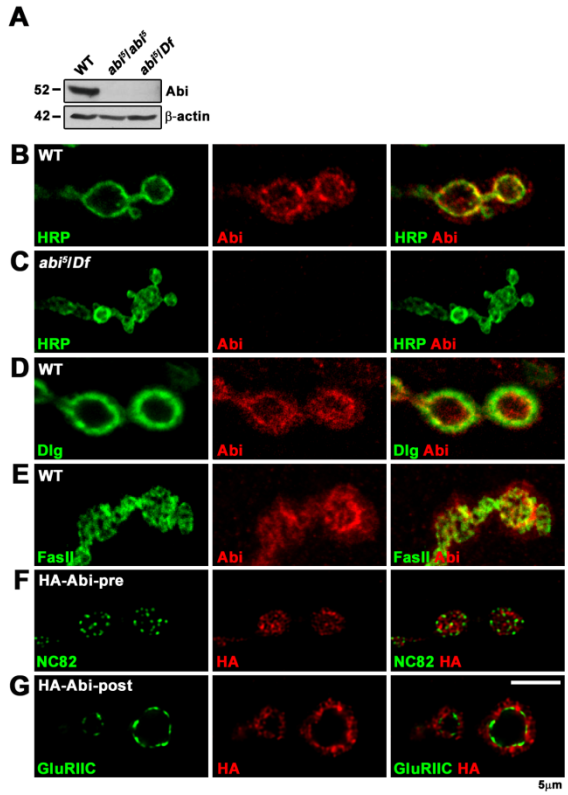
A
WT
abi5/abi5
abi5/Df
52
42
Abi
β-actin
B
WT
HRP
Abi
HRP Abi
C
abi5/Df
HRP
Abi
HRP Abi
D
WT
Dlg
Abi
Dlg Abi
E
WT
FasII
Abi
FasII Abi
F
HA-Abi-pre
NC82
HA
NC82 HA
G
HA-Abi-post
GluRIIC
HA
GluRIIC HA
5μm

adhesion molecule that defines the periactive zone (Figure 2E). A partial colocalization between Abi and FasII was seen (Figure 2E). I then expressed HA-Abi in motor neurons or muscles using the UAS/GAL4 system and compared the distribution of HA-Abi and active zone markers, such as the presynaptic protein Bruchpilot (Brp, refer to NC82; Figure 2F) and the postsynaptic glutamate receptor GluRIIC (Figure 2G). When expressed in neurons under the control of *C155-GAL4*, HA-Abi puncta showed a complementary distribution pattern to that of Brp (Figure 2F). Similarly, when expressed in muscles under the control of *24B-GAL4*, HA-Abi signals were present in non-overlapping areas around clusters of GluRIIC (Figure 2G). Together, these results suggest that Abi largely localizes to periactive zones within the pre- and postsynaptic membranes.

3. Abi Is Required Presynaptically for Normal NMJ Growth

Morphological analysis of abi^{5}/Df third instar larvae revealed a distinctive phenotype of NMJ overgrowth with excessive formation of satellite boutons, which are small boutons protruding from the main axis of the motor axon terminal (Dickman et al., 2006). This *abi* phenotype was observed at NMJ 6/7 (Figure 3A). To quantify the *abi* phenotype, the numbers of boutons and satellite boutons at NMJ 6/7 in abdominal segment 2 (A2) were measured. Compared with wild-type controls (w^{1118}), the number of boutons was increased by ~40% in abi^{5}/Df larvae. With normalization to muscle surface area, the number of boutons remained ~42% higher in abi^{5}/Df mutants than in control larvae (Figure 3B). abi^{5}/Df mutants also had an 87% increase in the number of satellite boutons (Figure 3B).

Figure 3. Abi Acts Presynaptically to Control Synaptic Growth

(A and B) Mutations in *abi* cause synaptic overgrowth at larval NMJs. (A) Confocal images of NMJ 6/7 (left panels) and NMJ 4 (right panels) labeled with anti-HRP taken from wild-type and $abi^{5}/Df(3R)Su(hw)$ (abi^{5}/Df) larvae. Magnified boutons of NMJ 6/7 are marked by white asterisks. Satellite boutons are marked with white arrowheads. Scale bar represents 20 μm. (B) Quantification of the number of total boutons normalized to the muscle surface area and satellite boutons of NMJ 6/7 in the following genotypes: wild-type, abi^{5}/Df, *C155-GAL4/+*; *UAS-HA-abi/+*; abi^{5}/Df (Abi rescue-pre), *C155-GAL4/+*; $UAS\text{-}HA\text{-}abi^{\Delta 30\text{-}65}/+$; abi^{5}/Df (AbiΔ30-65 rescue-pre), *C155-GAL4/+*; $UAS\text{-}HA\text{-}abi^{\Delta 123\text{-}175},Df/abi^{5}$ (AbiΔ123-175 rescue-pre), *C155-GAL4/+*; $UAS\text{-}HA\text{-}abi^{W456K},Df/abi^{5}$ (AbiW452K rescue-pre), *C155-GAL4/+*; $UAS\text{-}HA\text{-}abi^{4YE},Df/abi^{5}$ (Abi4YE rescue-pre), *C155-GAL4/+*; $UAS\text{-}HA\text{-}abi^{4YF},Df/abi^{5}$ (Abi4YF rescue-pre), and $24B\text{-}GAL4,abi^{5}/UAS\text{-}HA\text{-}abi,Df$ (Abi rescue-post). N=3; n=18, 21, 30, 21, 30, 21, 18, 18, 15, and 24, respectively. A one-way ANOVA was used for data analysis.

(C) Schematic of the domain structure of Abi and Abi transgenic mutants. Abbreviations of Abi domains are as follows: WAVE-binding (WAB) domain, homeodomain homologous region (HHR), proline region (P), SRC homology 3 (SH3) domain. Numbers on top of the domain structure indicate the number of amino acids.

All comparisons are with wild-type organisms unless otherwise indicated (*$p<0.001$). Error bars are SEM for all figures.

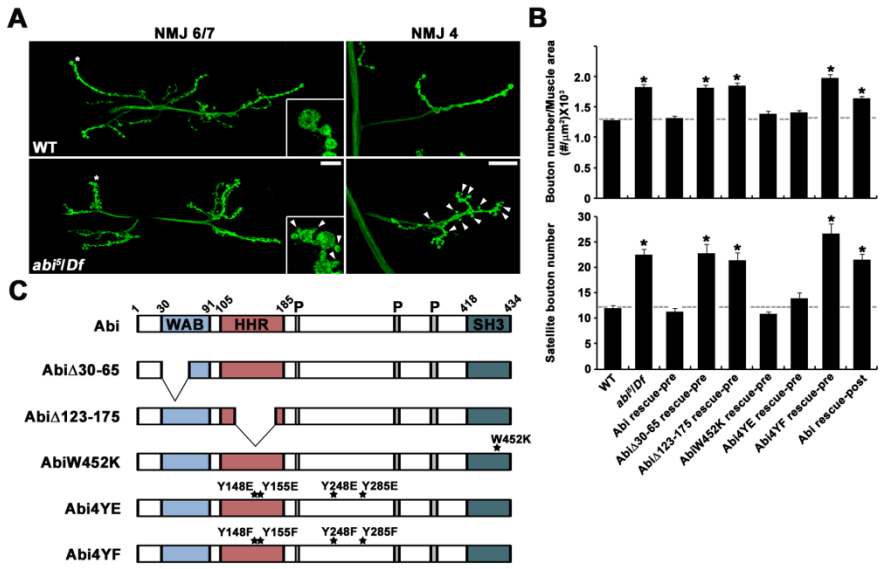
A
NMJ 6/7
NMJ 4
WT
abi5/Df
B
Bouton number/Muscle area (#/μm²)X10³
Satellite bouton number
WT
abi5/Df
Abi rescue-pre
Abi∆30-65 rescue-pre
Abi∆123-175 rescue-pre
AbiW452K rescue-pre
Abi4YE rescue-pre
Abi4YF rescue-pre
Abi rescue-post
C
Abi
WAB
HHR
SH3
Abi∆30-65
Abi∆123-175
AbiW452K
W452K
Abi4YE
Y148E Y155E Y248E Y285E
Abi4YF
Y148F Y155F Y248F Y285F

To examine whether Abi is required pre- or postsynaptically for normal NMJ development, I expressed Abi in *abi*^{5}*/Df* mutants using the UAS/GAL4 system. Expression of wild-type Abi in neurons using C155-GAL4 rescued the synaptic overgrowth defects (Figure 3B). In contrast, expression of Abi in muscles using 24B-GAL4 failed to rescue the synaptic overgrowth phenotype of *abi* mutants (Figure 3B). To verify whether presynaptic Abi is required for normal synaptic growth at the NMJ, I used GAL4-inducible RNAi mutants. I first confirmed the knock-down ability of *abi* double stranded RNA (dsRNA) by expressing *UAS-abi*^{RNAi} in *abi*-expressing tissues with *abi-GAL4* and performing subsequent western blot analyses. The levels of the Abi protein were diminished in *abi-GAL4/UAS-abi*^{RNAi} larvae compared to *abi-GAL4/+* larvae (Figure 4A). Moreover, expressing Abi-RNAi using *C155-GAL4* or *BG57-GAL4* (muscle drivers) reduced the presynaptic and postsynaptic expression of Abi at the NMJ (Figure 4B). Thus, western blot and immunohistochemistry analyses confirmed that transgenic expression of *abi* dsRNA efficiently inhibited Abi expression. Then, I tested whether synapses lacking presynaptic Abi showed defects in synaptic morphology. Compared with wild-type controls (*C155-GAL4/+*), the number of boutons, normalized to muscle surface area, was increased by ~29% in larvae with AbiRNAi expressed by *C155-GAL4*. However, loss of Abi driven by *24B-GAL4* resulted in no defect in synaptic growth compared to wild-type controls (*24B-GAL4/+*) (Figures 4C and 4D). Taken together, these results indicate that presynaptic Abi is necessary for normal NMJ growth.

To determine whether the satellite boutons featured in *abi*^{5}*/Df* mutants were true synaptic boutons, I characterized them with pre- and postsynaptic protein markers. The synaptic vesicle marker cystein-stiring protein (CSP; Figure 5A),

Figure 4. Loss of Presynaptic Abi Causes Synaptic Overgrowth at the Larval NMJ

(A) Western blot analysis of total protein extracts from *abi-GAL4*/+ and *abi-GAL4*/*UAS-abi*^{RNAi} third instar larvae probed with anti-Abi and anti-β–actin.

(B) Single confocal slices of NMJ 6/7 branches with type I boutons of third instar larvae. *C155-GAL4*/+, *C155-GAL4*/+; *UAS-abi*^{RNAi}/+, *BG57-GAL4*/+, *UAS-abi*^{RNAi}/+;*BG57-GAL4*/+ larvae were stained with presynaptic membrane marker anti-HRP (green) and anti-Abi (red) antibodies. Scale bar represents 5 μm.

(C) Confocal images of NMJ 6/7 labeled with anti-HRP taken from *C155-GAL4*/+, *C155-GAL4*/+; *UAS-abi*^{RNAi}/+, *24B-GAL4*/+, *UAS-abi*^{RNAi}/+; *24B-GAL4*/+ larvae. Magnified boutons of NMJ 6/7 are marked by white asterisks. Scale bar represents 20 μm.

(D) Quantification of the numbers of total boutons normalized to the muscle surface area and satellite boutons of NMJ 6/7. Control is *C155-GAL4/+* in the white box and *24B-GAL4/+* in the gray box. N=3, n = 12, 15, 12, and 18, respectively. Student's t-test was used for data analysis. All comparisons are with the control unless otherwise indicated (*$p<0.001$). Error bars are SEM for all figures.

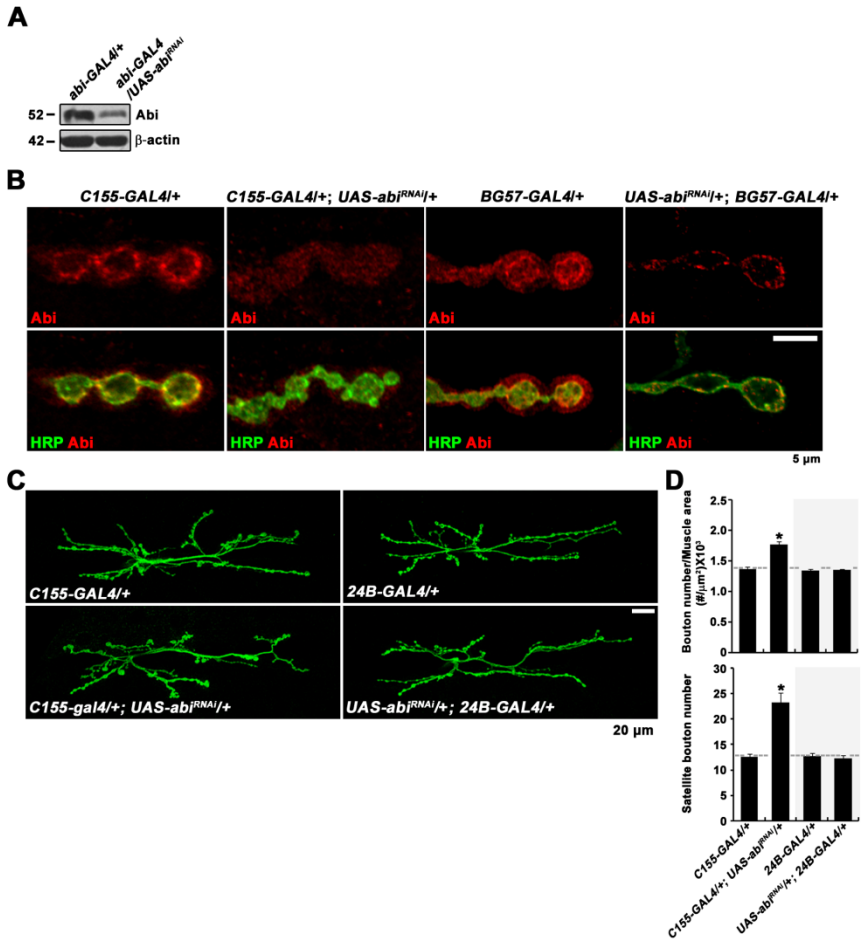
A
abi-GAL4/+
abi-GAL4 /UAS-abi^RNAi
52–
Abi
42–
β-actin
B
C155-GAL4/+
C155-GAL4/+; UAS-abi^RNAi/+
BG57-GAL4/+
UAS-abi^RNAi/+; BG57-GAL4/+
Abi
HRP Abi
5 μm
C
C155-GAL4/+
24B-GAL4/+
C155-gal4/+; UAS-abi^RNAi/+
UAS-abi^RNAi/+; 24B-GAL4/+
20 μm
D
Bouton number/Muscle area (#/μm²)X10³
Satellite bouton number
C155-GAL4/+
C155-GAL4/+; UAS-abi^RNAi/+
24B-GAL4/+
UAS-abi^RNAi/+; 24B-GAL4/+

Figure 5. Satellite Bouton Characterization in Loss of *abi* Mutants

(A-D) Satellite boutons shown in abi^{5}/Df mutants are functional synaptic boutons. Single confocal slices of NMJ 6/7 doubly labeled with anti-HRP (green) and anti-CSP (red) (A), anti-NC82 (red) (B), anti-Dlg (red) (C), or anti-GluRIIC (red) (D) antibodies from wild-type and abi^{5}/Df larvae. Scale bar represents 5 μm.

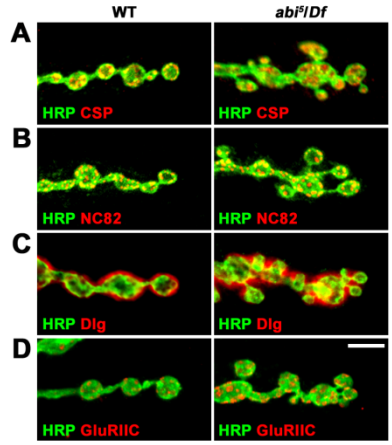
WT
abi5/Df
A
HRP CSP
HRP CSP
B
HRP NC82
HRP NC82
C
HRP Dlg
HRP Dlg
D
HRP GluRIIC
HRP GluRIIC

active zone marker NC82 (Figure 5B), and postsynaptic glutamate receptors (GluRIIC; Figure 5C) were all present in these satellite boutons. In addition, every satellite bouton was surrounded by the SSR marker Dlg (Figure 5C). Therefore, the small supernumerary boutons present in *abi*^{5}*/Df* mutants are functional synaptic boutons.

4. Presynaptic Requirements for Functional Abi Domains

Abi proteins consist of an N-terminal WAVE-binding (WAB) domain, a homeodomain homologous region (HHR), a proline-rich region (PRR), and a C-terminal SH3 domain. The Abi protein binds SCAR/WAVE and Kette/NAP1 through its N-terminal WAB domain and central HHR, respectively (Echarri et al, 2004, Bogdan et al., 2005). In addition, Abi can interact with WASP via the C-terminal SH3 domain (Bogdan et al., 2005). The Abl tyrosine kinase binds at the C-terminal SH3 domain of the Abi protein (Dai and Pendergast, 1995; Shi et al., 1995), and it has been shown that four tyrosine (Y) residues (Y148, Y155, Y248, Y285) in Abi are phosphorylated by Abl (Juang and Hoffmann, 1999; Huang et al., 2007).

GST pull-down experiments confirmed that deletion of amino acids 30-65 or 123-175 of Abi impairs its interaction with SCAR/WAVE or Kette, respectively (Figure 6B). In contrast, substitution of a key tryptophan residue in the SH3 domain to lysine (W452K) abrogated Abi interaction with WASP (Figure 6B). After confirming the interaction between Abi and SCAR, Kette, and WASP, I generated UAS transgenes of HA-AbiΔ30-65, HA-AbiΔ123-175, and HA-AbiW452K to investigate whether the function of Abi in the regulation of synapse

Figure 6. Physical Interaction between Abi and its Binding Partners

(A) Schematic representation of the deletion and point-mutation mutants of GST fusion Abi proteins. Abbreviations of Abi domains are as follows: WAVE-binding (WAB) domain, homeodomain homologous region (HHR), proline region (P), SRC homology 3 (SH3) domain.

(B) In GST pull-down assays, GST alone, GST-Abi-N (Abi N-terminus, amino acids 1-387), GST-Abi-SH3 (amino acids 387-473), and GST-Abi-N-Δ30-65 (Abi N-terminus with amino acids 30-65 deleted) were incubated with lysates from S2R+ cells and probed with anti-SCAR. GST, GST-Abi-N, GST-Abi-SH3, and GST-Abi-N-Δ123-175 (Abi N-terminus with amino acids 123-175 deleted) were incubated with lysates from S2R+ cells transiently expressing Kette-Myc and probed with anti-Myc. GST, GST-Abi-N, GST-Abi-SH3, and GST-Abi-SH3-W452K were incubated with lysates from S2R+ cells and probed with anti-WASP.

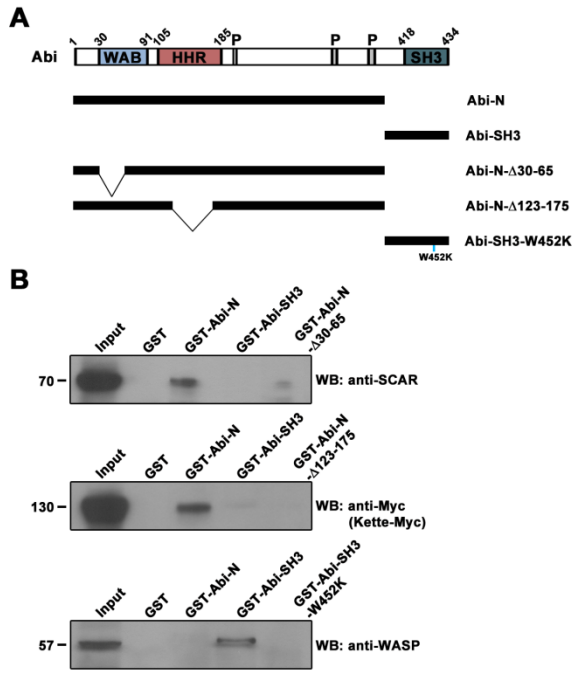
A
Abi
1
30
91
105
185
P
P
P
418
434
WAB
HHR
SH3
Abi-N
Abi-SH3
Abi-N-Δ30-65
Abi-N-Δ123-175
Abi-SH3-W452K
W452K
B
Input
GST
GST-Abi-N
GST-Abi-SH3
GST-Abi-N -Δ30-65
70
WB: anti-SCAR
Input
GST
GST-Abi-N
GST-Abi-SH3
GST-Abi-N -Δ123-175
130
WB: anti-Myc (Kette-Myc)
Input
GST
GST-Abi-N
GST-Abi-SH3
GST-Abi-SH3 -W452K
57
WB: anti-WASP

Figure 7. Analysis of Transgenic Expression of Abi and Its Mutants

(A) Western blot analysis of whole fly extracts using anti-HA and anti-β-actin antibodies in the following genotypes: *da-GAL4*/+ (control), *da-GAL4*/*UAS-HA-abi* (HA-Abi), *UAS-HA-abi*$^{\Delta 30\text{-}65}$/+; *da-GAL4* (HA-Abi*Δ*30-65), *da-GAL4/UAS-HA-abi*$^{\Delta 123\text{-}165}$ (HA-Abi*Δ*123-165), *da-GAL4*/*UAS-HA-abi*^{W452K} (HA-AbiW452K), *da-GAL4*/*UAS-HA-abi*^{4YE} (HA-Abi4YE), and *da-GAL4*/*UAS-HA-abi*^{4YF} (HA-Abi4YF). (B) Transgenic expression of HA-Abi and HA-Abi mutants. Single confocal slice images of third-instar larvae VNC stained with anti-HA (red) and bouton terminals of NMJ 6/7 double-labeled with anti-HA (red) and anti-HRP (green) taken from the following genotypes: *C155-GAL4/+*; *UAS-HA-abi/+*; *abi*^{5}*/Df* (HA-Abi), *C155-GAL4/+*; *UAS-HA-abi*$^{\Delta 30\text{-}65}$/+; *abi*^{5}*/Df* (HA-Abi*Δ*30-65), *C155-GAL4/+*; *UAS-HA-abi*$^{\Delta 123\text{-}175}$*,Df/abi*^{5} (HA-Abi*Δ*123-165), *C155-GAL4/+*; *UAS-HA-abi*^{W456K}*,Df/abi*^{5} (HA-AbiW452K), *C155-GAL4/+*; *UAS-HA-abi*^{4YE}*,Df/abi*^{5} (HA-Abi4YE), and *C155-GAL4/+*; *UAS-HA-abi*^{4YF}*, Df/abi*^{5} (HA-Abi4YF). Scale bars represent 50 μm (VNC) or 5 μm (NMJ termini).

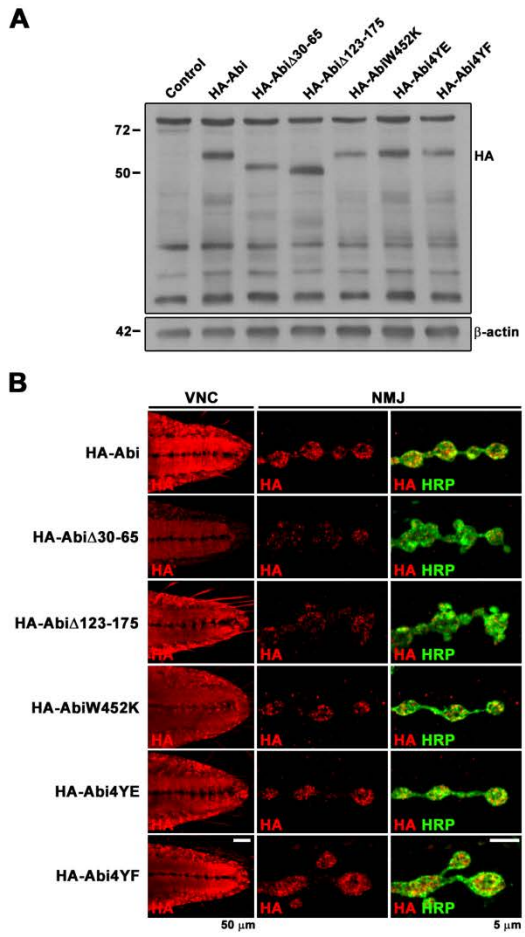
A
Control
HA-Abi
HA-AbiΔ30-65
HA-AbiΔ123-175
HA-AbiW452K
HA-Abi4YE
HA-Abi4YF
72
50
HA
42
β-actin
B
VNC
NMJ
HA-Abi
HA-AbiΔ30-65
HA-AbiΔ123-175
HA-AbiW452K
HA-Abi4YE
HA-Abi4YF
HA
HA HRP
50 μm
5 μm

development depends on the WAVE complex and WASP (Figure 3C). In addition, four tyrosine residues (Y148, Y155, Y248, Y285) were individually replaced by glutamate (E) or phenylalanine (F) to generate UAS transgenes of HA-Abi4YE (phosphor-mimic form of Abi) or HA-Abi4YF (phosphor-defective form of Abi) to further test whether phosphorylation of Abi by Abl kinase is necessary for regulating synaptic growth at the NMJ. These transgenes were expressed at levels similar to that of wild-type HA-Abi when driven by the *da-GAL4* driver (Figure 7A). Like wild-type HA-Abi, all HA-Abi variants were efficiently targeted to the presynaptic terminal of motor neurons (Figure 7B).

I then tested the ability of HA-AbiΔ30-65, HA-AbiΔ123-175, HA-Abi-W452K, HA-Abi4YE, and HA-Abi4YF to rescue the NMJ growth defects seen in abi^{5}/Df mutants. The increases in the numbers of overall and satellite boutons in abi^{5}/Df mutants were fully rescued by neuronal C155-GAL4-driven expression of *UAS-HA-abi*^{W452K} and *UAS-HA-abi*^{4YE}, but not *UAS-HA-abi*$^{\Delta 30\text{-}65}$, *UAS-HA-abi*$^{\Delta 123\text{-}175}$, or *UAS-HA-abi*^{4YF} (Figure 3B). Therefore, Abi interactions with the WAVE complex, but not with WASP, are critical for normal presynaptic development. In addition, Abl phosphorylation of Abi is essential for proper synaptic growth control. Together, these results suggest that Abi regulates synaptic growth through the WAVE complex and Abl kinase but not WASP.

5. Abi, the WAVE Complex, and Rac1 Act Together to Regulate Synaptic Growth

Based on the results of my biochemical and genetic experiments (Figure 3 and Figure 6), I hypothesized that Rac1 and components of the WAVE complex

may act together with Abi to regulate synaptic growth. To verify this hypothesis, I first examined the synaptic morphology of NMJs in larvae expressing dominant-negative Rac1 (UAS-*rac1*^{N17}), *scar* dsRNA (*UAS-scar*^{RNAi}), and *kette* dsRNA (*UAS-kette*^{RNAi}) in neurons using the *C155-GAL4* driver. Expressing presynaptic Rac1N17, ScarRNAi, and KetteRNAi increased the total bouton number and satellite bouton number in a manner similar to that seen with *abi* loss-of-function mutants (Figures 8A and 8B). This result confirmed that Rac1, SCAR, and Kette are required presynaptically for bouton formation. Therefore, Rac1 and the WAVE complex may regulate synaptic growth together with Abi in same signaling pathway. To confirm this possibility, I performed transheterozygous interaction experiments between *rac1*, *scar*, or *kette* and *abi* during synaptic growth. NMJ morphology of larvae lacking a single copy of *abi*, *rac1*, *scar*, or *kette* was similar to that of wild-type larvae. However, *abi-rac1*, *abi-scar*, and *abi-kette* transheterozygotes exhibited significantly increased numbers of overall boutons and satellite boutons (Figure 8C). Moreover, transheterozygotes of *abi* and *wasp* showed no differences in synaptic morphology (Figure 8C), supporting the idea that Abi and WASP do not genetically interact to regulate synaptic growth. These data suggest that Abi, Rac1, and components of the WAVE complex function in the same pathway to restrain synaptic growth.

Previous studies have shown that Rac1 acts upstream of the WAVE complex to activate actin nucleation of Arp2/3, which promotes actin polymerization. To confirm that Rac1 signals through Abi at the NMJ, I tested the epistatic relationship between *abi* and *rac1*. Expressing constitutively-active Rac1 (*UAS-rac1*^{V12}) under the control of *C155-GAL4* resulted in an overgrowth phenotype at the larval NMJ compared to controls (*C155-GAL4/+*). Removing the

Figure 8. Rac1 and the WAVE Complex are Required for Abi-Dependent Regulation of Synaptic Growth

(A and B) Loss of presynaptic Rac and the WAVE complex results in synaptic overgrowth at larval NMJs. (A) Confocal images of NMJ 6/7 (left panels) and NMJ 4 (right panels) labeled with anti-HRP taken from *C155-GAL4*/+, *C155-GAL4*/+; *UAS-rac1*^{N17}/+, *C155-GAL4*/+; *UAS-scar*^{RNAi}/+, and *C155-GAL4*/+; *UAS-kette*^{RNAi}/+ larvae. Scale bar represents 20 μm. (B) Quantification of the number of total boutons normalized to the muscle surface area and satellite boutons at NMJ 6/7 in the indicated genotypes. N=3, n=12, 9, 18, and 12, respectively. One-way ANOVA was used for data analysis. (C) Transheterozygous interaction between *abi*, *Abl*, *rac1*, *scar*, *kette*, and *wasp* shows that Abi interacts with Rac and the WAVE complex at the NMJ, but not with WASP. Quantification of number of overall boutons normalized to the muscle surface area and satellite boutons at NMJ 6/7. N=3, n=24, 15, 12, 30, 15, 9, 12, 30, 30, and 15, respectively. One-way ANOVA was used for data analysis.

(D) Abi acts as a downstream effecter for Rac1 in regulating synaptic growth. Quantification of the synaptic structure in the indicated genotypes.

All comparisons are with controls unless otherwise indicated (*$p<0.001$; **$p<0.01$). Error bars are SEM for all figures.

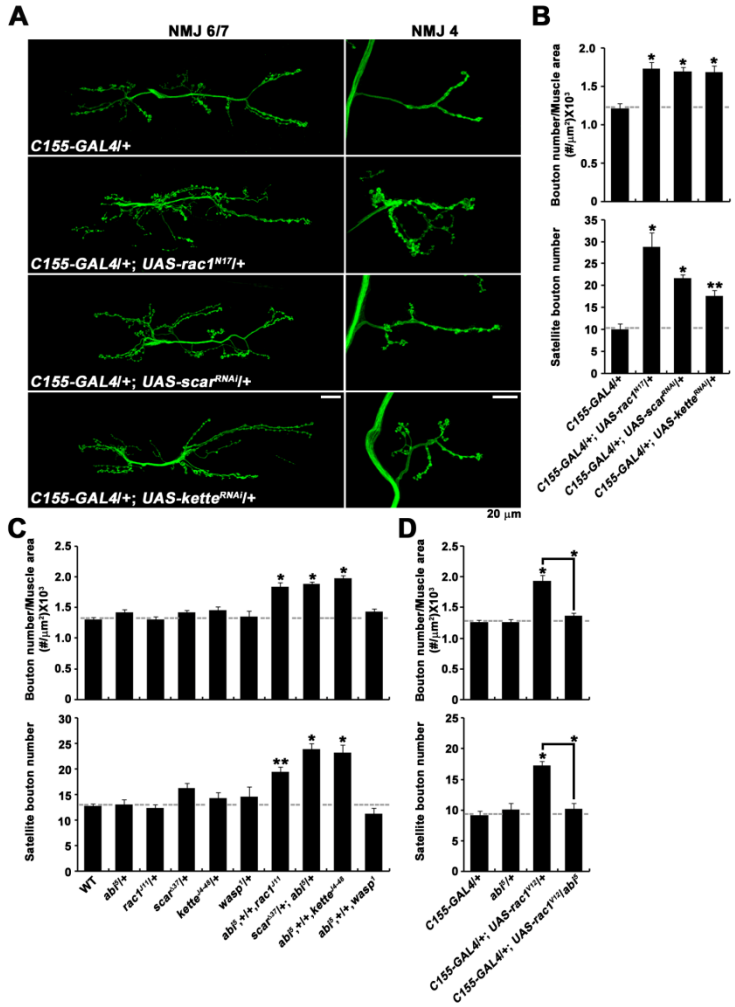
A
NMJ 6/7
NMJ 4
C155-GAL4/+
C155-GAL4/+; UAS-rac1N17/+
C155-GAL4/+; UAS-scarRNAi/+
C155-GAL4/+; UAS-ketteRNAi/+
20 μm
B
Bouton number/Muscle area (#/μm²)X10³
Satellite bouton number
C155-GAL4/+
C155-GAL4/+; UAS-rac1N17/+
C155-GAL4/+; UAS-scarRNAi/+
C155-GAL4/+; UAS-ketteRNAi/+
C
Bouton number/Muscle area (#/μm²)X10³
Satellite bouton number
WT
abl1/+
rac1J11/+
scarΔ37/+
ketteJ4-8/+
wasp1/+
abl1,+/+,rac1J11
scarΔ37/+; abl1/+
abl1,+/+,ketteJ4-8
abl1,+/+,wasp1
D
Bouton number/Muscle area (#/μm²)X10³
Satellite bouton number
C155-GAL4/+
abl1/+
C155-GAL4/+; UAS-rac1J11/+
C155-GAL4/+; UAS-rac1J11/abl1

single copy of *abi* completely suppressed the phenotype shown in larval NMJ presynaptically expressing Rac1V12, confirming that Rac1 acts as an upstream molecule of Abi to inhibit synaptic growth (Figure 8D).

6. Abi Acts Downstream of Abl Kinase during Synaptic Growth

The cytoplasmic tyrosine kinase Abelson (Abl) interacts with and phosphorylates Abi, suggesting a functional relationship between Abi and Abl (Juang and Hoffmann, 1999; Huang et al., 2007). In mammals, Abl has been implicated in the regulation of synaptic morphology (Moresco et al, 2003); in *Drosophila*, Abl is required for normal synaptic growth and axon guidance (Lin et al., 2009). Previous findings and genetic evidence (Figure 3B) support the idea that Abi phosphorylation by Abl may be required for normal synaptic growth. To prove this hypothesis, first, I examined whether *Abl* mutants exhibit the same phenotype as *abi* loss-of function mutants. Compared to wild-type controls, overall bouton and satellite bouton formation was elevated in Abl^{1}/Abl^{4} mutants (Figures 9A and 9D). To confirm whether the kinase activity of Abl in the presynapse is necessary in proper synaptic growth, I examined the NMJ morphology that occurred when the kinase-inactive Abl mutant (AblKN) was expressed in both neurons and muscles. Expression of *UAS-*Abl^{KN} by *C155-GAL4* was sufficient to increase the numbers of total boutons and of satellite boutons at the larval NMJ; however, *UAS-*Abl^{KN} expression driven by *24B-GAL4* showed no effect, supporting the idea that Abi phosphorylated by Abl in the presynapse may function in synaptic development (Figure 9B).

Figure 9. Abl Is Required for Abi-Dependent Regulation of Synaptic Growth

(A and B) Loss of Abl causes excessive formation of synaptic boutons, and Abl kinase activity at the presynapse is necessary for synaptic growth at larval NMJs. (A) Confocal images of NMJ 6/7 (left panel) and NMJ 4 (right panel) stained with anti-HRP (green) shown in wild-type, Abl^{1}/Abl^{4}, *C155-GAL4*/+, and *C155-GAL4*/+; *UAS-*Abl^{KN}/+ larvae. Scale bar represents 20 μm. (B) Quantification of numbers of total boutons normalized to the muscle surface area and satellite boutons at NMJ 6/7 in the indicated genotypes. N=3, n=15, 12, 12, 15, 15, and 18, respectively. Student's t-test was used for data analysis.

(C) Transheterozygous interaction between *abi* and *Abl*. Quantification of the synaptic structure at NMJ 6/7 in the indicated genotypes. N=3, n=15, 12, 15, and 30, respectively. One-way ANOVA was used for data analysis.

(D) Abl is an upstream molecule of Abi, and the kinase activity of Abl on Abi is necessary for regulating synaptic growth. Quantification of the synaptic structure at NMJ 6/7 in indicated genotypes. N=3, n=15, 12, 15, 12, 12, 15, 12, 15, 12, 15, and 12, respectively. One-way ANOVA was used for data analysis.

All comparisons are with controls unless otherwise indicated (*$p<0.001$; **$p<0.01$; ***$p<0.05$; n.s., not significant). Error bars are SEM for all figures.

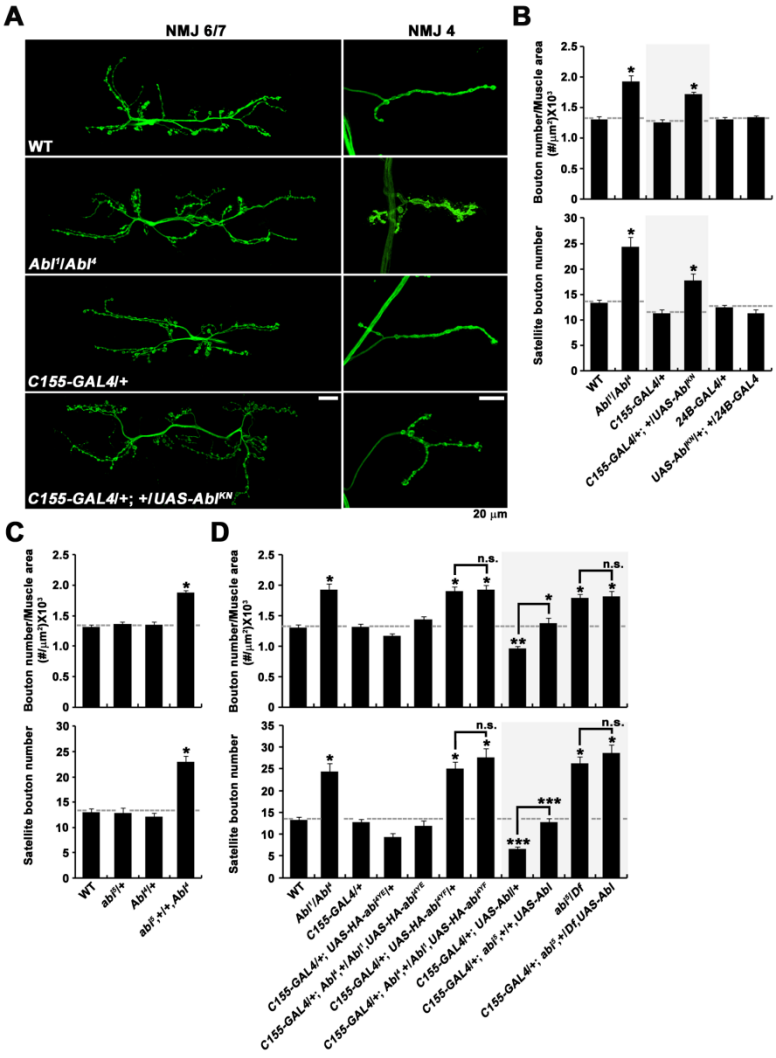
A
NMJ 6/7
NMJ 4
WT
Abl1/Abl4
C155-GAL4/+
C155-GAL4/+; +/UAS-AblKN
20 μm
B
Bouton number/Muscle area (#/μm2)X103
Satellite bouton number
WT
Abl1/Abl4
C155-GAL4/+
C155-GAL4/+; +/UAS-AblKN
24B-GAL4/+
UAS-Abl[c]/+; +/24B-GAL4
C
Bouton number/Muscle area (#/μm2)X103
Satellite bouton number
WT
abl[c]/+
Abl1/+
abl[c],+/+,Abl1
D
Bouton number/Muscle area (#/μm2)X103
Satellite bouton number
n.s.
WT
Abl1/Abl4
C155-GAL4/+
C155-GAL4/+; UAS-HA-abl[KE]/+
C155-GAL4/+; Abl4,+/Abl1,UAS-HA-abl[KE]
C155-GAL4/+; UAS-HA-abl[KN]
C155-GAL4/+; Abl4,+/Abl1,UAS-HA-abl[KN]/+
C155-GAL4/+; UAS-Abl/+
C155-GAL4/+; abl[c],+/+,UAS-Abl
abl[c]/Df
C155-GAL4/+; abl[c],+/Df,UAS-Abl

Next, I examined transheterozygous interactions between *abi* and *Abl* to confirm the possibility that Abi and Abl function in a common signaling pathway at the NMJ. Heterozygous abi^{5}/+ or Abl^{4}/+ larvae displayed normal NMJ morphology, whereas the numbers of overall boutons and satellite boutons increased after removal of both the abi^{5} and Abl^{4} alleles (Figure 9C). Thus, Abi and Abl regulate synaptic growth together in the same signaling cascade.

To address the requirement of Abl phosphorylation for Abi function and to examine their epistatic relationship, I performed genetic interaction experiments between *abi* and *Abl*. First, to determine whether the phosphorylation of Abi has any effect on synaptic growth, I examined the synaptic structure in the phospho-mimic form of Abi (HA-Abi4YE) or phospho-defective form of Abi (HA-Abi4YF) expressed in neurons. Overexpression of *UAS-HA-*abi^{4YE} in the wild-type background using *C155-GAL4* resulted in a similar phenotype to that of *C155-GAL4*/+ larvae. In contrast, overexpression of *UAS-HA-*abi^{4YF} in the wild-type background using *C155-GAL4* resulted in significantly increased numbers of total boutons and satellite boutons, which means that HA-Abi4YF has a dominant-negative effect in the NMJ (Figure 9D). Then, I expressed *UAS-HA-*abi^{4YE} *or UAS-HA-*abi^{4YF} in the *Abl* mutant background to examine whether phosphorylation of Abi is required for Abl. Expression of *UAS-HA-*abi^{4YE} by *C155-GAL4* in the Abl^{1}/Abl^{4} background suppressed the overgrowth phenotype seen in the *Abl* mutant (Figure 9D). However, expression of presynaptic HA-Abi4YF in *Abl* mutants culminated in a similar synaptic defect phenotype to that of *Abl* mutants or wild-type larvae with presynaptic expression of HA-Abi4YF (Figure 9D). These data suggest that phosphorylation of Abi is necessary for Abl to function in synaptic development. Lastly, I further examined the epistatic relation of *abi* and *Abl* using

Abl gain-of-function larvae and *abi* null mutants. Presynaptic expression of *Abl* in a wild-type background reduced overall bouton and satellite bouton formation compared to controls, which was the opposite result of that observed in *Abl* mutant larvae. The gain-of-function phenotype seen with presynaptic expression of *Abl* was rescued by removing a single copy of *abi* and further suppressed by removing both copies of *abi*, which resulted in the same phenotype as that of *abi* mutant larvae (Figure 9D). Taken together, these data support the idea that Abl acts upstream of Abi, and its kinase activity on Abi is required for proper synaptic development.

7. Abi, Abl, and Rac1 Restrain Synaptic Growth via Inhibition of Retrograde BMP Signaling

Like the *abi* mutant, *Abl* mutant, or pre-Rac1N17 phenotype, overactivation of retrograde BMP signaling induces synaptic overgrowth with excessive satellite bouton formation at the *Drosophila* NMJ (Nahm et al., 2013; O'Connor-Giles et al., 2008; Sweeney and Davis, 2002). This raises the possibility that synaptic overgrowth in larvae lacking *abi*, *Abl*, *rac1*, *scar*, or *kette* may be attributable to over-activation of BMP signaling at the NMJ. To test this hypothesis, I first examined phosphorylated Mad (P-Mad) as a molecular readout of BMP signaling activity. Levels of P-Mad were significantly higher in *abi* and *Abl* mutants than in wild-type controls, both at NMJ terminals and in motor neuron nuclei (Figures 10A and 10B). Also, presynaptic expression of dominant-negative Rac1, *scar* dsRNA, or *kette* dsRNA resulted in elevated P-Mad level in both motor neuron termini and nuclei. These data suggest that Abi, Abl, Rac1, and components

Figure 10. Abi, Abl, and Presynaptic Rac1 Are Required for P-Mad Accumulation at the Synaptic Terminal and Motor Neuron Nucleus

(A) Single confocal slices of NMJ 6/7 and VNC labeled with both anti-P-Mad (red) and anti-HRP (green; NMJ) or anti-Elav (green; VNC) taken from wild-type, *abi*^{5}*/Df*, *Abl*^{1}*/Abl*^{4}, *C155-GAL4*/+, and *C155-GAL4*/+; *UAS-rac1*^{N17}/+ larvae. Scale bar represents 5 μm.

(B) Quantification of P-Mad intensity at the NMJ terminus and motor neuron nucleus in the VNC in indicated genotypes. P-Mad intensity was divided by those of HRP (NMJ) or Elav (VNC) and normalized to controls. N=3, n=36, 36, 36, 45, 15, 36, and 18, respectively (synaptic terminal). N=3, n=30, 21, 27, 45, 33, 30, and 18, respectively (nuclei). One-way ANOVA was used for data analysis.

All comparisons are with controls unless indicated (*$p<0.001$). Error bars are SEM for all figures.

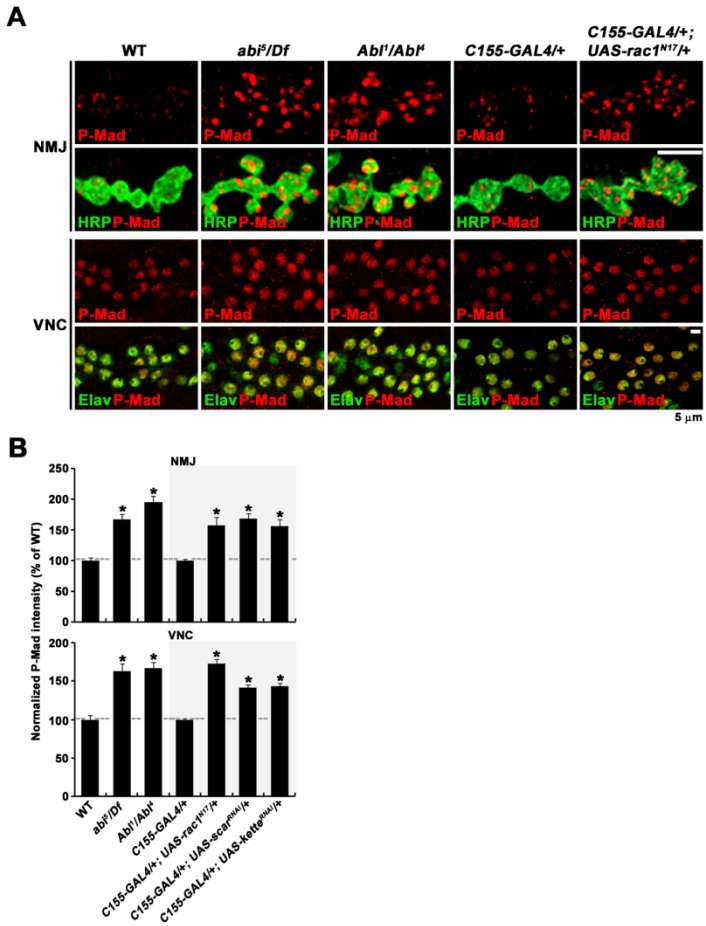
A
WT
abi5/Df
Abl1/Abl4
C155-GAL4/+
C155-GAL4/+; UAS-rac1N17/+
NMJ
VNC
P-Mad
HRP P-Mad
Elav P-Mad
5 μm
B
NMJ
VNC
Normalized P-Mad intensity (% of WT)
250
200
150
100
50
0
WT
abi5/Df
Abl1/Abl4
C155-GAL4/+
C155-GAL4/+; UAS-rac1N17/+
C155-GAL4/+; UAS-scarWAU/+
C155-GAL4/+; UAS-ketteWAU/+

of the WAVE complex are negative regulators of the BMP signaling pathway at the NMJ. I then examined the genetic interactions between *abi*, *Abl*, or presynaptic Rac1N17 and the BMP receptor *wit*. As reported previously (Aberle et al., 2002; Marques et al., 2002), single *wit* mutants showed significant synaptic undergrowth (Figures 11A and 11B). *wit* heterozygote mutants showed normal synaptic morphology compared to that of wild-type controls, but removing a single copy of *wit* suppressed the synaptic overgrowth phenotype of abi^{5}/Df, Abl^{1}/Abl^{4}, *C155-GAL4*/+, and *UAS-*$rac1^{N17}$/+ mutants (Figures 11A and 11B). Furthermore, in *wit,abi*, *wit,Abl*, and *wit,*pre-$rac1^{N17}$ double mutants, I also observed a synaptic undergrowth phenotype comparable to that of *wit* single mutants (Figures 11A and 11B). All together, these data suggest that Abi, Abl, and Rac1 restrain synaptic growth via inhibition of BMP signaling. Also, these results gave me the idea that Rac1-WAVE signaling, which activates actin polymerization, may not directly regulate synaptic development, but instead may regulate synaptic growth through regulation of BMP signaling at the NMJ.

8. Abi, Abl, and Rac1 Regulate Synaptic Growth through Modulation of Microtubule Stability

Previous studies have revealed that BMP signaling promotes synaptic growth by repressing the expression of *Drosophila* fragile X mental retardation protein (dFMRP) (Nahm et al., 2013). dFMRP subsequently inhibits the expression of the MAP1B ortholog Futsch to regulate microtubule stability and synaptic growth (Zhang et al., 2001). Futsch-mediated regulation of microtubule (MT) stability is critical for normal synaptic growth, as demonstrated by the synaptic

Figure 11. Synaptic Growth Regulated by Abi, Abl, and Presynaptic Rac1 Depends on BMP Signaling

(A) Confocal images of NMJ 6/7 (left panel) and NMJ 4 (right panel) stained with anti-HRP (green) taken from *C155-GAL4*/+; *UAS-rac1*^{N17}/+, *C155-GAL4*/+; *UAS-rac1*^{N17}/*wit*^{B11}, *wit*^{A12}/*wit*^{B11}, and *C155-GAL4*/+; *UAS-rac1*^{N17}, *wit*^{B11}/+,*wit*^{A12} larvae. Scale bar represents 20 μm.

(B) Quantification of the synaptic structure at NMJ 6/7 in the indicated genotypes. N=3, n=15, 18, 15, 15, 18, 15, 15, 15, 15, 15, 9, 12, and 18, respectively. One-way ANOVA was used for data analysis.

All comparisons are with controls unless otherwise indicated (*$p<0.001$; n.s., not significant). Error bars are SEM for all figures.

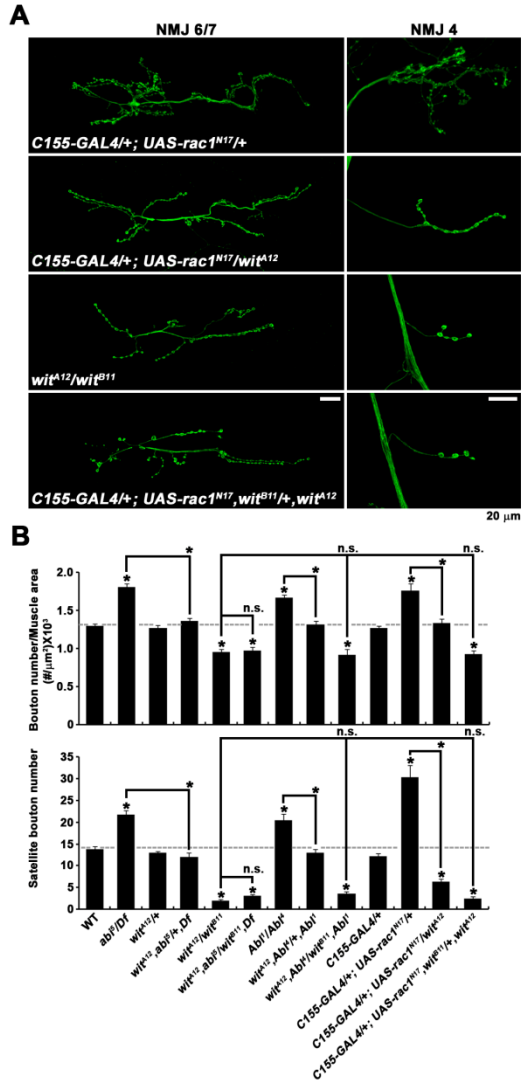
A
NMJ 6/7
NMJ 4
C155-GAL4/+; UAS-rac1N17/+
C155-GAL4/+; UAS-rac1N17/witA12
witA12/witB11
C155-GAL4/+; UAS-rac1N17,witB11/+,witA12
20 μm
B
Bouton number/Muscle area (#/μm²)X10³
Satellite bouton number
n.s.
WT
abf/Df
wit+/+
wit+/+,abf/+,Df
wit+/+/witB11
wit+/+,abf/witB11,Df
Abl/Abl
wit+/+,Abl/+,Abl
wit+/+,Abl/witB11,Abl
C155-GAL4/+
C155-GAL4/+; UAS-rac1N17/+
C155-GAL4/+; UAS-rac1N17/witA12
C155-GAL4/+; UAS-rac1N17,witB11/+,witA12

undergrowth seen in *futsch* mutants (Roos et al., 2000). Genetic evidences and the enhancement of BMP signaling in *abi*, *abl*, and *rac1* mutants support the possibility that Abi, Abl, and Rac1 may function through the dFMRP-Futsch pathway to regulate synaptic growth. To test this hypothesis, I examined the effects of *abi* and *Abl* mutations or presynaptic dominant-negative *rac1* mutations on *dfmr1* mRNA expression by qRT-PCR. *dfmr1* levels in the larval CNS (brain and ventral nerve cord) of abi^{5}/Df, Abl^{1}/Abl^{4}, or *C155-GAL4*/+;*UAS-*$rac1^{N17}$/+ mutants were significantly lower than in that of wild-type controls (Figure 12A). I then examined the genetic interactions between *dfmr1* and *abi*, *Abl*, or presynaptic Rac1N17 to test whether synaptic growth regulated by dFMRP is dependent on Abi/Abl/Rac1. Larvae that were transheterozygous for $dfmr1^{\Delta 50M}$ and abi^{5}, Abl^{4}, or presynaptic-Rac1N17 showed increased numbers of overall boutons and satellite boutons (Figure 12B), which gave me the clue that Abi/Abl/Rac1 and dFMRP may function together in a common signaling pathway to control synaptic development. Therefore, I investigated the epistatic relationship between *dfmr1* and *abi, abl,* or *rac1*. The synaptic overgrowth phenotype seen in abi^{5}/Df, Abl^{1}/Abl^{4}, or *C155-GAL4*/+;*UAS-*$rac1^{N17}$/+ mutants was suppressed by expressing *UAS-dfmr1* using the *C155-GAL4* driver (Figure 12C). These results suggest that Abi, Abl, and Rac1 activate dFMRP expression to regulate synaptic growth at the NMJ.

Next, to examine whether Abi, Abl, and the Rac1-WAVE complex affect Futsch expression to regulate microtubule stability, I measured the level of Futsch in abi^{5}/Df, Abl^{1}/Abl^{4}, *C155-GAL4*/+; *UAS-*$rac1^{N17}$/+, *C155-GAL4*/+; *UAS-*$scar^{RNAi}$/+, and *C155-GAL4*/+;*UAS-*$kette^{RNAi}$/+ larvae. The level of Futsch in the motor axon terminus of *abi* or *Abl* mutant, presynaptic *scar* or *kette* knock-down, and presynaptic *rac1* dominant-negative larvae were higher than that of the control

Figure 12. Abi, Abl, and Rac1 Require dFMRP to Regulate Synaptic Growth

(A) Abi, Abl, and Rac1 regulate the mRNA expression of *dfmr1* in the larval VNC. Quantification of relative *dfmr1* mRNA expression using quantitative real-time PCR in wild-type, abi^{5}/Df, Abl^{1}/Abl^{4}, *C155-GAL4*/+, and *C155-GAL4*/+; *UAS-*$rac1^{N17}$/+ larvae. Samples were run in duplicate in four independent experiments, and *rp49* was used as an internal control. Ten larvae were used for each experiment. A one-way ANOVA and Student's t-test were used for data analysis.

(B and C) *abi*, *rac1*, and *Abl* genetically interact with *dfmr1*. (B) Transheterozygous interaction of *abi*, *Abl*, *rac1*, and *dfmr1*. Quantification of the synaptic structure at NMJ 6/7 in the indicated genotypes. N= 3, n=15, 15, 15, 12, 12, 12, 12, and 12, respectively. One-way ANOVA was used for data analysis. (C) Overexpression of presynaptic *dfmr1* in *abi* or *Abl* mutants and presynaptic Rac1 dominant negative larvae exhibit decreased bouton formation at larval NMJs. Quantification of the synaptic structure at NMJ 6/7 in the indicated genotypes. N=3, n=15, 12, 15, 12, 12, 18, 12, 12, and 15, respectively. One-way ANOVA was used for data analysis.

All comparisons are with wild-type organisms unless otherwise indicated (*$p<0.001$; ***$p<0.05$; n.s., not significant). Error bars are SEM for all figures.

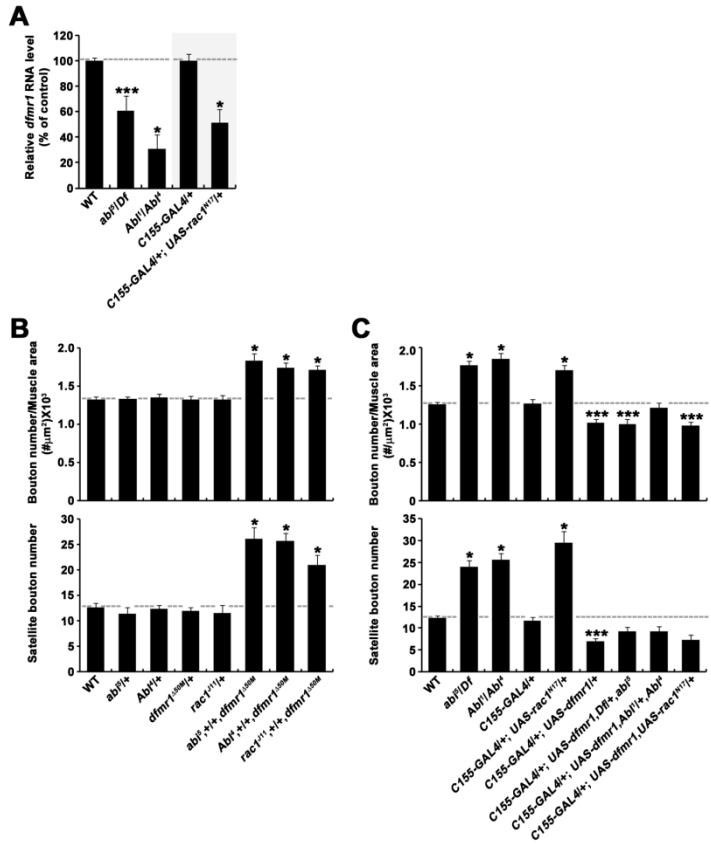
A
Relative dfmr1 RNA level (% of control)
WT
abl1/Df
Abl1/Abl1
C155-GAL4/+
C155-GAL4/+; UAS-rac1V17/+
B
Bouton number/Muscle area (#/μm²)X10³
Satellite bouton number
WT
abl1/+
Abl1/+
dfmr1Δ50M/+
rac1J11/+
abl1,+/+,dfmr1Δ50M
Abl1,+/+,dfmr1Δ50M
rac1J11,+/+,dfmr1Δ50M
C
Bouton number/Muscle area (#/μm²)X10³
Satellite bouton number
WT
abl1/Df
Abl1/Abl1
C155-GAL4/+
C155-GAL4/+; UAS-rac1V17/+
C155-GAL4/+; UAS-dfmr1/+
C155-GAL4/+; UAS-dfmr1,Df/+,abl1
C155-GAL4/+; UAS-dfmr1,Abl1/+,Abl1
C155-GAL4/+; UAS-dfmr1,UAS-rac1V17/+

Figure 13. Abi, Abl, and Rac1 Regulate Synaptic Growth by Modulating Futsch and Microtubule Stability

(A and B) Futsch immunoreactivity is increased in *abi* and *Abl* mutant and presynaptic Rac1 dominant negative motor axon terminals. (A) Single confocal slice of NMJ 6/7 stained with anti-Futsch (22C10) (red) and anti-HRP (green) taken from wild-type, abi^{5}/Df, Abl^{1}/Abl^{4}, *C155-GAL4*/+, and *C155-GAL4*/+; *UAS-*$rac1^{N17}$/+ larvae. Arrowheads represent Futsch-positive loops. Scale bar represents 5 μm. (B) Quantification of the ratio of mean 22C10 to HRP at NMJ 6/7 in the indicated genotypes. N=3, n=30, 15, 24, 24, 27, 18, and 12, respectively. One-way ANOVA was used for data analysis.

(C) Vinblastine (VB) administration suppresses the synaptic overgrowth caused by *abi* and *Abl* mutations and loss of presynaptic *rac1*, *scar*, and *kette*. Quantification of the numbers of boutons normalized to the muscle surface area and satellite boutons at NMJ 6/7 in the indicated genotypes grown in the absence (0 μM) or presence (1 μM) of VB.

All comparisons are with wild-type organisms unless otherwise indicated (*$p<0.001$; **$p<0.01$; n.s., not significant). Error bars are SEM for all figures.

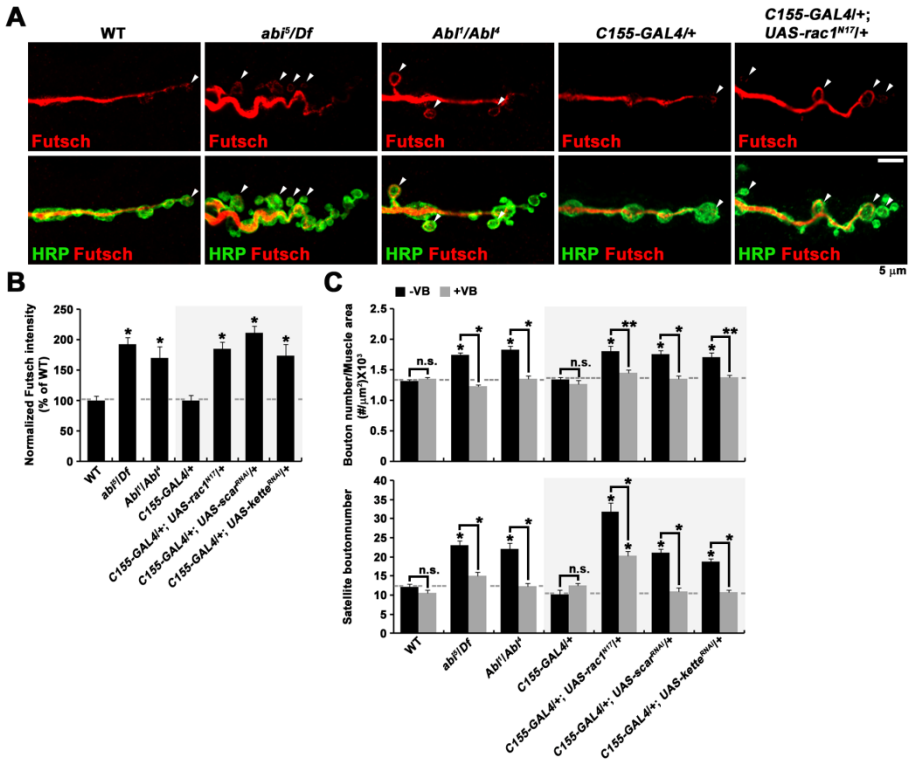
A
WT
abi5/Df
Abl1/Abl4
C155-GAL4/+
C155-GAL4/+; UAS-rac1N17/+
Futsch
HRP Futsch
5 μm
B
Normalized Futsch intensity (% of WT)
C
-VB
+VB
Bouton number/Muscle area (#/μm2)X10-3
Satellite boutonnumber
n.s.
WT
abi5/Df
Abl1/Abl4
C155-GAL4/+
C155-GAL4/+; UAS-rac1N17/+
C155-GAL4/+; UAS-scarnull/+
C155-GAL4/+; UAS-kettenull/+

(Figures 13A and 13B). Moreover, these mutants displayed an increased number of loop formations at the NMJ, which suggest that lack of *abi*, *Abl*, *rac1* and components of the WAVE complex enhances microtubule stability at the NMJ (Figure 13A). Therefore, I administered the microtubule severing drug vinblastine to Abi, Abl, Rac1, SCAR, or kette mutants to directly test the effect of microtubule stability on synaptic growth. The feeding of 1 μM vinblastine to wild-type larvae did not affect their synaptic growth. In contrast, the structural defects seen in *abi*, *Abl*, *rac1*, *scar*, or *kette* mutants were suppressed completely by the feeding of 1 μM vinblastine compared to non-fed (0 μM vinblastine) mutant larvae (Figure 13C). Overall, these results suggest that Abi, Abl, and Rac1 regulate synaptic growth via the dFMRP-Futsch pathway controlling microtubule stability.

9. Abi Interacts with Endocytic Mutants to Regulate Synaptic Growth

The key mechanism attenuating BMP signaling is endocytosis, which leads to endocytic degradation of the BMP receptor during synaptic development (Sweeny et al., 2002; O'Connor-Giles et al., 2008; Nahm et al., 2013). Activation of BMP signaling causes excessive satellite bouton formation at the NMJ, which resembles the phenotype of the endocytic mutants. Also, endocytosis requires actin polymerization, and many actin regulators are involved in endocytosis (Smythe and Ayscough et al., 2006). The small GTPase Rac1 and the WAVE complex, including Abi, SCAR, and Kette, are the major regulators of the Arp2/3 complex, which initiates actin polymerization. Mutation in *rac1* and components of the WAVE complex results in significantly increased satellite bouton formation.

Therefore, Abi may attenuate BMP signaling by BMP receptor endocytosis. To examine this hypothesis, I tested whether Abi functions with endocytic proteins to regulate synaptic growth by performing transheterozygous interaction experiments between *abi* and *dap160* or *endoA*. Loss of a single copy of each mutant allele resulted in no defect in bouton formation. However, deletion of both a single copy of the mutant allele for *abi* and *dap160* or of *abi* and *endoA* resulted in elevated overall bouton and satellite bouton formation (Figures 14A and 14B). This genetic evidence raises the possibility that Abi may negatively regulate BMP signaling through endocytic mechanisms in the NMJ. In a previous study, Nwk has been identified as a WASP interactor for regulating synaptic growth (Coyle et al., 2004). Nwk also interacts with the BMP type I receptor Thickveins (Tkv) and Dap160 or EndoA to inhibit retrograde BMP signaling during synaptic growth (O'Connor-Gailes et al., 2008). However, transheterozygotes for *abi* and *nwk* displayed no differences in synaptic growth. This result is consistent with the data showing that Abi and WASP have no genetic relationship with regard to synaptic growth control, and that Nwk and Abi regulate BMP signaling through a distinct pathway.

If endocytosis caused by Abi inhibits BMP signaling, internalization of the BMP receptor from the plasma membrane should be inhibited in *abi* mutants. To determine this possibility, I compared the surface expression of the type I BMP receptor Tkv in control and *abi* mutant backgrounds. To label surface Tkv, *UAS-Myc-tkv* was expressed by the *C155-GAL4* driver in wild-type and abi^{5}/Df larvae. Myc-Tkv expressed at the bouton surface was increased by ~79% in the *abi* mutant background compared to expression in the wild-type background, indicating that internalization of Tkv may be inhibited in *abi* null mutants (Figures 14C and 14D). These data suggest the hypothesis that Abi is required for regulation of surface Tkv

Figure 14. Abi Interacts with Endocytic Mutants to Regulate Synaptic Growth

(A and B) Transheterozygous interaction between *abi* and endocytic mutants. (A) Confocal images of NMJ 6/7 stained with anti-HRP (green) taken from the indicated genotypes. Scale bar represents 20 μm. (B) Quantification of the synaptic structure at NMJ 6/7 in the following genotypes: wild-type, abi^{5}/+, $endoA^{\Delta 4}$/+, $dap160^{\Delta 1}$/+, nwk^{1}/+, abi^{5},+/+,$endoA^{\Delta 4}$, abi^{5},+/+,$dap160^{\Delta 1}$, and abi^{5},+/+,nwk^{1}. N=3, n=12, 12, 12, 12, 12, 12, 12, and 12, respectively. One-way ANOVA was used for data analysis.

(C and D) Abi regulates surface expression of Tkv at the NMJ. (C) Confocal images of NMJ 6/7 labeled with anti-Myc (red) and anti-HRP taken from the indicated genotypes. (D) Quantification of the ratio of mean Myc-Tkv to HRP fluorescence intensity, with the values as percentages of the intensities seen in *C155-GAL4*/+; *UAS-Myc-tkv* larvae (control). All comparisons are with wild-type organisms unless otherwise indicated (*$p<0.001$). Error bars are SEM for all figures.

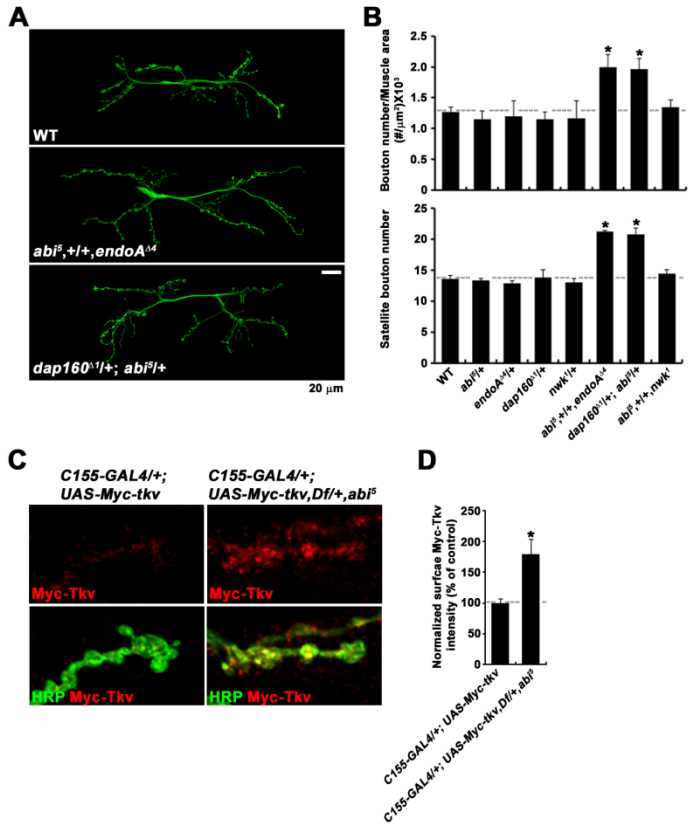
A
WT
abi5,+/+,endoAΔ4
dap160Δ1/+; abi5/+
20 μm
B
Bouton number/Muscle area (#/μm²)X10³
Satellite bouton number
WT
abi5/+
endoAΔ4/+
dap160Δ1/+
nwk1/+
abi5,+/+,endoAΔ4
dap160Δ1/+; abi5/+
abi5,+/+,nwk1
C
C155-GAL4/+; UAS-Myc-tkv
C155-GAL4/+; UAS-Myc-tkv,Df/+,abi5
Myc-Tkv
HRP Myc-Tkv
D
Normalized surface Myc-Tkv intensity (% of control)
C155-GAL4/+; UAS-Myc-tkv
C155-GAL4/+; UAS-Myc-tkv,Df/+,abi5

expression. Altogether, BMP signaling is restrained by Abi-dependent BMP receptor endocytosis at the NMJ.

10. Gbb Induces Macropinocytosis in a Dose-Dependent Manner in Cultured Neurons

My results so far suggest that Abi, Abl, and Rac1 negatively regulate BMP signaling to control synaptic growth via BMP receptor endocytosis. However, the specific endocytic mechanism regulating BMP signaling remained unclear. Many studies have revealed that the Rac1-Abi-WAVE complex is a key regulator of macropinocytosis (Kerr and Teasdale, 2009; Fujii et al., 2013). Macropinocytosis is an inducible, actin-dependent, endocytic mechanism that requires external signals, such as EGF or other signaling molecules, to degrade the extra particles and receptors expressed in the membrane (Lim and Gleeson, 2011). However, the role of macropinocytosis in neurons and the requirement of BMP signaling in macropinocytosis are unknown. Therefore, I first test whether BMP signaling induces macropinocytosis in neurons. To perform a macropinocytosis assay in *Drosophila* neuronal cells, BG2-c2 cells, I produced Gbb conditioned media from S2R+ cells. Cells expressing *pAc-gbb* produced more than 200 ng/ml of secreted Gbb, which was determined by western blot analysis (Figure 15A). I then treated BG2-c2 cells with low to high doses (5, 10, 50, 100, and 200 ng/ml) of Gbb and assayed macropinocytosis activity using 70 kDa dextran conjugated to tetramethylrhodamine (TMR), a high molecular weight dextran selectively internalized to macropinosomes (Figures 15B and 15C) (Cosimo et al., 2014; Lei et al., 2015). For the macropinocytosis assay, cells were treated with various

Figure 15. Gbb Induces Macropinocytosis in a Dose-Dependent Manner in Cultured Neurons

(A) Western blot analysis of Gbb-conditioned media (50 and 100 ng/ml) probed with anti-Gbb. Processed Gbb (14 kDa) secreted from *pAc-gbb* expressing S2R+ cells is detected.

(B) BG2-c2 cells were serum starved for 6 hr and, prior to the macropinocytosis assay, cells were treated with (5, 10, 50, 100, and 200 ng/ml) or without (0 ng/ml) Gbb. Then, cells were pulsed with 2 mg/ml 70 kDa TMR-dextran in the presence or absence of Gbb for 5 min. TMR-dextran is internalized in the presence of high concentrations of Gbb, but not with 0 ng/ml Gbb. Z-stack images of BG2-c2 cells with TMR-dextran uptake (red) and stained with DAPI (blue). For all following macropinocytosis assays performed in BG2-c2 cells, 2mg/ml of 70kDa TMR-dextran and 50 ng/ml Gbb were used. Scale bar represents 5 μm.

(C) Quantification of total fluorescence intensity of TMR-dextran (A.U., arbitrary units) and the number of macropinosomes in the presence of Gbb (5 ng/ml, 20 ng/ml, 50 ng/ml, 100 ng/ml, 200 ng/ml) in BG2-c2 cells. The punctate structures of TMR-dextran (indicating a diameter greater than 0.2 μm) were counted in each cell to quantify the number of macropinosomes present. To quantify the total fluorescence intensity and number of macropinosomes, each cell was imaged with Z-slices throughout the whole cell at 0.33-μm intervals and maximal projection. Quantifications were done in three independent experiments with a total of 42 cells per condition.

Error bars are SEM for all figures.

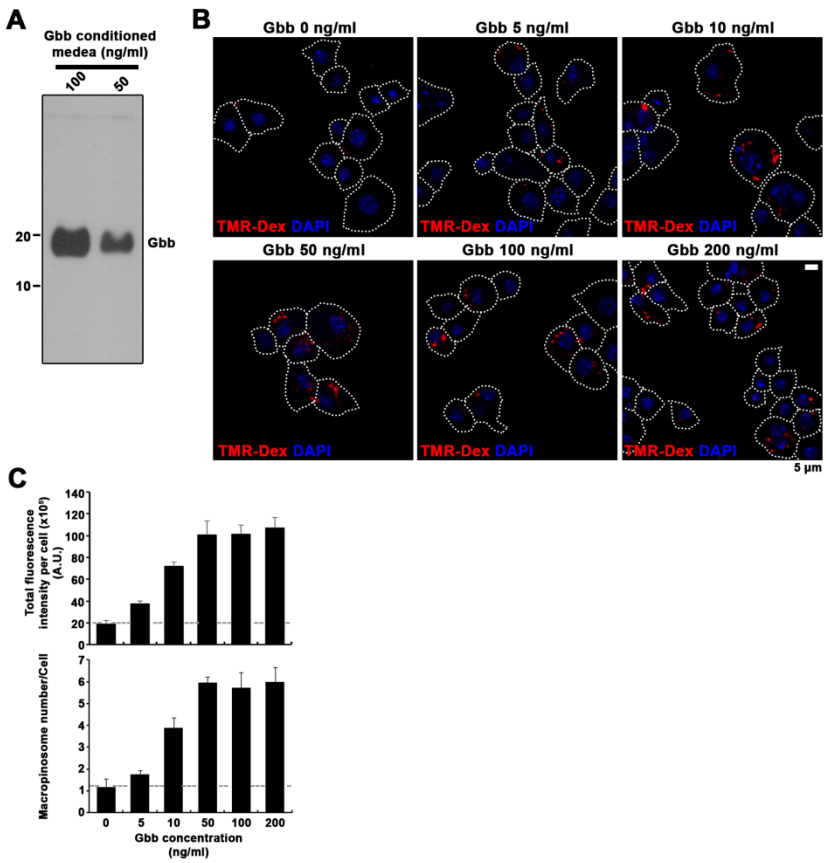
A
Gbb conditioned medea (ng/ml)
100
50
20
10
Gbb
B
Gbb 0 ng/ml
Gbb 5 ng/ml
Gbb 10 ng/ml
Gbb 50 ng/ml
Gbb 100 ng/ml
Gbb 200 ng/ml
TMR-Dex DAPI
5 µm
C
Total fluorescence intensity per cell (x10⁶) (A.U.)
Macropinosome number/Cell
Gbb concentration (ng/ml)
0
5
10
50
100
200

concentrations (1, 2, 5, 10, 50, 100, or 200 ng/ml) of Gbb or without Gbb (0 ng/ml) for 10 min. Then, TMR-dextran was sequentially pulsed for 5 min, and the number or intensity of internalized TMR-dextran puncta (>0.2 μm) was measured. TMR-dextran puncta with diameters over 0.2 μm indicate macropinosomes (Kerr and Teasdale, 2009). Cells treated without Gbb (0 ng/ml) or with low concentrations of Gbb (1 and 2 ng/ml, data not shown) did not uptake TMR-dextran, and treatment with 5 ng/ml Gbb also resulted in little to no effect on the cells (Figures 15B and 15C). On the contrary, the total number and fluorescence intensity of TMR-dextran puncta were five times higher in cells treated with high doses of Gbb (50, 100, or 200 ng/ml) than in cells without Gbb induction (Figures 15B and 15C). These data support the hypothesis that Gbb induces macropinocytosis in neurons.

To validate whether the dextran internalization activity induced by Gbb is truly macropinocytosis, I tested the requirement of known macropinocytosis regulators for Gbb-induced micropinocytosis by knock-down experiments and pharmacological approaches in BG2-c2 cells. Cells treated with *rabankyrin* (a macropinocytosis regulator) dsRNA showed reduced macropinocytosis activity induced by Gbb when compared with control cells (Figures 16B and 16C). Moreover, macropinocytosis activated by Gbb was inhibited by 25 μM LY294002 (a PI3-kinase inhibitor which specifically inhibits macropinocytosis) or 100 μM 5-N-ethyl-N-isopropyl-amiloride (EIPA, an inhibitor of the Na+/H+ exchanger and subsequent endocytosis) treatment in BG2-c2 cells, which was consistent with previous observations (Figure 16C). Together, these results demonstrated that Gbb triggers macropinocytosis in BG2-c2 cells.

Figure 16. Abi, Abl, Rac1, and the Wave Complex Are Required for Gbb-Induced Macropinocytosis in BG2-c2 Cells

(A) RT-PCR analysis of BG2-c2 cells transfected with dsRNA against *abi*, *Abl*, *rac1*, *scar*, *kette*, *rabankyrin*, *endophilin A* (*endoA*), or *nervous wreck* (*nwk*). The efficacy and specificity of each dsRNA were determined by RT-PCR analysis. The expression level of *rp49* was used as an internal control.

(B and C) Gbb-induced macropinocytosis is defective in cells with *abi*, *Abl*, *rac1*, *scar*, or *rabankyrin* knock-down. (B) For the macropinocytosis assay, BG2-c2 cells were induced with Gbb for 10 min and pulsed with TMR-dextran in media containing Gbb for 5 min. Z-stack images of BG2-c2 cells showing TMR-dextran uptake (red) and nuclei stained with DAPI (blue). Scale bar represents 5 μm. (C) The total fluorescence intensity (A.U.) and number of macropinosomes per cell are depleted by *abi*, *Abl*, *rac1*, *scar*, *kette*, *rabankyrin*, *endoA*, *dap160*, and *nwk* dsRNA compared with controls (white box) and by treatment with macropinosome-specific inhibitors (LY294002, EIPA) compared with treatment with DMSO (control) (gray box). Cells were treated with DMSO, 25 μM LY294002, or 100 μM 5-N-ethyl-N-isopropyl-amiloride (EIPA) at 25°C for 30 min before incubation with conditioned medium containing Gbb and TMR-dextran. Quantification was done in three independent experiments with a total of 30 cells per condition. All comparisons in white box are with control and all comparisons in gray box are with DMSO (control) (*$p<0.001$).

(D) Quantification of total fluorescence intensity (A.U.) of TMR-dextran per cell in HA-abi-, HA-abiΔ30-65-, HA-abiΔ123-175-, HA-abi4YE-, or HA-abi4YF-expressing BG2-c2 cells with *abi* knock-down by *abi* dsRNA treatment. All

comparisons are with HA-Abi-expressing cells without Gbb treatment (-Gbb) (*p<0.001).

Error bars are SEM for all figures.

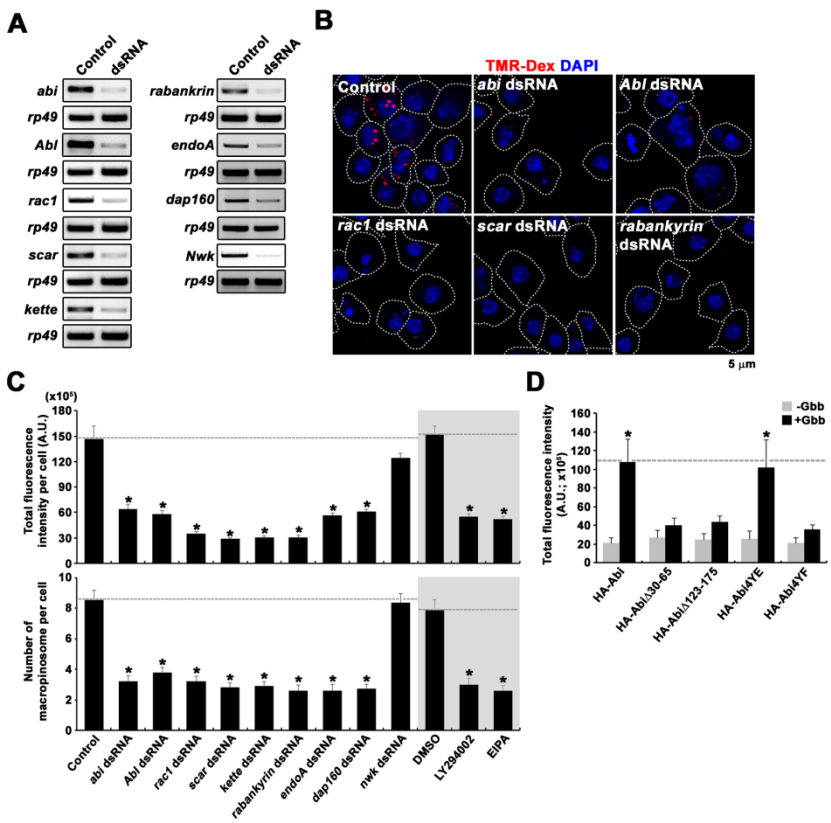

11. Abi, Abl, and the WAVE Complex Is Required for Macropinocytosis in BG2-c2 Cells

Previous studies have shown that Abi1 and components of the WAVE complex are essential for Rac1-dependent macropinocytosis in non-neuronal cells, such as fibroblasts or macrophages (Dubielecka et al., 2010; Innocenti et al, 2005; Seastone et al., 2001) Therefore, to address whether Abi is involved in Gbb-induced macropinocytosis in neurons, I knocked-down *abi* in BG2-c2 cells through treatment with *abi* dsRNA. The knock-down efficiency of *abi* dsRNA was tested by RT-PCR, and the transcript level of *abi* in *abi* dsRNA-treated cells was reduced compared to control cells (Figure 16A). Additionally, macropinocytosis was reduced in the cells lacking *abi* compared to control cells (Figures 16B and 16C). This result supports the hypothesis that Abi is required for Gbb-induced macropinocytosis in cultured neurons.

Next, to investigate the requirement of SCAR/Kette binding and Abi phosphorylation for macropinocytosis in neurons, I determined whether expression of HA-AbiΔ30-65, HA-AbiΔ123-175, HA-Abi4YE, or HA-Abi4YF restores the reduction of macropinocytosis in cells lacking *abi*. Without Gbb (-Gbb), activity indicative of macropinocytosis was not shown in HA-Abi-, HA-AbiΔ30-65-, HA-AbiΔ123-175-, HA-Abi4YE-, or HA-Abi4YF-expressing cells (Figure 16D), which demonstrates that Abi itself does not induce macropinocytosis. When Gbb was applied (+Gbb), HA-Abi and HA-Abi4YE expression rescued the *abi* knock-down phenotype, whereas expression of HA-AbiΔ30-65, HA-AbiΔ123-175, or HA-Abi4YF did not reverse the defect of macropinocytosis activity caused by *abi* knock-down (Figure 16D). These data support the hypothesis that binding of

SCAR or Kette and the phosphorylation of Abi by Abl kinase are necessary to regulate Gbb-induced macropinocytosis in BG2-c2 cells. Finally, to further investigate whether the Rac1 and Abi binding partners Abl, SCAR, and Kette are also required for macropinocytosis in neurons, I knocked-down each of these genes in BG2-c2 cells using dsRNA and performed macropinocytosis assays. The expression levels of *abl*, *rac1*, *scar*, and *kette* mRNA in BG2-c2 cells treated with dsRNA for each gene was quantified by RT-PCR, and the results showed an ~80% reduction in mRNA expression for each gene compared to non-treated cells (control) (Figure 16A). In comparison to mock-treated cells (control), reduction of *abl*, *rac1*, *scar*, or *kette* expression caused a decrease in both the number and staining intensity of the macropinosomes, showing phenotypic similarity to *abi* knock-down cells (Figures 16B and 16C). I concluded from these experiments that Abl, Rac1, and the WAVE complex are also critical for regulating Gbb-activated macropinocytosis in cultured neurons.

12. Macropinocytosis and Maturation of Macropinosomes in BG2-c2 Cells

The stages of macropinocytosis may differ between cell types, and the mechanisms underlying the maturation of macropinosomes in neurons are unknown. Therefore, I monitored Gbb-induced macropinosome formation and maturation in BG2-c2 cells to dissect the macropinocytosis process in neurons. For evaluation of the early stage of macropinocytosis, PLCδ_1-PH-GFP (a marker of membrane ruffles and cup closure, which binds to PI(4,5)P2), and Akt-PH-GFP (a marker of macropinosome cup closure and closed macropinosomes (early

macropinosome), which binds to PI(3,4,5)P3) were used (Figures 17 and Figure 18). Maturation of macropinosomes from the early to the later stage was monitored with Rabankyrin-GFP (an early macropinosome to early endosome marker), GFP-Rab5 (an early endosome marker), and Rab7-GFP (a late endosome marker) (Figures 19, 20, and 21). Serum-starved BG2-c2 cells were activated by treatment with Gbb, pulsed for 2 min with TMR-dextran, and chased for 0, 1, 3, 8, or 18 min to assess the early to later steps of macropinosome maturation. At the 2min pulse time, TMR-dextran colocalized mostly with PLCδ_1-PH-GFP (~84%) and Akt-PH-GFP (~90%), but neither Rabankyrin nor early/late endosome markers colocalized with TMR-dextran. These data indicate that the membrane ruffles were not fully closed to form macropinosomes in BG2-c2 cells at this time point. Next, when TMR-dextran was internalized for 3 min, Akt-PH-GFP (~85%) was still highly colocalized with TMR-dextran, GFP-Rabankyrin (~30%) had started to colocalize with TMR-dextran, and a few GFP-Rab5 signals (~14%) were co-labeled with TMR-dextran. These data show that the membrane ruffles were already closed, and macropinosomes were formed at this time point. When 5 to 10 min passed, TMR-dextran was highly colocalized with GFP-Rabankyrin and GFP-Rab5, and the colocalization rate of TMR-dextran with PLCδ_1-PH or Akt-PH was decreased, indicating that the macropinosomes were fused with early endosomes. Finally, when TMR-dextran was internalized for 20 min, only Rab7-GFP (82.5%) remained colocalized with TMR-dextran. In conclusion, macropinocytosis in neurons is first accompanied by PLC and Akt in the first 2 to 3 min to form the membrane ruffles and macropinocytic cups. Next, Rabankyrin is recruited to the early macropinosomes 3 to 5 min after induction of macropinocytosis. Finally, internalized macropinosomes are trafficked to early endosomes and late endosomes

Figure 17. Monitoring of Macropinosomes in BG2-c2 Cells with PLCδ_1-PH-GFP

BG2-c2 cells transiently expressing *pAc-PLCδ_1-PH-GFP* were serum starved for 6 hr; treated with 50 ng/ml Gbb for 10 min; pulsed for 2 min with TMR-dextran mixed with Gbb; chased for 0 min, 1 min, 3 min, 8 min, or 18 min; and finally fixed. TMR-dextran pulsed for 2 min is co-localized with PLCδ_1-PH-GFP, a membrane ruffle and unclosed macropinocytic cup marker. Maximal projected image of BG2-c2 cells stained with DAPI (blue). Arrowheads represent dextran co-labeled with PLCδ_1-PH-GFP. Scale bar represents 5 μm.

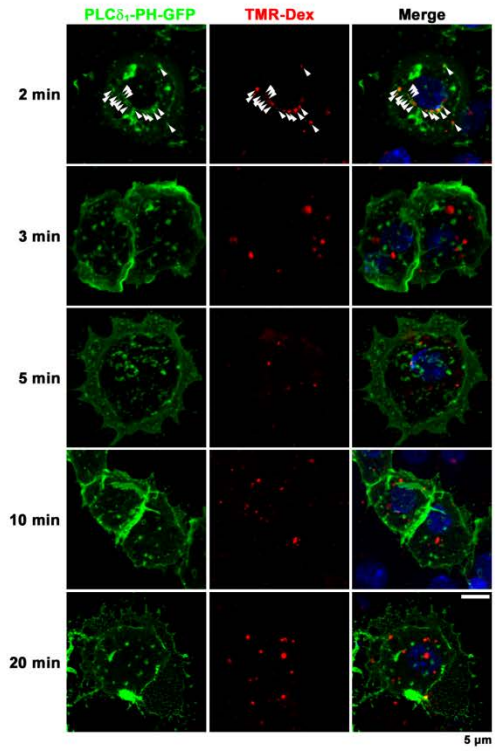
PLCδ1-PH-GFP
TMR-Dex
Merge
2 min
3 min
5 min
10 min
20 min
5 µm

Figure 18. Monitoring of Macropinosomes in BG2-c2 Cells with Akt-PH-GFP

BG2-c2 cells transiently expressing *pAc-Akt-PH-GFP* were serum starved for 6 hr; induced by treatment with 50 ng/ml Gbb for 10 min; pulsed for 2 min with TMR-dextran mixed with 50 ng/ml Gbb; chased for 0 min, 1 min, 3 min, 8 min, or 18 min; and finally fixed. At early pulse-chase times (2 min pulse and 0 or 1 min chase), TMR-dextran is co-localized to Akt-PH-GFP, a closed early macropinosome marker. Maximal projected confocal images of BG2-c2 cells stained with DAPI (blue). Arrowheads represent internalized dextran co-labeled with PLC-PH-GFP. Scale bar represents 5 μm.

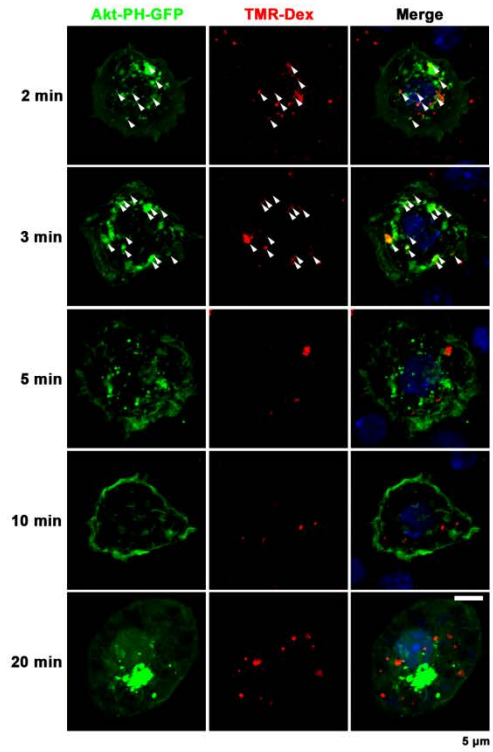
Akt-PH-GFP
TMR-Dex
Merge
2 min
3 min
5 min
10 min
20 min
5 µm

Figure 19. Monitoring of Macropinosomes in BG2-c2 Cells with GFP-Rabankyrin

BG2-c2 cells transiently expressing *pAc-GFP-Rabankyrin* were serum starved for 6 hr; induced by treatment with 50 ng/ml Gbb for 10 min; pulsed for 2 min with TMR-dextran mixed with Gbb; chased for 0 min, 1 min, 3 min, 8 min, or 18 min; and finally fixed. GFP-Rabankyrin (a macropinosome marker) is mostly co-localized with dextran at 5 min and 10 min (2 min pulse and 3 or 8 min chase). Maximal projected confocal images of BG2-c2 cells stained with DAPI (blue). Arrowheads represent internalized dextran co-labeled with GFP-Rabankyrin. White dotted line indicates cortical membranes of BG2-c2 cell. Scale bar represents 5 μm.

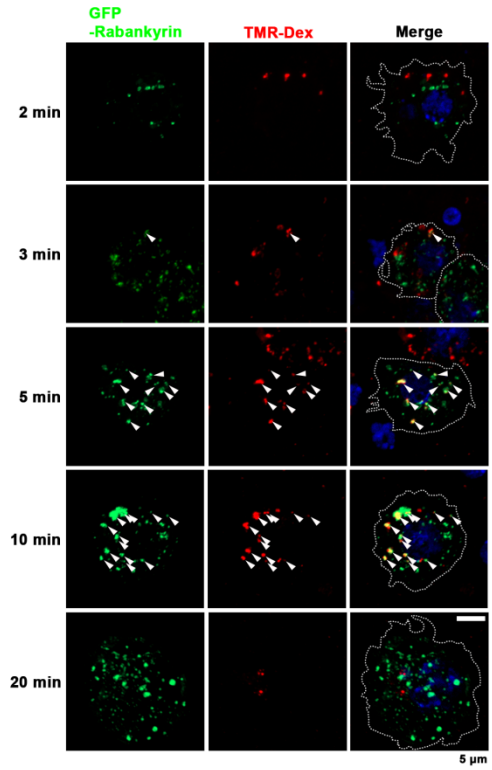
GFP
-Rabankyrin
TMR-Dex
Merge
2 min
3 min
5 min
10 min
20 min
5 μm

Figure 20. Monitoring of Macropinosomes in BG2-c2 Cells with GFP-Rab5

BG2-c2 cells transiently expressing *pAc-GFP-Rab5* were serum starved for 6 hr; activated by treatment with 50 ng/ml Gbb for 10 min; pulsed for 2 min with TMR-dextran mixed with Gbb; chased for 0 min, 1 min, 3 min, 8 min, or 18 min; and finally fixed. The majority of GFP-Rab5 (an early endosome marker) is co-labeled with dextran at 10 min (2 min pulse and 8 min chase). Maximal projected confocal images of BG2-c2 cells stained with DAPI (blue). Arrowheads represent internalized dextran co-labeled with GFP-Rab5. White dotted line indicates cortical membranes of BG2-c2 cell. Scale bar represents 5 μm.

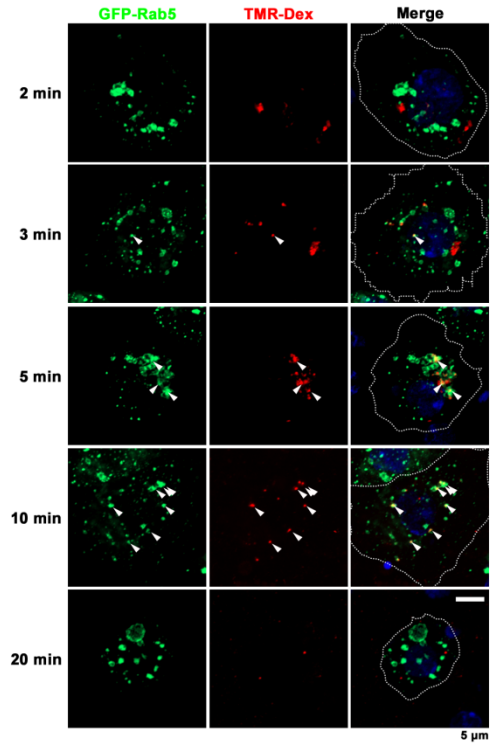
GFP-Rab5
TMR-Dex
Merge
2 min
3 min
5 min
10 min
20 min
5 µm

Figure 21. Monitoring of Macropinosomes in BG2-c2 Cells with Rab7-GFP

BG2-c2 cells transiently expressing *pAc-GFP-Rab7* were serum starved for 6 hr; induced by treatment with 50 ng/ml Gbb for 10 min; pulsed for 2 min with TMR-dextran mixed with Gbb; chased for 0 min, 1 min, 3 min, 8 min, or 18 min; and finally fixed. Dextran is co-labeled with Rab7-GFP (a late endosome marker) at minute 20 of the TMR-dextran pulse-chase experiment. Maximal projected confocal images of BG2-c2 cells stained with DAPI (blue). Arrowheads represent internalized dextran co-labeled with GFP-Rab5. White dotted line indicates cortical membranes of BG2-c2 cell. Scale bar represents 5 μm.

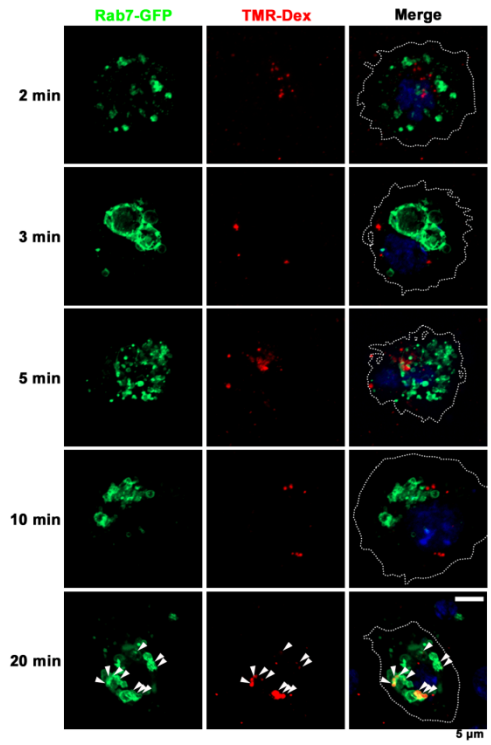
Rab7-GFP
TMR-Dex
Merge
2 min
3 min
5 min
10 min
20 min
5 µm

Figure 22. Abi is Involved in the Early Stages of Macropinocytosis

(A and B) Abi is associated with macropinosomes at the early macropinocytosis stage in BG2-c2 cells. (A) BG2-c2 cells expressing *pAc-HA-Abi* were serum starved for 6 hr, treated with 50 ng/ml Gbb for 10 min, pulsed for 2 min with TMR-dextran mixed with Gbb, and chased (0, 1, 2, 3, 8 or 18 min) in serum-free medium lacking TMR-dextran and Gbb. HA-Abi is associated with TMR-dextran at 2 min and 3 min. Times indicate the summation of pulse and chase times. Maximal projected confocal images of BG2-c2 cells stained with DAPI (blue). Arrowheads represent internalized dextran associated with HA-Abi. White dotted line indicates cortical membranes of BG2-c2 cells. Scale bar represents 5 μm. (B) Quantification of the amount of TMR-dextran co-localized with PLCδ_1-PH-GFP (blue line), Akt-PH-GFP (purple line), GFP-Rabankyrin (red line), GFP-Rab5 (orange line), or GFP-Rab7 (green line) and TMR-dextran associated with HA-Abi (black dotted line) from the results of the pulse-chase assay. Quantification was done in three independent experiments with a total of six cells per condition. Data represent mean ± SEM.

(C) Still frames showing the formation of a GFP-Abi-labeled early macropinosome. Live image of GFP-Abi (green) and latex bead (red). BG2-c2 cells expressing *pAc-GFP-abi* were serum starved for 6 hr, treated with conditioned medium containing 50 ng/ml Gbb and 20 μg/ml latex beads, and live-imaged with confocal microscopy. Both GFP-Abi and the latex bead were filmed from the initial internalization of the latex bead (0 min) to the detaching of GFP-Abi from the latex bead (5 min). White dotted line indicates the cortical membranes of BG2-c2 cells. Scale bar represents 0.5 μm.

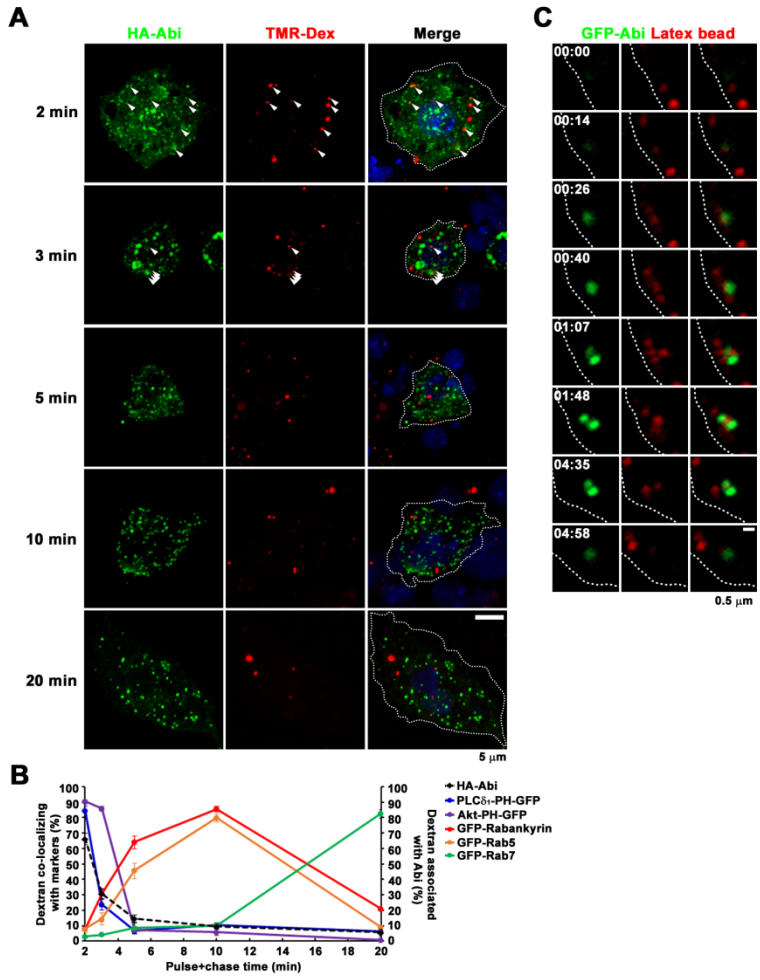
A
HA-Abi
TMR-Dex
Merge
2 min
3 min
5 min
10 min
20 min
5 μm
C
GFP-Abi Latex bead
00:00
00:14
00:26
00:40
01:07
01:48
04:35
04:58
0.5 μm
B
Dextran co-localizing with markers (%)
Dextran associated with Abi (%)
Pulse+chase time (min)
HA-Abi
PLCδ1-PH-GFP
Akt-PH-GFP
GFP-Rabankyrin
GFP-Rab5
GFP-Rab7

by the small GTPases Rab5 and Rab7 10 to 20 min after the beginning of macropinocytosis (Figures 17, 18, 19, 20, 21, and 22B).

13. Abi Is Involved in the Early Stages of Macropinocytosis

During macropinocytosis, Rac1 is required for membrane ruffling and macropinocytic cup formation, the initial step of macropinocytosis (Fujii et al., 2013). Rac1 relays signals to the WAVE complex to activate actin polymerization. Therefore, I hypothesized that Abi might be required for early macropinocytosis in neurons. To test this hypothesis, I performed a pulse-chase experiment with TMR-dextran in Gbb-induced BG2-c2 cells expressing *pAc-HA-abi*. At the early time point (2 min), when membrane ruffling and macropinocytic cup formation occur, over 66% of HA-Abi was associated with TMR-dextran, and its association decrease rapidly after 3 to 5 min, the time when macropinosomes associate with Rabankyrin and are referred to as early macropinosomes (Figures 22A and 22B). At later times (10~20 min), when early macropinosomes become late macropinosomes, only 6% of HA-Abi was associated with TMR-dextran (Figures 22A and 22B). These data support the idea that Abi is required at early step of macropinocytosis. Next, early association of Abi with macropinosomes was directly observed by time-lapse live imaging in BG2-c2 cells. Latex beads (a macropinosome marker) with 50 ng/ml Gbb were applied to GFP-Abi expressing cells, and the movement of GFP-Abi was monitored. Live images of GFP-Abi and latex beads showed that GFP-Abi rapidly targeted to the internalizing latex beads at 15 to 30 sec, and after 2 to 3 min, GFP-Abi was detached from the latex beads

(Figure 22C). Therefore, Abi is involved in the early stage of Gbb-induced macropinocytosis in cultured neurons.

14. Abl Kinase Activity Is Necessary for Abi Targeting to Macropinocytic Structure

Given that cells activated by Gbb formed macropinosomes, and that Abi was involved in the early stage of this process, I questioned whether Abi is transiently targeted to macropinocytic structures at the plasma membrane after Gbb induction. To test this hypothesis, I co-expressed HA-Abi and PLCδ_1-PH-GFP in BG2-c2 cells with (+Gbb) or without (-Gbb) Gbb and then pulsed the cells with TMR-dextran for 2 min. Without Gbb treatment, the distribution of HA-Abi was diffuse in the cytoplasm with no specific pattern, and that of PLCδ_1-PH-GFP was diffuse under the plasma membrane, which showed no sign of ruffling or macropinocytosis activity (Figure 23A; -Gbb). After Gbb treatment, TMR-dextran started to internalize within 2 min of the pulse, which was associated with HA-Abi immunosignals in a punctuated pattern. Moreover, this punctate HA-Abi staining was located on PLCδ_1-PH-GFP-positive membranes (Figure 23A; +Gbb). Thus, Abi was localized to the macropinocytic structure in the early stage of macropinocytosis after Gbb activation.

Next, I examined whether Abl kinase or the WAVE complex is required for Abi targeting to macropinosomes using HA-Abi mutants lacking the WAVE complex binding domain (HA-Abi Δ30-65, HA-Abi Δ123-175) or phosphorylation activity (HA-Abi4YE, HA-Abi4YF). In Gbb non-treated cells, the distribution of HA-Abi, HA-AbiΔ30-65, HA-AbiΔ123-175, or HA-Abi4YF was diffuse in the

Figure 23. Abl-Mediated Phosphorylation of Abi Is Essential for Its Localization to Early Macropinocytic Structures

(A and B) Abi is targeted to early macropinosomes upon Gbb stimulation, and Abi phosphorylation is necessary for Abi targeting to macropinocytic structures. (A) BG2-c2 cells expressing PLCδ_1-PH-GFP and HA-Abi were serum starved for 6 hr, treated with 50 ng/ml Gbb (+Gbb) or without Gbb (-Gbb) for 10 min, and pulsed with TMR-dextran with Gbb (+Gbb) or without Gbb (-Gbb) for 2 min. A single confocal section showing BG2-c2 cells; arrowheads indicate that HA-Abi (blue) is co-localized with both TMR-dextran (red) and PLCδ_1-PH-GFP (green). Scale bar represents 5 μm. (B) Quantification of HA-Abi puncta colocalizing with PLC-PH-GFP in BG2-c2 cells. BG2-c2 cells expressing both *pAc-PLCδ_1-PH-GFP* and *abi* constructs (*pAc-HA-abi*, *pAc-HA-abiΔ30-65*, *pAc-HA-abiΔ123-175*, *pAc-HA-abi4YE*, and *pAc-HA-abi4YF*) depleted of *abi* by *abi* dsRN*A* treatment were serum starved for 6 hr and then incubated with Gbb (+Gbb) or without Gbb (-Gbb) for 10 min. The cells were fixed for 10 min with 4% formaldehyde in PBS, permeabilized with PBS containing 0.1% saponin for 10 min, and then stained with an anti-HA antibody and an appropriate fluorescent-conjugated secondary antibody. Quantification was done in three independent experiments with a total of five cells per condition. All comparisons are with HA-AbiWT without Gbb unless otherwise indicated (*$p<0.001$). Error bars are SEM for all figures.

(C) The kinase activity of Abl is necessary for Abi targeting to the early macropinosomes. BG2-c2 cells expressing HA-Abi and Abl-Myc or Abl^{KN}-Myc were serum starved for 6 hr, treated with 50 ng/ml Gbb (+Gbb) or without Gbb (-Gbb) for 10 min, and pulsed with TMR-dextran with Gbb (+Gbb) or without Gbb

(-Gbb) for 2 min. Triple colocalization of HA-Abi (green), Abl-Myc (white), and TMR-dextran (red) is shown with arrowheads. Scale bar represents 5 μm.

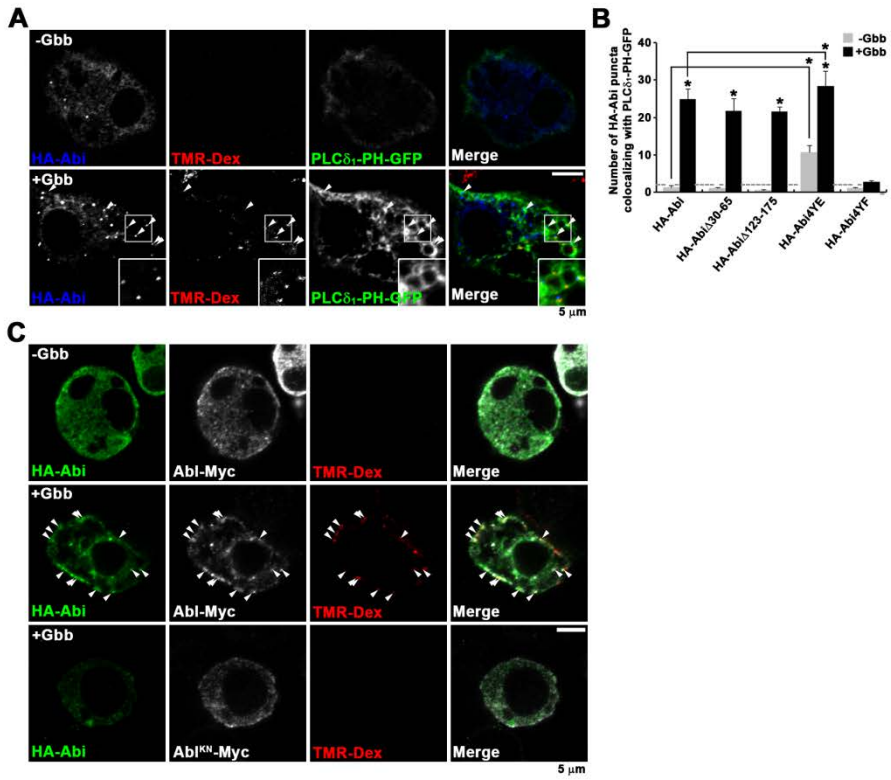

cytoplasm. However, the amount of HA-Abi4YE targeted to the plasma membrane was 8-fold higher than that of HA-Abi in cells without Gbb treatment, indicating that phosphorylation facilitates the targeting of Abi to the membrane (Figure 23B; gray bars, -Gbb). In the Gbb induced state (+Gbb), HA-Abi, HA-AbiΔ30-65, HA-AbiΔ123-175, and HA-Abi4YE were all localized to the PLCδ_1-PH-GFP-positive membrane, but HA-Abi4YF was still diffuse, as in the non-stimulated state (-Gbb) (Figure 23B; black bars, +Gbb). Together, these results indicate that the targeting of Abi by Gbb stimuli requires the phosphorylation of Abi but not interaction with the WAVE complex. Therefore, Abl kinase activity may be involved in Abi translocation to the macropinocytic site in the membrane. Finally, to directly examine this idea, I cotransfected BG2-c2 cells with either wild-type Abl-Myc or dominant-negative Abl-Myc (AblKN-Myc) and HA-Abi and conducted macropinocytosis assays. In the non-stimulated state (-Gbb), HA-Abi and Abl-Myc staining was diffuse in the cytoplasm, showing no special pattern, and macropinocytosis did not occur (Figure 23C). After Gbb treatment (+Gbb), HA-Abi and Abl-Myc were colocalized at the macropinosome-enriched area of the plasma membrane. In contrast, HA-Abi expressed with AblKN-Myc in Gbb-stimulated cells displayed the same immunoreactivity pattern as that of HA-Abi in cells without Gbb induction (Figure 23C), indicating that, if Abl kinase activity is inhibited, Abi is not able to localize to the macropinocytic site. These results support the notion that Gbb not only activates macropinocytosis, but also activates Abl kinase in order to target phosphorylated Abi to the site where macropinocytosis may occur.

15. The Kette- and SCAR-Binding Domains of Abi are Essential for Localized Actin Polymerization at Macropinocytic Structures

When macropinocytosis is induced, the WAVE complex, activated by Rac1, promotes actin cytoskeleton rearrangement underneath the plasma membrane to form ruffles (Fujii et al., 2013; Kerr and Teasdale, 2009). Thus, I hypothesized that Abi and its binding with components of the WAVE complex are required for actin polymerization at macropinocytic structures after Abi translocation to these sites. Macropinocytosis assays were conducted using BG2-c2 cells transfected with HA-Abi, HA-AbiΔ30-65, HA-AbiΔ123-175, HA-Abi4YE, or HA-Abi4YF, and F-actin was visualized using phalloidine. After activation with Gbb, HA-Abi and HA-Abi4YE were localized to macropinosomes enriched with F-actin (Figures 24A and 24B). However, although their immunosignals were shown in punctate structures, HA-AbiΔ30-65- or HA-AbiΔ123-175-expressing cells were lacking TMR-dextran. Moreover, F-actin was not colocalized with HA-AbiΔ30-65 or HA-AbiΔ123-175 puncta, and the overall expression of F-actin in these cells was lower than in wild-type HA-Abi-expressing cells (Figures 24A and 24B). HA-Abi4YF-expressing cells displayed diffuse expression of Abi and reduction of both macropinocytosis and actin polymerization (Figure 24B). These results suggest that Abi- and WAVE complex-dependent actin polymerization is responsible for Gbb-induced macropinosome formation.

Figure 24. The Kette- & SCAR-Binding Domains of Abi are Essential for Localized Actin Polymerization at Macropinocytic Structures

(A) Serum starved BG2-c2 cells expressing HA-Abi, HA-AbiΔ30-65, or HA-AbiΔ123-175 in *abi* dsRNA treated conditions were pre-activated with 50 ng/ml Gbb for 10 min, pulsed with TMR-dextran with Gbb for 2 min, and finally fixed. Permeabilized cells were than stained with anti-HA and phalloidine (F-actin). Arrowheads indicate HA-Abi (green) puncta with F-actin (white) and TMR-dextran (red). Scale bar represents 5 μm.

(B) Quantification of the number of HA-Abi puncta colocalizing with F-actin and TMR-dextran in HA-abi-, HA-abiΔ30-65-, HA-abiΔ123-175-, HA-abi4YE-, or HA-abi4YF-expressing BG2-c2 cells treated with *abi* dsRNA. All comparisons are with HA-AbiWT (*$p<0.001$). Error bars are SEM for all figures.

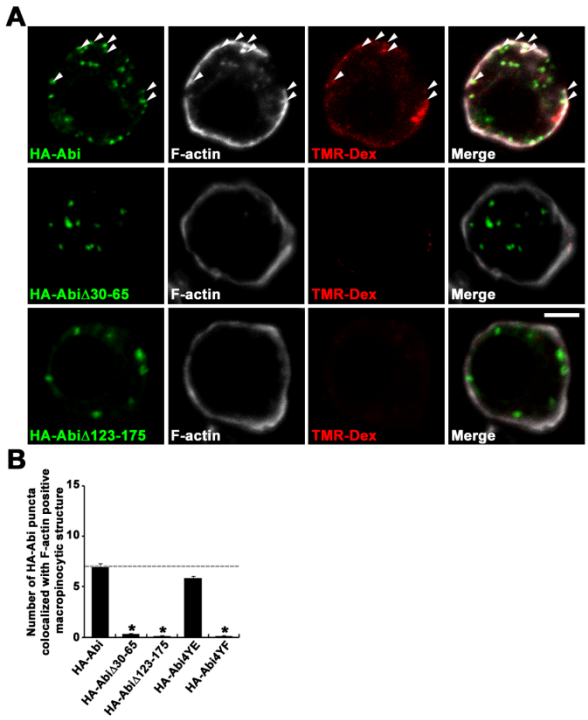
A
HA-Abi
F-actin
TMR-Dex
Merge
HA-AbiΔ30-65
F-actin
TMR-Dex
Merge
HA-AbiΔ123-175
F-actin
TMR-Dex
Merge
B
Number of HA-Abi puncta colocalized with F-actin positive macropinocytic structure
15
10
5
0
HA-Abi
HA-AbiΔ30-65
HA-AbiΔ123-175
HA-Abi4YE
HA-Abi4YF

16. BMPR Internalization via Abi-Dependent Macropinocytosis Is Indispensable for Downregulation of BMPR

Abi may negatively regulate BMP signaling at the NMJ by mediating endocytosis of the BMP receptor. The endocytic mechanism controlling receptor internalization, however, remains unknown. In the preceding experiments, I showed that Gbb induced macropinocytosis in cultured neuronal cells in an Abi-dependent manner. Therefore, I hypothesized that Abi-dependent macropinocytosis induced by Gbb signaling may regulate the endocytic degradation of the BMP receptor. To test this hypothesis, I used several approaches.

First, to examine internalization of BMP receptors through Gbb-induced macropinocytosis, I quantified the number of internalized BMP receptor puncta and the percentage of internalized Myc-Tkv puncta colocalizing with macropinosomes after Gbb induction. For Myc-Tkv internalization assays, non-fixed, Myc-Tkv-expressing BG2-c2 cells were probed with anti-Myc containing conditioned media with or without Gbb for 30 min at 4℃ (at this temperature, endocytosis is blocked) to label Myc-Tkv located on the plasma membrane surface only. Then, cells were pulsed and chased for 3 min with TMR-dextran in conditioned media containing (+Gbb) or not containing (-Gbb) Gbb at 25℃. In Gbb-treated cells, the number of internalized Myc-Tkv puncta was 5.3-fold higher than in cells not treated with Gbb, which showed little or no internalized Myc-Tkv. Approximately 70% of the internalized Myc-Tkv puncta were colocalized with macropinosomes in Gbb-stimulated cells (Figures 25A and 25B). These data indicate that Gbb stimulation activates BMP receptor internalization, and that BMP

Figure 25. Macropinocytosis Mediates Gbb/BMP-Induced BMPR Internalization in an Abi-Dependent Manner in BG2-c2 Cells

(A) Single confocal sections through the middle of cells showing Myc-Tkv (green) and TMR-dextran (red). BG2-c2 cells expressing Myc-Tkv in combination with or without the indicated dsRNA were serum-starved for 6 hr, incubated with conditioned medium containing anti-Myc and 0 ng/ml (-Gbb) or 50 ng/ml (+Gbb) Gbb for 30 min at 4ºC, and then further pulse-chased at 25ºC for 5 min (2 min pulse and 3 min chase) in the presence of TMR-dextran and 0 or 50 ng/ml Gbb. After washing with ice-cold 0.2 M sodium acetate buffer (pH 4.5) containing 0.5 M NaCl to remove bound anti-Myc antibodies, BG2-c2 cells were immediately fixed for 10 min with 4% formaldehyde in PBS, permeabilized with PBS containing 0.1% saponin for 10 min, and then stained with fluorescent-conjugated secondary antibodies in blocking buffer (PBS containing 0.2% BSA) for 1 hr. Arrows indicate internalized Myc-Tkv colocalized with TMR-dextran, and arrowheads demonstrate internalized Myc-Tkv without TMR-Dextran. Scale bar represents 5 μm.

(B) Quantification of the numbers of internalized Myc-Tkv puncta and internalized Myc-Tkv puncta colocalized with TMR-dextran in BG2-c2 cells from experiments performed under the indicated conditions as in (A). Cells were treated with DMSO, 25 μM LY294002, or 100 μM EIPA at 25°C for 30 min before incubation with conditioned medium containing Gbb and TMR-dextran. Quantification was done in three independent experiments with a total of five cells per condition. Comparisons are with Gbb-treated (white box) or DMSO/Gbb-treated (grey box) controls (*$p<0.001$). Error bars are SEM for all figures.

(C) Single confocal sections of the middle part of cells are shown. The experiment was done using Myc-Tkv- and HA-Abi-expressing BG2-c2 cells induced by 50

ng/ml Gbb and pulse-chased for 3 min (2 min pulse and 1 min chase) with TMR-dextran. The overall procedure was equivalent to that of (A). An early time point was used to detect early stage macropinosomes, as determined by HA-Abi and Myc-Tkv staining. Arrowheads indicate the puncta triply stained with Myc-Tkv (green), TMR-dextran (red), and HA-Abi (blue). Scale bar represents 5 μm.

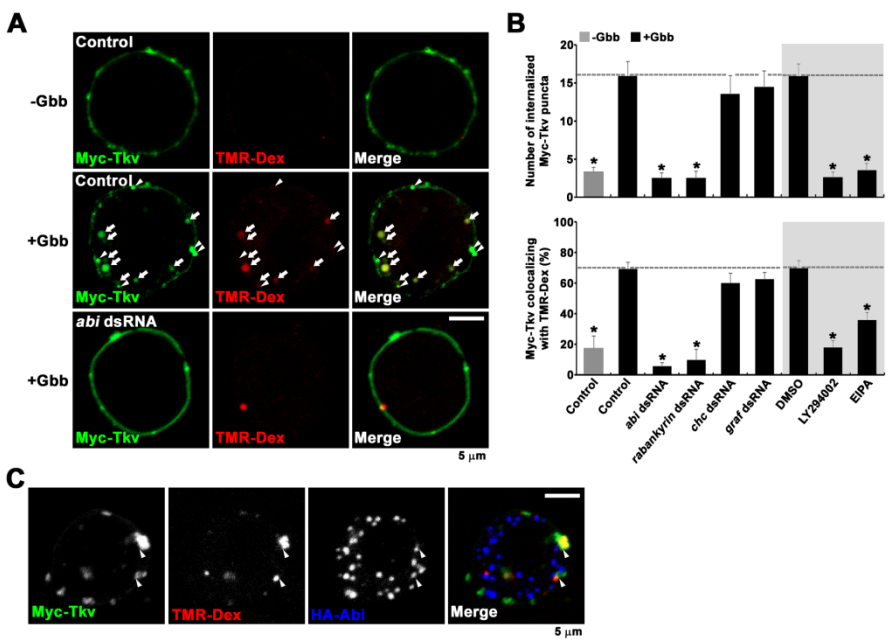

may be internalized through macropinocytosis. To further investigate whether the BMP receptor is internalized specifically via macropinocytosis under Gbb-stimulated conditions, I conducted knock-down and pharmacological experiments. To inhibit macropinocytosis, I treated BG2-c2 cells with *rabankyrin* dsRNA (a macropinocytosis regulator) and the macropinocytosis inhibitors LY294002 or EIPA. Treatment with *rabankyrin* dsRNA and macropinocytosis inhibitors restrained Myc-Tkv internalization, and colocalization of Myc-Tkv with TMR-dextran was reduced compared to non-treated control cells. In contrast, when clathrin-dependent (CD) endocytosis was blocked by *clathrin heavy chain* (*chc*) dsRNA, Gbb-induced Myc-Tkv internalization and colocalization of Myc-Tkv to macropinosomes were unaffected. In addition, internalization of both the BMP receptor and macropinosomes remained active when GPI-enriched endocytic compartment (GEEC) endocytosis, one of the clathrin-independent (CI) endocytic processes known to degrade surface EGF receptors, was inhibited by *GTPase regulator associated with focal adhesion kinase* (*graf*) dsRNA (Figure 25B) (Kim et al., 2017). These data suggest that the Gbb-induced endocytic mechanism that results in the internalization of the BMP receptor involves macropinocytosis, but not CD endocytosis or other CI endocytosis.

Next, to investigate whether the Gbb-induced macropinocytosis of the BMP receptor is dependent on Abi, I knocked-down *abi* in BG2-c2 cells with *abi* dsRNA and conducted a BMP receptor internalization assay with TMR-dextran under Gbb-induced conditions. Internalization of surface Myc-Tkv was inhibited in *abi* knock-down cells, as in non-stimulated (Gbb-) cells or in cells treated with *rabankyrin* dsRNA and macropinocytosis inhibitors (Figures 25A and 25B). Additionally, at the early macropinocytosis step (pulse-chase time: 1-2 min), TMR-

dextran, HA-Abi, and Myc-Tkv were all colocalized in the same compartment (Figure 25C). These data support the idea that macropinocytosis mediates Gbb-induced BMP receptor internalization in an Abi-dependent manner in BG2-c2 cells.

Then, I tested whether Gbb-induced BMP receptor internalization through macropinocytosis promotes endosomal trafficking of the BMP receptor to lysosomes. Gbb-treated, Myc-Tkv-expressing BG2-c2 cells were pulsed and chased with TMR-dextran for 20 min (the time point when macropinosomes were colocalized with lysosomes); then, lysosomes were visualized with lysotracker (a lysosome marker). At this time point, 70% of internalized Myc-Tkv was colocalized with lysotracker and TMR-dextran. However, only 20% of internalized Myc-Tkv was colocalized with lysotracker in *abi* knock-down cells (Figures 26A and 26B). Inhibition of macropinocytosis by LY294002 or EIPA and reduction of *rabankyrin* expression in Gbb-induced BG2-c2 cells resulted in a similar phenotype to that of *abi* dsRNA treated cells (Figure 26B). CD endocytosis and GEEC endocytosis were not involved in the lysosomal trafficking of Myc-Tkv activated by Gbb (Figure 26B). Thus, Gbb-induced macropinocytosis is associated with the sorting of internalized BMPR to lysosomes.

Finally, I directly determined the role of Gbb in BMPR degradation and its signaling. Myc-Tkv-expressing BG2-c2 cells were incubated with or without Gbb for 0, 5, 60, or 120 min. Then, I examined the protein expression levels of Myc-Tkv by western blot analysis. In control conditions, the expression levels of Myc-Tkv and P-Mad signal were stable through 120 min (Figures 26C, 26D and 26E; -Gbb). When Gbb was present, Myc-Tkv protein expression started to drop from 60 min onward, and BMP signaling was almost completely abolished

Figure 26. Macropinocytosis Is Required for Ligand-Induced BMPR Degradation

(A and B) Abi-dependent macropinocytosis is necessary for the lysosomal targeting of the BMP receptor. (A) Single confocal slices of the middle section of cells are shown. BG2-c2 cells expressing Myc-Tkv with or without *abi* dsRNA were pretreated with 50 ng/ml Gbb and anti-Myc antibody and then pulse-chased with TMR-dextran for 20 min (2 min pulse and 18 min chase) at 25 ºC. Cells were then incubated with 1 μM lysotracker at 25 ºC for 5 min. Next, BG2-c2 cells were fixed with 4% formaldehyde in PBS and permeabilized with PBS containing 0.1% saponin for 10 min. After washing with PBS, BG2-c2 cells were stained with a fluorescent-conjugated secondary antibody. Arrowheads represent Myc-Tkv (blue), lysotracker (red), and TMR-dextran (green). Scale bar represents 5 μm. (B) Quantification of Myc-Tkv colocalizing with lysotracker in BG2-c2 cells under the indicated conditions. Quantification was done in three independent experiments with a total of five cells per condition. Comparisons are with Gbb-treated (white box) or DMSO/Gbb-treated (grey box) controls (*$p<0.001$).

(C-E) Abi-dependent macropinocytosis is associated with efficient Myc-Tkv degradation and inhibition of its signaling. (C) Western blot analysis of total BG2-c2 cell lysates expressing Myc-Tkv treated with or without the indicated dsRNA. Serum starved cells were pretreated with 100 μg/ml cycloheximide for 3 hr before Gbb treatment. Cells were then incubated in the presence of 50 ng/ml Gbb at 25ºC for the indicated times. (D) Quantification of the expression level of Myc-Tkv normalized to β-actin. The mean values from three independent experiments are plotted against incubation time. (E) Quantification of nuclear P-mad level normalized to the level of DAPI in Myc-Tkv-expressing BG2-C2 cells. Serum-

starved cells were fixed (0 min) or incubated with (+Gbb) or without (-Gbb) Gbb for 120 min and then fixed. Quantification was done in Z-stacked images of BG2-c2 cells to measure P-mad levels. Comparisons are with controls treated with Gbb for 120 min (gray bar graph) unless otherwise indicated (*p<0.001; **p<0.001). Error bars are SEM for all figures.

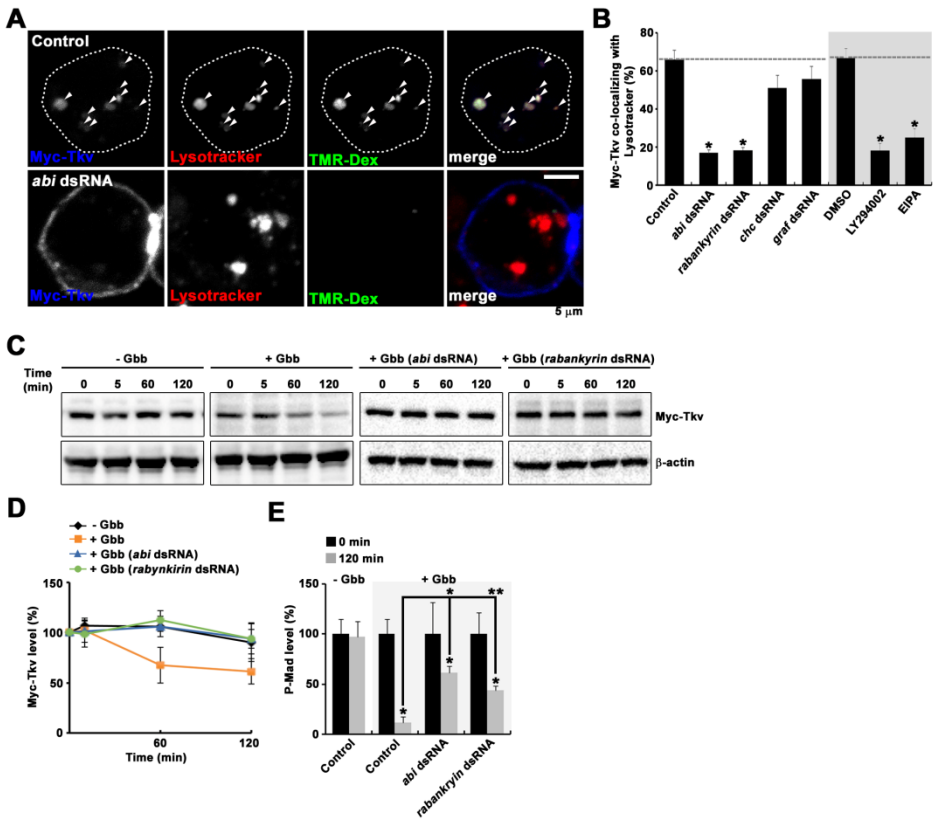

(Figures 26C, 26D and 26E; +Gbb). Loss of *abi* or *rabankyrin* expression inhibited the degradation of Myc-Tkv, and BMP signaling stayed at a higher level compared to that of control cells (Figures 26C, 26D and 26E; +Gbb). Overall, these results suggest that Abi-dependent macropinocytosis initiated by Gbb is the main endocytic route of the BMP receptor, which is an essential step for BMP receptor degradation.

17. Abi and BMP Signaling Is Required for Gbb-Induced Macropinocytosis at the NMJ

If BMP signaling is inhibited by Abi-dependent macropinocytosis at the NMJ, as seen in cultured neurons, loss of *abi* function should cause defects in Gbb-induced macropinocytosis at the NMJ. To prove this hypothesis, I first examined whether macropinocytosis activated by Gbb also exists in the *Drosophila* NMJ. To perform macropinocytosis assays at the NMJ, I dissected third instar wandering larvae in HL3.1 buffer, incubated the larvae in conditioned media containing 50 ng/ml Gbb generated from S2R+ cells for 10 min, and then pulsed them with TMR-dextran for 5 min. When Gbb was applied to the larvae, TMR-dextran was internalized, and a punctate pattern showing the locations of macropinosomes was detected in the synaptic boutons. Without Gbb application, however, the intensity of TMR-dextran was 54% lower than in the Gbb-treated NMJ (Figures 27A and 27B). Then, I tested the necessity of Abi, Abl, and Rac1 for the regulation of Gbb-induced macropinocytosis at the NMJ. Lack of *abi* and *Abl* or presynaptically expressed dominant-negative Rac1 caused a reduction in TMR-dextran uptake at the NMJ of Gbb-treated larvae compared to wild-type larvae (Figures 27A and

Figure 27. Gbb/BMP-Induced Macropinocytosis at the NMJ Is Impaired by Loss of Abi-Abl-Rac1 and the BMP Receptor Wit

(A) A macropinocytosis assay performed in third instar larvae. Z-stacked images of NMJ 6/7 stained with anti-HRP (green) and internalized TMR-dextran (red) from the indicated genotypes.

(B) Quantification of TMR-dextran intensity normalized to HRP in the indicated genotypes. All comparisons are with wild-type (w^{1118}) or *C155-GAL4/+* treated with Gbb (*p<0.001). Error bars are SEM for all figures.

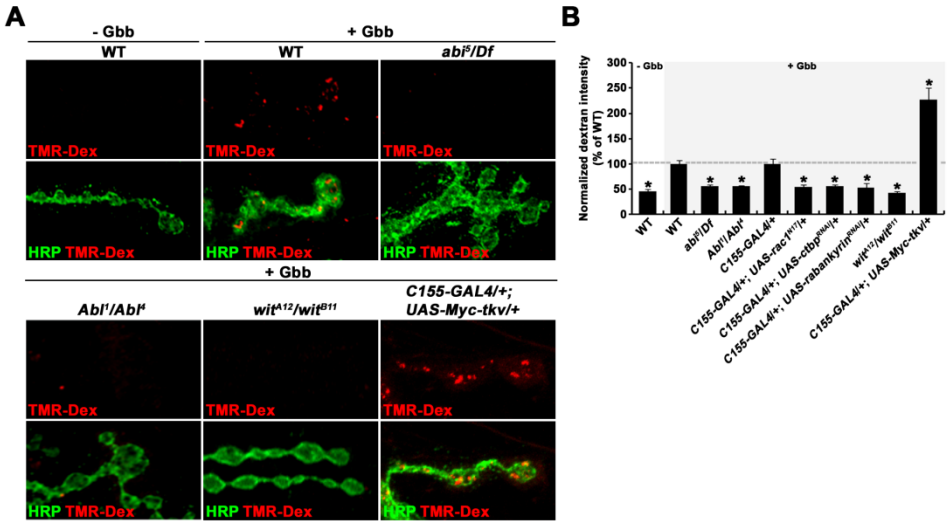
A
- Gbb
+ Gbb
WT
WT
abi5/Df
TMR-Dex
HRP TMR-Dex
+ Gbb
Abl1/Abl4
witA12/witB11
C155-GAL4/+;
UAS-Myc-tkv/+
B
Normalized dextran intensity
(% of WT)
300
250
200
150
100
50
0
- Gbb
+ Gbb
WT
abi5/Df
Abl1/Abl4
C155-GAL4/+
C155-GAL4/+; UAS-rac1V17/+
C155-GAL4/+; UAS-ctbpRNAi/+
C155-GAL4/+; UAS-rabankyrinRNAi/+
witA12/witB11
C155-GAL4/+; UAS-Myc-tkv/+

27B). Then, I expressed CtBPRNAi or RabankyrinRNAi using the *C155-GAL4* driver to test the specificity of macropinocytosis at the NMJ. Lack of presynaptic macropinocytosis regulators *ctbp* or *rabankyrin* resulted in a decreased level of TMR-dextran intensity under Gbb-induced conditions (Figures 27A and 27B). Lastly, to validate whether macropinocytosis is dependent on BMP signaling at the NMJ, macropinocytic activity was measured in *wit* loss-of-function or *tkv* gain-of-function larvae. When treated with Gbb, the intensity of TMR-dextran was reduced ~57% in *wit* mutants compared to controls. On the other hand, overexpression of Tkv under the *C155-GAL4* driver resulted in a ~2.2 fold-higher TMR-dextran intensity than that of controls (Figures 27A and 27B). These data indicate that Gbb-induced macropinocytosis requires BMP signaling at the NMJ. Overall, Gbb-induced macropinocytosis is dependent on both Abi/Abl/Rac1 and BMP signaling at the NMJ. In this study, I present the first evidence of a macropinocytic mechanism existing at the neuromuscular synapse.

Next, to test whether Abi and macropinocytic regulators are responsible for surface expression of the BMP receptor at the NMJ, I first examined the localization of Tkv with Abi, CtBP, or Rabankyrin. I then evaluated the expression level of surface Tkv in mutants lacking *abi* or *rabankyrin*. At basal state, Myc-tkv was localized at motor neuron terminals in a punctate pattern, and GFP-Rabankyrin, CtBP-GFP, and HA-Abi were each colocalized with Myc-Tkv at these patches (Figure 28A). The fact that internal or surface BMP receptors localized with Abi or regulators of macropinocytosis implies the possibility that the BMP receptor may internalize though macropinocytosis. In addition, I tested the level of Tkv expressed on the surface of boutons in a RabankyrinRNAi background. Loss of presynaptic *rabankyrin* caused a ~73% increase in the expression of surface Tkv

Figure 28. Internalization of the BMP Receptor Requires Abi and Macropinocytosis Regulators

(A) Tkv is colocalized partially with macropinocytosis regulators and Abi in the NMJ at baseline. Single confocal slices of NMJ 6/7 doubly expressing presynaptic Myc-Tkv and GFP-Rabankyrin, CtBP-GFP, or HA-Abi in a wild-type background. Arrowheads indicate co-existing presynaptic Myc-Tkv and GFP-Rabankyrin, CtBP-GFP, or HA-Abi.

(B and C) Rabankyrin regulates surface expression of Tkv at the NMJ. (B) Confocal images of NMJ 6/7 labeled with anti-Myc (red) and anti-HRP (green) taken from the indicated genotypes. (C) Quantification of the ratio of mean Myc-Tkv to HRP fluorescence intensities; the values are expressed as percentages of the intensities of C155-GAL4/+; UAS-Myc-tkv larvae (control). All comparisons are with controls (*$p<0.001$). Error bars are SEM for all figures.

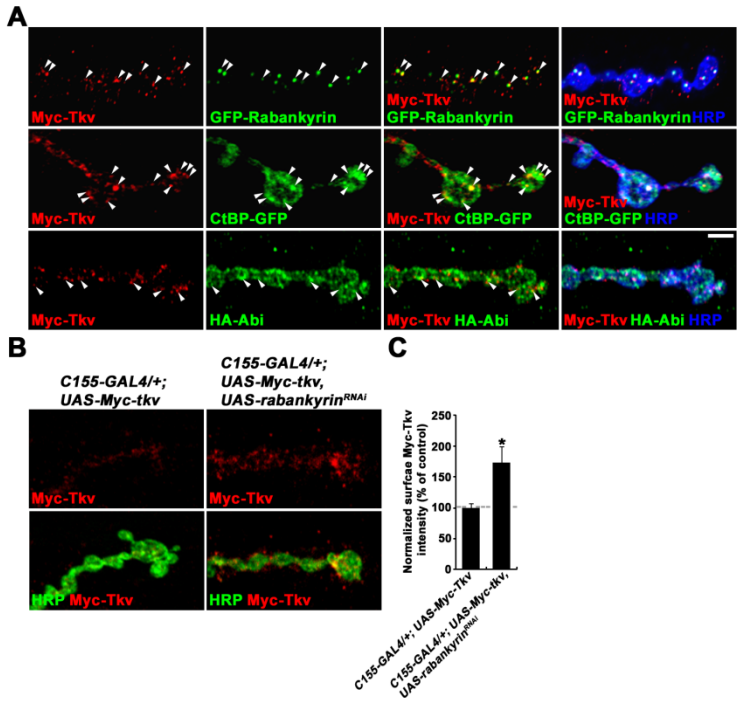
A
Myc-Tkv
GFP-Rabankyrin
Myc-Tkv GFP-Rabankyrin
Myc-Tkv GFP-Rabankyrin HRP
Myc-Tkv
CtBP-GFP
Myc-Tkv CtBP-GFP
Myc-Tkv CtBP-GFP HRP
Myc-Tkv
HA-Abi
Myc-Tkv HA-Abi
Myc-Tkv HA-Abi HRP
B
C155-GAL4/+; UAS-Myc-tkv
C155-GAL4/+; UAS-Myc-tkv, UAS-rabankyrinRNAi
Myc-Tkv
HRP Myc-Tkv
C
Normalized surface Myc-Tkv intensity (% of control)
250
200
150
100
50
0
*
C155-GAL4/+; UAS-Myc-Tkv
C155-GAL4/+; UAS-Myc-tkv, UAS-rabankyrinRNAi

compared to controls, which was equivalent to that of *abi* null mutants (Figures 28B and 28C). Together, these results support the possibility that Abi-dependent macropinocytosis is the major endocytic route that restrains BMP signaling by promoting receptor internalization at the NMJ.

18. Rabankyrin and CtBP, Regulators of Macropinocytosis, Also Control BMP Signaling at the NMJ

The data so far raise the possibility that regulators of macropinocytosis may control synaptic growth through restraining BMP signaling. To test this hypothesis, I performed several experiments using a variety of approaches.

First, I tested whether CtBP and Rabankyrin control synaptic growth at the NMJ by expressing *ctbp* dsRNA or *rabankyrin* dsRNA with *C155-GAL4*. The numbers of overall boutons and satellite boutons were increased in organisms with presynaptic knock-down of *ctbp* or *rabankyrin* compared with controls, as seen in *abi* null mutants (Figures 29A and 29B).

Next, to verify the possibility that CtBP and Rabankyrin negatively regulate BMP signaling at the NMJ, the genetic interaction between *wit* mutants and presynaptic CtBPRNAi or RabankyrinRNAi was tested. Single copy deletion of *wit* in both *C155-GAL4*/+; *UAS-ctbp*^{RNAi} and *C155-GAL4*/+; *UAS-rabankryin*^{RNAi} larvae suppressed the synaptic overgrowth caused by reduction of *ctbp* or *rabankyrin* expression at the presynaptic side of the NMJ. Double copy deletion of *wit* further suppressed the excessive formation of both total boutons and satellite boutons caused by *C155-GAL4*/+; *UAS-ctbp*^{RNAi} or *C155-GAL4*/+; *UAS-rabankryin*^{RNAi} (Figure 29B), indicating a dose-dependent genetic interaction. This

Figure 29. Dysregulation of BMP-Dependent Synaptic Growth in Loss of Presynaptic *ctbp* and *rabankyrin*

(A and B) Loss of presynaptic ***ctbp* and *rabankyrin*** results in excessive bouton formation, which is dependent on BMP signaling. (A) Confocal images of NMJ 6/7 (left panels) and NMJ 4 (right panels) labeled with anti-HRP taken from *C155-GAL4/+*, *C155-GAL4/+; UAS-ctbp^{RNAi}/+*, and *C155-GAL4/+; UAS-rabankyrin^{RNAi}* larvae. Scale bar represents 20 μm. (B) Quantification of the synaptic structure at NMJ 6/7 in the indicated genotypes.

(C and D) CtBP and Rabankyrin are necessary for P-Mad accumulation in the NMJ and motor neuron nucleus. (C) Single confocal slices of NMJ 6/7 and the VNC stained with both anti-P-Mad (red) and anti-HRP (green; NMJ) or anti-Elav (green; VNC) taken from *C155-GAL4/+*, *C155-GAL4/+; UAS-ctbp^{RNAi}/+*, and *C155-GAL4/+; UAS-rabankyrin^{RNAi}* larvae. Scale bar represents 5 μm. (D) Quantification of P-Mad to HRP intensity ratio (NMJ) and P-Mad to Elav intensity ratio (VNC).

(E) Transheterozygous interaction between *abi* and macropinocytosis regulators**.** Quantification of the synaptic structure at NMJ 6/7 in the indicated genotypes. N=3, n=12, 12, 12, 12, 12, 12, 12, and 12, respectively. One-way ANOVA was used for data analysis.

All comparisons are with controls unless otherwise indicated (*$p<0.001$; **$p<0.01$; n.s., not significant). Error bars are SEM for all figures.

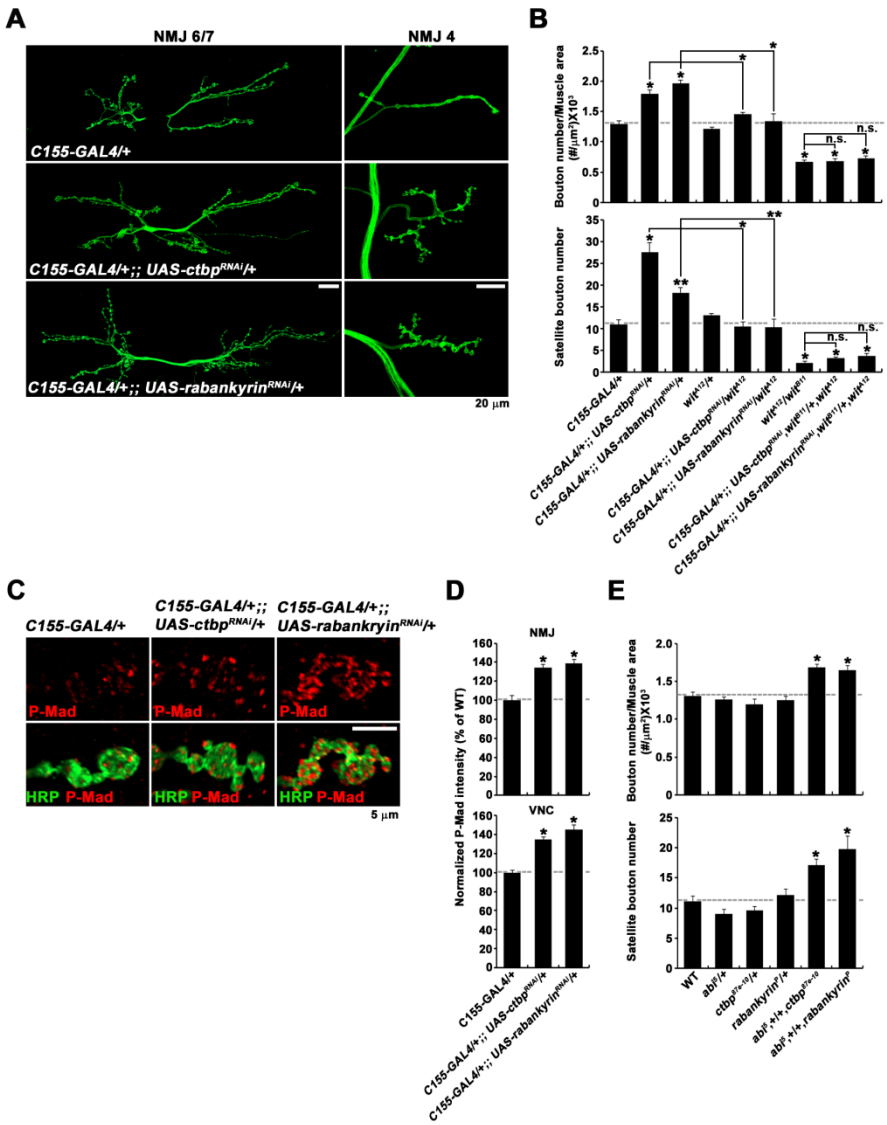
A
NMJ 6/7
NMJ 4
C155-GAL4/+
C155-GAL4/+;; UAS-ctbp^RNAi/+
C155-GAL4/+;; UAS-rabankyrin^RNAi/+
20 μm
B
Bouton number/Muscle area (#/μm²)X10³
Satellite bouton number
n.s.
C155-GAL4/+
C155-GAL4/+;; UAS-ctbp^RNAi/+
C155-GAL4/+;; UAS-rabankyrin^RNAi/+
wlt^12/+
C155-GAL4/+;; UAS-ctbp^RNAi/wlt^12
C155-GAL4/+;; UAS-rabankyrin^RNAi/wlt^12
wlt^12/wlt^11
C155-GAL4/+;; UAS-ctbp^RNAi ;wlt^11/+,wlt^12
C155-GAL4/+;; UAS-rabankyrin^RNAi ;wlt^11/+,wlt^12
C
C155-GAL4/+
C155-GAL4/+;; UAS-ctbp^RNAi/+
C155-GAL4/+;; UAS-rabankyrin^RNAi/+
P-Mad
HRP P-Mad
5 μm
D
NMJ
VNC
Normalized P-Mad intensity (% of WT)
C155-GAL4/+
C155-GAL4/+;; UAS-ctbp^RNAi/+
C155-GAL4/+;; UAS-rabankyrin^RNAi/+
E
Bouton number/Muscle area (#/μm²)X10³
Satellite bouton number
WT
abl^F/+
ctbp^Flox-10/+
rabankyrin^7/+
abl^F,+/+,ctbp^Flox-10
abl^F,+/+,rabankyrin^7

genetic evidence showed that *ctbp* and *rabankyrin* act upstream of the BMP signaling cascade to regulate synaptic growth. To directly examine the effect of CtBP or Rabankyrin on the regulation of BMP signaling, I quantified the level of P-Mad in motor axon termini and nuclei. The expression level of P-Mad in both the NMJ and motor neuron nuclei was elevated in *C155-GAL4*/+; *UAS-ctbp*^{RNAi} and *C155-GAL4*/+; *UAS-rabankryin*^{RNAi} larvae, indicating that CtBP and Rabankyrin are negative regulators of BMP signaling at the NMJ (Figures 29C and 29D).

Finally, I explored whether CtBP and Rabankyrin are required for Futsch-mediated MT stability in the regulation of synaptic growth. I first examined the level of Futsch and extent of loop formation in motor axon termini. Lack of presynaptic *ctbp* or *rabankyrin* caused elevated expression of Futsch and increased loop formation. This result indicates that CtBP and Rabankyrin regulate BMP signaling to control Futsch expression and MT stability at the NMJ (Figures 30A and 30B). To directly test the involvement of MT stability in the regulation of synaptic growth by CtBP and Rabankyrin, I applied Vinblastine to both *C155-GAL4*/+; *UAS-ctbp*^{RNAi} and *C155-GAL4*/+; *UAS-rabankryin*^{RNAi} larvae. The synaptic overgrowth phenotype featured in *C155-GAL4*/+; *UAS-ctbp*^{RNAi} or *C155-GAL4*/+; *UAS-rabankryin*^{RNAi} larvae was suppressed with vinblastine application (Figure 30C). Altogether, these data support the hypothesis that regulators of macropinocytosis are required for the canonical BMP-Futsch-MT signaling pathway to restrain synaptic growth at the NMJ.

Figure 30. CtBP and Rabankyrin Regulate Microtubule Stability to Modulate Synaptic Growth

(A and B) The level of Futsch staining intensity in the NMJ is increased by loss of presynaptic CtBP and Rabankyrin. (A) Single confocal slice of NMJ 6/7 stained with anti-Futsch (22C10) (red) and anti-HRP (green) in *C155-GAL4/+*, *C155-GAL4/+; UAS-ctbp^{RNAi}/+*, and *C155-GAL4/+; UAS-rabankyrin^{RNAi}* larvae. Arrowheads represent Futsch-positive loops. Scale bar represents 5 μm. (B) Quantification of Futsch-to-HRP ratio in the indicated genotypes.

(C) Quantification of the numbers of overall boutons normalized to muscle surface area and satellite boutons at NMJ 6/7 in the absence (-VB; 0 μM) or presence (+VB; 1 μM) of vinblastine.

All comparisons are with controls unless otherwise indicated (*$p<0.001$; **$p<0.01$; ***$p<0.05$; n.s., not significant). Error bars are SEM for all figures.

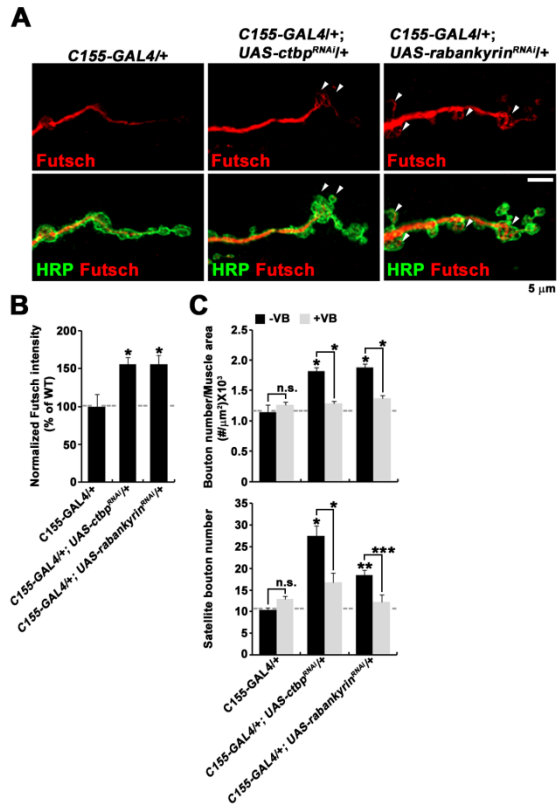
A
C155-GAL4/+
C155-GAL4/+; UAS-ctbp^RNAi/+
C155-GAL4/+; UAS-rabankyrin^RNAi/+
Futsch
HRP Futsch
5 μm
B
Normalized Futsch intensity (% of WT)
C155-GAL4/+
C155-GAL4/+; UAS-ctbp^RNAi/+
C155-GAL4/+; UAS-rabankyrin^RNAi/+
C
-VB
+VB
Bouton number/Muscle area (#/μm²)X10³
Satellite bouton number
n.s.

IV. Discussion

In this thesis, I present the first model of the Abi-dependent macropinocytic regulation of retrograde BMP signaling at the neuromuscular *Drosophila* synapse. These findings provided evidence of an indirect mechanism of Rac1-Abi-SCAR/WAVE-dependent actin polymerization in the regulation of synaptic growth, in which actin acts as a driving force of macropinocytosis to restrain BMP signaling. This study also showed that Gbb induces macropinocytosis in neurons, and that the major endocytic mechanism for the internalization of the BMP receptor is macropinocytosis. Therefore, this thesis demonstrated that Abi acts together with Abl and Rac1-SCAR/WAVE to regulate synaptic growth by regulating Gbb-induced Tkv macropinocytosis to attenuate retrograde BMP signaling.

1. The Role of Abi in Retrograde BMP Signaling-Dependent Synaptic Growth

Arp2/3 activation of actin polymerization by signal transduction of the Rac1-WAVE complex has been studied in several cell contexts, including in neurons. However, the *in vivo* mechanism of the Rac1-WAVE complex-dependent actin polymerization regulating synaptic development is unclear. Moreover, the genetic interaction between components of the WAVE complex has not been studied thoroughly. The *abi* mutant demonstrated severe morphological defects in the NMJ, showing increased numbers of overall boutons and satellite boutons (Figures 3 and 4). The increased bouton formation represents synaptic overgrowth,

which suggests that Abi is a crucial protein for regulating synaptic development. It has been reported that Abi acts as a scaffolding protein linking WAVE, Kette, and Sra-1 to form the WAVE complex in order to relay Rac1 signals to Arp2/3, which in turn activates actin polymerization (Eden et al, 2002). The integrity of these proteins is important for the stability of the WAVE complex, and reduction in Abi function leads to degradation of these components of the WAVE complex (Kunda et al., 2003; Innocenti et al., 2004). Thus, Abi and Rac1-SCAR-Kette may function together to control synaptic development at the NMJ. Transheterozygous interactions and other genetic evidence confirming the epistatic relationship strongly suggest that Abi and Rac1, SCAR/WAVE, or Kette genetically interact to regulate synaptic growth in the same signaling pathway, and that Rac1 acts upstream of Abi in the regulation of synaptic morphology at the NMJ (Figure 8). Interestingly, the number of satellite boutons was increased significantly in mutation or knock-down of *abi*, *rac1*, *scar*, and *kette* (Figures 8A and 8B). The transheterozygous interactions between *abi*, *rac1*, *scar*, and *kette* mutants also displayed excessive satellite bouton formation (Figure 8C). Abi is also known for being a non-receptor tyrosine kinase Abl interactor protein. Tyrosine phosphorylation of Abi by Abl is important for Abi subcellular localization and for Abi/Rac1-modulated F-actin polymerization regulating cell shape and motility. Interaction between Abi1 and Abl also promotes WAVE2 transocalization and activity for actin polymerization (Leng at al., 2005). Therefore, these studies suggest that Abi and Abl may regulate synaptic growth in the same signaling pathway. Genetic interaction experiments between Abi and Abl showed that phosphorylation of Abi by Abl kinase is important in the regulation of bouton and satellite bouton formation (Figure 9). All together, these data suggest that Abi acts

together with Abl and the Rac1-SCAR/WAVE complex to regulate synaptic growth in the same signaling pathway at the NMJ.

Then, in which pathway do Abi, Abl, and Rac1-SCAR/WAVE have a role in regulating synaptic growth? Or does Abi, Abl, and Rac1-SCAR/WAVE-activated F-actin polymerization directly regulate synaptic development? It has been proposed that BMP signaling has an instructive role in regulating synaptic growth, and that it is the major signaling pathway during synaptic development at the NMJ (Marques et al., 2002). Overactivation of BMP signaling by *daughters against decapentaplegic* (*dad*) mutation or constitutive activation of presynaptic Tkv also results in significantly increased satellite bouton formation (Nahm et al., 2013; O'Connor-Giles et al., 2008). Moreover, loss of certain endocytic proteins, including Dap160, EndoA, Nwk, and WASP, results in excessive satellite bouton formation (Coyle et al., 2002; O'Connor-Giles et al., 2008). The actin regulator WASP interacts with Nwk to downregulate BMP signaling by endocytic machinery (O'Connor-Giles et al., 2008). This indicates that actin polymerization regulated by the WASP family is involved in the endocytosis regulating the surface expression of signaling receptors at the NMJ (O'Connor-Giles et al., 2008). The formation of satellite boutons is a unique phenotype seen in the context of impairment of endocytosis or activation of BMP signaling, and it has been revealed that endocytosis is the main mechanism to attenuate the BMP signaling pathway (O'Connor-Giles et al., 2008). SCAR/WAVE is member of the WASP family that regulates Arp2/3-dependent actin polymerization. Moreover, Rac-WAVE complex signaling-dependent macropinocytosis, one of the CI endocytic mechanisms, has been reported. Thus, I first hypothesized that Abi, Abl, and Rac1-SCAR/WAVE

may be required for the BMP signaling to regulate NMJ growth. The level of BMP signaling readout P-Mad and the genetic interaction between *wit* and *abi*, *Abl*, and *rac1* suggest that Abi, Abl, and Rac1-SCAR/WAVE control synaptic development by inhibiting BMP signaling (Figures 10 and 11). To further verify this idea, I tested the relationships between Abi, Abl, or Rac1 and the BMP signaling downstream effectors dFMRP and Futsch/MAP1B, which were first revealed by Nahm et al., 2013. The BMP-dFMRP-Futsch/MAP1B signaling is responsible for synaptic development controlled by microtubule stability (Nahm et al., 2013). Therefore, it is possible that Abi, Abl, and Rac1-SCAR/WAVE may signal through the BMP-dFMRP-Futsch/MAP1B pathway for regulation of microtubule stability at the NMJ. Abi, Abl and Rac1 genetically interact with dFMRP as an upstream molecule, and the expression of the *dfmr1* transcript was decreased after loss of *abi*, *Abl*, and *rac1* (Figure 12). The level of Futsch/MAP1B was increased in those mutants, and they displayed Futsch-positive loops at their synaptic boutons, indicating that mutation in *abi*, *Abl*, and *rac1* resulted in increased microtubule stability (Figure 13). Treatment with vinblastine, a microtubule-severing drug, directly suppressed the synaptic overgrowth phenotype seen in those mutants (Figure 13). This evidence indicates that the actin cytoskeleton does not directly regulate synaptic morphology and growth. Instead, actin polymerization controlled by the Rac/WAVE complex inhibits synaptic growth through BMP signaling regulating microtubule stability at the NMJ. It was surprising that actin regulators regulate microtubule stability in the synapse to control synaptic development, rather than directly affecting the synaptic structure. Therefore, I concluded that actin polymerization regulated by Abi, Abl, and components of the WAVE complex do not directly regulate bouton formation; rather, these regulators restrain

BMP signaling to regulate microtubule stability and synaptic growth. In future studies, it will be interesting to test whether other components of the WAVE complex, including CYFIP (Sra-1) and HSPC300, are required for BMP signaling and microtubule stability at the NMJ.

Next, I questioned whether Rac1-Abi-SCAR/WAVE and Abl-dependent actin polymerization play a role in BMP receptor endocytosis. Transheterozygous interactions between *abi* and endocytic mutants, such as *dap160, endoA* and *nwk*, showed that Abi genetically interacts with Dap160 and EndoA, but not with Nwk (Figure 14). This indicates that Abi may have a role in endocytosis. Nwk interacts with WASP to regulate the endocytosis of Tkv and synaptic growth (O'Connor-Giles et al., 2008). However, in this study, Nwk and WASP did not genetically interact with Abi at the NMJ (Figures 8C and 14B). Abi is known to physically interact with both WAVE and WASP to regulate actin polymerization through distinct actions (Innocenti et al., 2005). Interaction between Abi and WAVE is necessary for Rac1 signaling-dependent macropinocytosis, and Abi-WASP interactions regulate epidermal growth factor receptor (EGFR) endocytosis and trafficking in HEK293 cells (Innocenti et al., 2005). These distinct roles of Abi in the regulation of WASP and WAVE activity suggest that Abi may interact with WASP to regulate different aspects of synaptic function.

2. Macropinocytosis of the BMP Receptor and Its Regulation by Abi-Abl-Rac1 Signaling

Even though Abi showed genetic interaction with endocytic mutants, the exact endocytic mechanism regulating BMP receptor internalization is unclear.

Receptors in the TGF-β superfamily are known to be internalized by both clathrin-coated vesicles and caveolin-positive vesicles (Ye-Guang Chen, 2009; Guaglielmo et al., 2003). Usually, lipid raft-mediated endocytosis of TGF-β receptors facilitates receptor degradation and inhibits signal transduction, and it was reported that inhibiting clathrin-dependent endocytosis did not affect the internalization of TGF-β receptors (Ye-Guang Chen, 2009; Guaglielmo et al., 2003). However, the endocytic pathway responsible for BMP receptor internalization at the NMJ is unknown. Previous studies have shown that Abi and Rac-SCAR/WAVE complex-activated actin polymerization plays a major role in macropinocytosis in non-neuronal cells (Innocenti et al, 2005; Dubielecka et al., 2010; Rottner et al, 2010). Macropinocytosis is known for non-selective engulfment of extracellular viruses or antigens in macrophages; however, there is some evidence that macropinocytosis is also associated with the internalization of certain receptors to inhibit receptor signaling (Basagiannis et al, 2016). Moreover, WAVE1 and EndoA1 regulate dendrite outgrowth by facilitating BDNF-induced TrkB internalization through clathrin-independent endocytosis (Xu et al., 2016). Therefore, I hypothesized that Abi and Rac-SCAR/WAVE may internalize BMP receptors by actin-dependent macropinocytosis to attenuate its signaling. Macropinocytosis is an inducible process that requires high concentrations of certain signals, such as growth factors. If BMP receptors are internalized by macropinocytosis, there must be signals inducing this mechanism. The receptors internalized through macropinocytosis are usually stimulated by their own signals in a manner that turn off the receptor signaling pathway (negative feedback loops). For example, vascular endothelial growth factor (VEGF) induces VEGFR2 internalization through macropinocytosis (Basagiannis et al, 2016). Therefore, I hypothesized that Gbb, the BMP signal

secreted from postsynaptic muscles, may stimulate macropinocytosis and the internalization of the BMP receptor. Macropinocytosis was detected when BG2-c2 cells were treated with high doses of Gbb (Figure 15), suggesting that Gbb induces macropinocytosis in neurons. I then questioned whether Abi, Abl, and Rac1-SCAR/Kette were required for Gbb-induced macropinocytosis. Treatment with *abi, Abl, rac1, scar, and kette* dsRNA in BG2-c2 cells efficiently blocked Gbb-induced macropinocytosis (Figure 16). In Gbb-induced cells, HA-Abi was translocated to the plasma membrane at the site of macropinocytosis (Figures 22 and 23A). Moreover, Abl kinase activity was critical for Abi to target to the early macropinocytic structure (Figure 23). Once Abi targeted the site of micropinocytosis, it interacted with the WAVE complex to form actin-rich macropinosomes (Figure 24). These results suggest that Abi phosphorylation by Abl and the Rac1-WAVE complex signal are required for Gbb-induced macropinocytosis. In the future, it will be interesting to test whether other components of the WAVE complex are required for Gbb-induced macropinocytosis in neurons. *dap160* or *endoA* dsRNA also inhibited macropinocytosis stimulated by Gbb (Figure 16), suggesting that Dap160 and EndoA may regulate macropinocytosis. The endocytic mechanisms of Dap160 and Endophilin are under debate, and it is unknown whether these proteins act in CD endocytosis, CI endocytosis, or both. Therefore, this study hints at the presence of the underlying endocytic mechanisms of Dap160 and Endophilin, and further study should be conducted to elucidate these mechanisms.

Next, I wondered whether internalization of the BMP receptor through macropinocytosis stimulates degradation of the BMP receptor, thereby inhibiting its signaling. Another question I had was whether macropinocytosis acts as a major

endocytic pathway for internalizing the BMP receptor. Endocytosis is major mechanism regulating surface receptor expression and negatively regulates receptor signaling, and macropinocytosis is also known for this action. Blocking CD endocytosis or other CI endocytosis did not affect the internalization of BMP receptors in the presence of Gbb. This indicates that macropinocytosis is the major endocytic mechanism internalizing BMP receptors in neurons (Figure 25). The effect of receptor degradation and P-Mad signaling was also tested to determine the role of macropinocytosis in BMP signaling. Gbb-induced macropinocytosis of the BMP receptor resulted in it being trafficked to lysosomes, and the expression of this receptor was rapidly reduced by Gbb treatment in an Abi-dependent manner (Figure 26). These data suggest that Abi-Abl-Rac1 attenuate BMP signaling by Gbb-induced macropinocytosis of Tkv, which lead to its degradation.

I then asked whether Gbb induces macropinocytosis at the NMJ. Ectopic treatment of Gbb induced macropinocytosis at the NMJ, and Abi-Abl-Rac1 and components of the BMP signaling pathway were required for this action (Figure 27). Furthermore, regulators of macropinocytosis negatively regulate synaptic growth by inhibiting BMP signaling and the surface expression of Tkv (Figures 29 and 30). These data suggest that Abi-dependent, Gbb-induced BMP receptor macropinocytosis is the major endocytic pathway regulating synaptic growth at the NMJ. The remaining questions left in this thesis are, when and how Gbb is secreted in the postsynaptic muscle. There is some evidence that retrograde BMP signaling regulates activity-dependent homeostasis at the NMJ. When synaptic activity is increased by high temperature or hyperexcitable K^+ channel double-mutants, such as *ether a go-go* (*eag*) or *Shaker* (*Sh*), synapse size is increased. Moreover, activity-dependent plasticity at the NMJ requires canonical retrograde BMP

signaling (Berke et al., 2013). *eag,sh* mutants are constitutively hyperactive, and if activity-dependent Gbb secretion in this mutant continuously increases at the synapse, the size of the NMJ will be continuously increasing. However, the number of total boutons in *eag,sh* mutants was lower than that of *abi* mutant or presynaptically overexpressed dominant-negative Rac1 larvae. These data may indicate that continuous or excessive Gbb secretion that is beyond the physiological range acts as a negative homeostatic signal, blocking extreme growth of the synapse which may be toxic to larvae. In other words, Gbb secreted in the physiological range acts as positive signal for synaptic growth. In contrast, Gbb secreted over the physiological range may act as negative signal to protect the synapse from excessive growth. Therefore, when synaptic growth is extremely increased, Gbb may be secreted in an activity-dependent manner to reduce surface expression of BMP receptors through Abi-dependent macropinocytosis. Altogether, Gbb-induced macropinocytosis may act as a negative homeostatic mechanism to protect synapses at the NMJ. To test this hypothesis, activity-dependent secretion of Gbb and macropinocytosis activity should by tested in hyperexcitable mutants, such as *eag* or *sh*, or by directly activating synapses with electric or chemical stimuli. To fully explore this hypothesis, it may also be interesting to examine whether larvae lacking either Abi or macropinocytosis regulators have a larger NMJ size in an *eag,sh* mutant background.

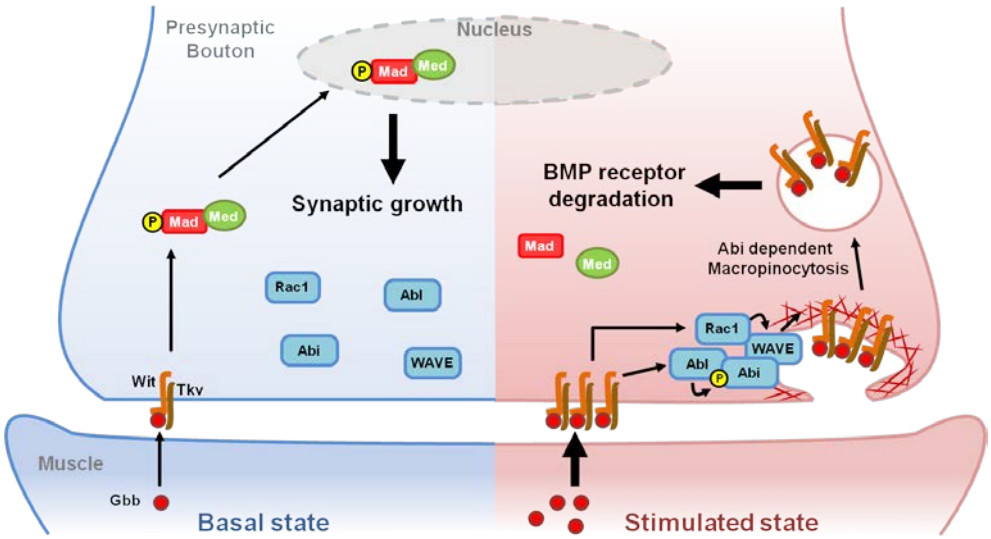

Figure 31. Proposed Model of Abi-Abl-Rac1-Dependent Gbb-Induced BMP Receptor Macropinocytosis at the NMJ

At basal state (left side of the synapse), Gbb signals positively regulate synaptic growth through the canonical BMP signaling cascade controlling the transcriptional expression of target genes regulating synaptic development. In the stimulated state (right side of the synapse), excessive Gbb is secreted from the postsynaptic muscle to trigger Abi/Abl/Rac1/WAVE signaling, activating actin polymerization and inducing macropinocytosis. Gbb-induced macropinocytosis then internalizes BMP receptors expressed on the surface of the synaptic membrane to attenuate BMP signaling and downregulate synaptic growth.

IV. REFERENCES

Aberle, H., Haghighi, A.P., Fetter, R.D., McCabe, B.D., Magalhaes, T.R., and Goodman, C.S. (2002). wishful thinking encodes a BMP type II receptor that regulates synaptic growth in Drosophila. Neuron *33*, 545-558.

Araki N, Egami Y, Watanabe Y, and Hatae T. (2007). Phosphoinositide metabolism during membrane ruffling and macropinosome formation in EGF-stimulated A431 cells. Exp Cell Res. *313*, 1496-507.

Basagiannis D, Zografou S, Murphy C, Fotsis T, Morbidelli L, Ziche M, Bleck C, Mercer J, and Christoforidis S. (2016). VEGF induces signalling and angiogenesis by directing VEGFR2 internalisation through macropinocytosis. J Cell Sci. 129, 4091-4104.

Berke B, Wittnam J, McNeill E, Van Vactor DL, and Keshishian H. (2013). Retrograde BMP signaling at the synapse: a permissive signal for synapse maturation and activity-dependent plasticity. J Neurosci. *33*, 17937-17950.

Bogdan S, Grewe O, Strunk M, Mertens A, Klämbt C. (2004). Sra-1 interacts with Kette and WASP and is required for neuronal and bristle development in Drosophila. Development *131*, 3981-3989.

Bogdan, S., Stephan, R., Lobke, C., Mertens, A., and Klambt, C. (2005). Abi activates WASP to promote sensory organ development. Nat Cell Biol *7*, 977-984.

Brand, A.H., and Perrimon, N. (1993). Targeted gene expression as a means of altering cell fates and generating dominant phenotypes. Development *118*, 401-415.

Bryant DM, Kerr MC, Hammond LA, Joseph SR, Mostov KE, Teasdale RD, and Stow JL. (2007). EGF induces macropinocytosis and SNX1-modulated recycling of E-cadherin. J Cell Sci. *120*, 1818-1828.

Budnik, V., Koh, Y.H., Guan, B., Hartmann, B., Hough, C., Woods, D., and Gorczyca, M. (1996). Regulation of synapse structure and function by the Drosophila tumor suppressor gene dlg. Neuron *17*, 627-640.

Commisso C, Flinn RJ, and Bar-Sagi D. (2014). Determining the macropinocytic index of cells through a quantitative image-based assay. Nat Protocols *9*, 182-192.

Coyle IP, Koh YH, Lee WC, Slind J, Fergestad T, Littleton JT, and Ganetzky B. (2004). Nervous wreck, an SH3 adaptor protein that interacts with Wsp, regulates synaptic growth in Drosophila. Neuron *41*, 521-534.

Dai Z and Pendergast AM. (1995). Abi-2, a novel SH3-containing protein interacts with the c-Abl tyrosine kinase and modulates c-Abl transforming activity. Genes Dev. *9*, 2569-2582.

Dickman, D.K., Lu, Z., Meinertzhagen, I.A., and Schwarz, T.L. (2006). Altered synaptic development and active zone spacing in endocytosis mutants. Curr Biol *16*, 591-598.

Dubielecka PM, Cui P, Xiong X, Hossain S, Heck S, Angelov L, and Kotula L. (2010). Differential regulation of macropinocytosis by Abi1/Hssh3bp1 isoforms. PLoS One. *5*, e10430.

Dubielecka PM, Ladwein KI, Xiong X, Migeotte I, Chorzalska A, Anderson KV, Sawicki JA, Rottner K, Stradal TE, and Kotula L. (2010). Essential role for Abi1 in embryonic survival and WAVE2 complex integrity. Proc Natl Acad Sci U S A. 108, 7022-7027.

Echarri A, Lai MJ, Robinson MR, and Pendergast AM. (2004). Abl interactor 1 (Abi-1) wave-binding and SNARE domains regulate its nucleocytoplasmic shuttling, lamellipodium localization, and wave-1 levels. Mol Cell Biol. 24, 4979-4993.

Eden S, Rohatgi R, Podtelejnikov AV, Mann M, and Kirschner MW. (2002). Mechanism of regulation of WAVE1-induced actin nucleation by Rac1 and Nck. Nature *418*, 790-793.

Egami Y, Taguchi T, Maekawa M, Arai H, and Araki N. (2014). Small GTPases and phosphoinositides in the regulatory mechanisms of macropinosome formation and maturation. Front Physiol. 5, 374.

Fujii M, Kawai K, Egami Y, and Araki N. (2013) Dissecting the roles of Rac1 activation and deactivation in macropinocytosis using microscopic photo-manipulation. Sci Rep. 3:2385

Fujii M, Kawai K, Egami Y, and Araki N. (2013). Dissecting the roles of Rac1 activation and deactivation in macropinocytosis using microscopic photo-manipulation. Sci Rep. *3*, 2385

Goley ED and Welch MD. (2006). The ARP2/3 complex: an actin nucleator comes of age. Nat Rev Mol Cell Biol. *7*, 713-726.

Hewlett LJ, Prescott AR, and Watts C. (1994). The coated pit and macropinocytic pathways serve distinct endosome populations. J Cell Biol. *124*, 689-703.

Huang EJ, Reichardt LF. (2001). Neurotrophins: roles in neuronal development and function. Annu Rev Neurosci. *24*, 677-736.

Huang, C.H., Lin, T.Y., Pan, R.L., and Juang, J.L. (2007). The involvement of Abl and PTP61F in the regulation of Abi protein localization and stability and lamella formation in Drosophila S2 cells. J Biol Chem *282*, 32442-32452.

Innocenti M, Zucconi A, Disanza A, Frittoli E, Areces LB, Steffen A, Stradal TE, Di Fiore PP, Carlier MF, and Scita G. (2004). Abi1 is essential for the formation and activation of a WAVE2 signalling complex. Nat Cell Biol. *6*, 319-27.

Innocenti, M., Gerboth, S., Rottner, K., Lai, F.P., Hertzog, M., Stradal, T.E., Frittoli, E., Didry, D., Polo, S., Disanza, A., Benesch, S., Di Fiore, P.P., Carlier, M.F., and Scita, G. (2005). Abi1 regulates the activity of N-WASP and WAVE in distinct actin-based processes. Nat Cell Biol *7*, 969-976.

Innocenti, M., Zucconi, A., Disanza, A., Frittoli, E., Areces, L.B., Steffen, A., Stradal, T.E., Di Fiore, P.P., Carlier, M.F., and Scita, G. (2004). Abi1 is essential for the formation and activation of a WAVE2 signalling complex. Nat Cell Biol *6*, 319-327.

Juang, J.L., and Hoffmann, F.M. (1999). Drosophila abelson interacting protein (dAbi) is a positive regulator of abelson tyrosine kinase activity. Oncogene *18*, 5138-5147.

Kerr MC and Teasdale RD. (2009). Defining macropinocytosis. Traffic *10*, 364-374

Keshishian, H., and Kim, Y.S. (2004). Orchestrating development and function: retrograde BMP signaling in the Drosophila nervous system. Trends Neurosci *27*, 143-147.

Kim S, Nahm M, Kim N, Kwon Y, Kim J, Choi S, Choi EY, Shim J, Lee C, and Lee S. (2017). Graf regulates hematopoiesis through GEEC endocytosis of EGFR. Development *144*, 4159-4172

Kunda P, Craig G, Dominguez V, and Baum B. (2003). Abi, Sra1, and Kette control the stability and localization of SCAR/WAVE to regulate the formation of actin-based protrusions. Curr Biol. 13, 1867-1875.

Lanzetti L, Palamidessi A, Areces L, Scita G, and Di Fiore PP. (2004). Rab5 is a signalling GTPase involved in actin remodelling by receptor tyrosine kinases. Nature. 429(6989), 309-314.

Lee, Y.S., and Carthew, R.W. (2003). Making a better RNAi vector for Drosophila: use of intron spacers. Methods *30*, 322-329.

Leng Y, Zhang J, Badour K, Arpaia E, Freeman S, Cheung P, Siu M, and Siminovitch K. (2005). Abelson-interactor-1 promotes WAVE2 membrane translocation and Abelson-mediated tyrosine phosphorylation required for WAVE2 activation. Proc Natl Acad Sci U S A. *102*, 1098-1103.

Li L, Wan T, Wan M, Liu B, Cheng R, and Zhang R. (2015). The effect of the size of fluorescent dextran on its endocytic pathway. Cell Biol Int *39*, 531-539

Liberali P, Kakkonen E, Turacchio G, Valente C, Spaar A, Perinetti G, Böckmann RA, Corda D, Colanzi A, Marjomaki V, and Luini A. (2008). The closure of Pak1-dependent macropinosomes requires the phosphorylation of CtBP1/BARS. EMBO J. *27*, 970-981.

Lim JP and Gleeson PA. (2011). Macropinocytosis: an endocytic pathway for internalising large gulps. Immunol Cell Biol. *89*, 836-843.

Lin, T.Y., Huang, C.H., Kao, H.H., Liou, G.G., Yeh, S.R., Cheng, C.M., Chen, M.H., Pan, R.L., and Juang, J.L. (2009). Abi plays an opposing role to Abl in Drosophila axonogenesis and synaptogenesis. Development *136*, 3099-3107.

Marques, G., Bao, H., Haerry, T.E., Shimell, M.J., Duchek, P., Zhang, B., and O'Connor, M.B. (2002). The Drosophila BMP type II receptor Wishful Thinking regulates neuromuscular synapse morphology and function. Neuron *33*, 529-543.

McCabe, B.D., Marques, G., Haghighi, A.P., Fetter, R.D., Crotty, M.L., Haerry, T.E., Goodman, C.S., and O'Connor, M.B. (2003). The BMP homolog Gbb

provides a retrograde signal that regulates synaptic growth at the Drosophila neuromuscular junction. Neuron *39*, 241-254.

Mooren, O.L., Galletta, B.J., and Cooper, J.A. (2012). Roles for actin assembly in endocytosis. Annu Rev Biochem *81*, 661-686.

Moresco EM and Koleske AJ. (2003). Regulation of neuronal morphogenesis and synaptic function by Abl family kinases. Curr Opin Neurobiol. *13*, 535-544.

Nahm, M., Kim, S., Paik, S.K., Lee, M., Lee, S., Lee, Z.H., Kim, J., Lee, D., Bae, Y.C., and Lee, S. (2010a). dCIP4 (Drosophila Cdc42-interacting protein 4) restrains synaptic growth by inhibiting the secretion of the retrograde Glass bottom boat signal. J Neurosci *30*, 8138-8150.

Nahm, M., Lee, M.J., Parkinson, W., Lee, M., Kim, H., Kim, Y.J., Kim, S., Cho, Y.S., Min, B.M., Bae, Y.C., Broadie, K., and Lee, S. (2013). Spartin regulates synaptic growth and neuronal survival by inhibiting BMP-mediated microtubule stabilization. Neuron *77*, 680-695.

Nahm, M., Long, A.A., Paik, S.K., Kim, S., Bae, Y.C., Broadie, K., and Lee, S. (2010b). The Cdc42-selective GAP rich regulates postsynaptic development and retrograde BMP transsynaptic signaling. J Cell Biol *191*, 661-675.

O'Connor-Giles, K.M., Ho, L.L., and Ganetzky, B. (2008). Nervous wreck interacts with thickveins and the endocytic machinery to attenuate retrograde BMP signaling during synaptic growth. Neuron *58*, 507-518.

Osterwalder, T., Yoon, K.S., White, B.H., and Keshishian, H. (2001). A conditional tissue-specific transgene expression system using inducible GAL4. Proc Natl Acad Sci U S A *98*, 12596-12601.

Pollitt AY and Insall RH. (2009). WASP and SCAR/WAVE proteins: the drivers of actin assembly. J Cell Sci. *122*, 2575-2578

Prokop, A. (2006). Organization of the efferent system and structure of neuromuscular junctions in Drosophila. Int Rev Neurobiol *75*, 71-90.

Qurashi A, Sahin HB, Carrera P, Gautreau A, Schenck A, Giangrande A. (2007). HSPC300 and its role in neuronal connectivity. Neural Dev. *2*, 18.

Racoosin EL and Swanson JA. (1993). Macropinosome maturation and fusion with tubular lysosomes in macrophages. J Cell Biol. *121*, 1011-1020.

Rawson, J.M., Lee, M., Kennedy, E.L., and Selleck, S.B. (2003). Drosophila neuromuscular synapse assembly and function require the TGF-beta type I receptor saxophone and the transcription factor Mad. J Neurobiol *55*, 134-150.

Roos, J., Hummel, T., Ng, N., Klambt, C., and Davis, G.W. (2000). Drosophila Futsch regulates synaptic microtubule organization and is necessary for synaptic growth. Neuron *26*, 371-382.

Schenck A, Qurashi A, Carrera P, Bardoni B, Diebold C, Schejter E, Mandel JL, Giangrande A. (2004). WAVE/SCAR, a multifunctional complex coordinating different aspects of neuronal connectivity. Dev Biol. *274*, 260-270.

Schmees C, Villaseñor R, Zheng W, Ma H, Zerial M, Heldin CH, Hellberg C. (2012). Macropinocytosis of the PDGF β-receptor promotes fibroblast transformation by H-RasG12V. Mol Biol Cell. *23*, 2571-2582.

Schnatwinkel C, Christoforidis S, Lindsay MR, Uttenweiler-Joseph S, Wilm M, Parton RG, and Zerial M. (2004). The Rab5 effector Rabankyrin-5 regulates and coordinates different endocytic mechanisms. PLoS Biol. 2, 1363-1380

Schuster CM, Davis GW, Fetter RD, and Goodman CS. (1996a). Genetic dissection of structural and functional components of synaptic plasticity. I. Fasciclin II controls presynaptic structural plasticity. Neuron. *17*, 655-667.

Seastone DJ, Harris E, Temesvari LA, Bear JE, Saxe CL, and Cardelli J. (2001). The WASp-like protein scar regulates macropinocytosis, phagocytosis and endosomal membrane flow in Dictyostelium. J Cell Sci. *114*, 2673-2683.

Shi Y, Alin K, and Goff SP. (1995). Abl-interactor-1, a novel SH3 protein binding to the carboxy-terminal portion of the Abl protein, suppresses v-abl transforming activity. Genes Dev. *9*, 2583-2597.

Smythe E and Ayscough KR. (2006). Actin regulation in endocytosis. J Cell Sci. *119*, 4589-4598.

Stephan, R., Gohl, C., Fleige, A., Klambt, C., and Bogdan, S. (2011). Membrane-targeted WAVE mediates photoreceptor axon targeting in the absence of the WAVE complex in Drosophila. Mol Biol Cell *22*, 4079-4092.

Swanson J. A. (2008). Shaping cups into phagosomes and macropinosomes. Nat Rev Mol Cell Biol. *9*, 639-649.

Swanson JA and Watts C. (1995). Macropinocytosis. Trends Cell Biol. *5*, 424-428.

Sweeney, S.T., and Davis, G.W. (2002). Unrestricted synaptic growth in spinster-a late endosomal protein implicated in TGF-beta-mediated synaptic growth regulation. Neuron *36*, 403-416.

Takenawa T and Suetsugu S. (2007). The WASP-WAVE protein network: connecting the membrane to the cytoskeleton. Nat Rev Mol Cell Biol. *8*, 37-48.

Tao HW and Poo M. (2001). Retrograde signaling at central synapses. Proc Natl Acad Sci U S A. *98*, 11009-11015.

Valdez G, Philippidou P, Rosenbaum J, Akmentin W, Shao Y, Halegoua S. (2007). Trk-signaling endosomes are generated by Rac-dependent macroendocytosis. Proc Natl Acad Sci U S A. 104, 12270-12275.

Wang, X., Shaw, W.R., Tsang, H.T., Reid, E., and O'Kane, C.J. (2007). Drosophila spichthyin inhibits BMP signaling and regulates synaptic growth and axonal microtubules. Nat Neurosci *10*, 177-185.

West MA, Prescott AR, Eskelinen EL, Ridley AJ, and Watts C. (2000). Rac is required for constitutive macropinocytosis by dendritic cells but does not control its downregulation. Curr Biol. *10*, 839-848.

Wodarz, A., Hinz, U., Engelbert, M., and Knust, E. (1995). Expression of crumbs confers apical character on plasma membrane domains of ectodermal epithelia of Drosophila. Cell *82*, 67-76.

Xiao, L., Michalski, N., Kronander, E., Gjoni, E., Genoud, C., Knott, G., and Schneggenburger, R. (2013). BMP signaling specifies the development of a large and fast CNS synapse. Nat Neurosci *16*, 856-864.

Xu C, Fu X, Zhu, and Liu JJ. (2016). Retrolinkin recruits the WAVE1 protein complex to facilitate BDNF-induced TrkB endocytosis and dendrite outgrowth. Mol Biol Cell. *27*, 3342-3356.

Yoshida S, Gaeta I, Pacitto R, Krienke L, Alge O, Gregorka B, and Swanson JA. (2015). Differential signaling during macropinocytosis in response to M-CSF and PMA in macrophages. Front Physiol. *6*, 8

Zhang, Y.Q., Bailey, A.M., Matthies, H.J., Renden, R.B., Smith, M.A., Speese, S.D., Rubin, G.M., and Broadie, K. (2001). Drosophila fragile X-related gene regulates the MAP1B homolog Futsch to control synaptic structure and function. Cell *107*, 591-603.

Zhao L, Wang D, Wang Q, Rodal AA, Zhang YQ. (2013). Drosophila cyfip regulates synaptic development and endocytosis by suppressing filamentous actin assembly. PLoS Genet. *9*, e1003450.

국문 초록

Abl 상호작용 단백질인 Abi 에 의한 BMP 의존적 시냅스 성장 및 macropinocytosis 조절

김나진

협동과정 유전공학전공

서울대학교 대학원

초파리의 근육에서 발현되는 glass bottom boat(Gbb)는 bone morphogenetic protein(BMP) 계열의 성장인자로서, 신경근육 이음부에서 시냅스 발생 및 가소성을 조절하는 중요한 역방향 신호로 작용한다. 기존연구에 의하여 과도한 BMP 신호전달의 활성화를 억제하는 endocytosis 의 기능이 잘 규명되었으나, BMP 수용체를 세포 내로 이입되는 과정에 대한 분자적, 세포생물학적 기전에 대해서는 알려진 바가 없는 실정이다. 인산화 효소인 Abl 과 상호 작용하는 동시에 기질로 알려진 Abi 단백질은 SCAR/WAVE 복합체의 주요 인자로

기능하는 바, SCAR/WAVE 복합체는 Rac 의 하위인자로서 macropinocytosis 에 필수적인 액틴의 중합반응을 조절한다. 본 연구는 Abi 에 의한 macropinocytosis 의 조절이 BMP 의존적 시냅스 발생이 정상적으로 일어나는데 매우 중요함을 규명하고자 하였다. 유전학적 기법을 통하여 Abi 가 Abl 와 Rac1 신호전달의 하위 인자로 작용하여 BMP 신호전달을 조절함으로써 시냅스의 성장을 억제함을 규명하였다. 다음으로 Abi 가 다양한 endocytic 단백질들과 상호 작용하여 시냅스 성장을 억제함을 규명하였다. 또한 Gbb 가 신경세포 및 신경근육 이음부에서 macropinocytosis 를 유발할 수 있는 바, 이 과정에서 Rac-SCAR/WAVE 신호전달 경로와 Abl 에 의한 Abi 의 인산화가 필요함을 규명하였다. 한편 Gbb 에 의해 유발된 macropinocytosis 는 BMP 수용체의 내재화를 통한 세포 내 분해를 촉진함을 규명하였다. 마지막으로 macropinocytosis 의 주요 인자로 알려진 Rabankyrin 과 CtBP 의 경우에도 BMP 신호전달을 억제하여 시냅스의 성장을 조절하는 기능이 있음을 규명하였다. 이러한 연구 결과들은 Abi 단백질이 Abl 과 Rac-SCAR/WAVE 신호전달의 통합을 통하여 macropinocytosis 를 촉진함으로써 BMP 수용체의 세포 내 분해를 유도하여 시냅스 성장을 저해함을 제시한다.

주 요 어: Abi, Abl, Rac, Gbb, BMP 수용체, Macropinocytosis,
시냅스 성장, 신경근육 이음부, 초파리

학 번: 2010-20212